

DESIGN STUDIES AND PROTOTYPE DEVELOPMENT OF A 325 MHz 4-ROD RFQ

DISSERTATION

zur Erlangung des Doktorgrades
der Naturwissenschaften

vorgelegt beim Fachbereich Physik
der Johann Wolfgang Goethe - Universität
in Frankfurt am Main
von

BENJAMIN KOUBEK
aus Schwäbisch Hall

Frankfurt am Main 2014
(D 30)



vom Fachbereich Physik der
Johann Wolfgang von Goethe - Universität als Dissertation angenommen.

Dekan:	Prof. Dr. Joachim Stroth
Gutachter:	Prof. Dr. Alwin Schempp
	Prof. Dr. Holger Podlech

Datum der Disputation: 23.10.2014

Contents

0	Zusammenfassung	1
1	Introduction	6
1.1	GSI and the FAIR Project	8
1.2	Proton Linac	12
2	Theory	14
2.1	Radio Frequency Quadrupole	14
2.1.1	Principle of an RFQ	15
2.1.2	Resonator Concepts	21
2.1.3	RF-Fields in an RFQ	24
2.1.4	Characteristic RF Parameters	29
2.1.5	Modes	34
2.2	CST Microwave Studio	39
3	Analysis of the 4-rod Structure at 325 MHz	42
3.1	Dipole Field	43
3.1.1	RF Design of the Prototype	44
3.1.2	Compensation of the Dipole Field	44
3.1.3	Prototype	53
3.2	Fringe Fields	57
3.2.1	Longitudinal Fields	57
3.2.2	Boundary Conditions	57
3.2.3	Fringe Fields at the FNAL RFQ	64
3.3	Improvement of the 325 MHz 4-rod Prototype	66
3.3.1	Stem Thickness	67
3.3.2	Tuning Plate Height	68
3.3.3	Stem Shape	68
3.3.4	Summary	69

4	Comparison of Alternative RFQ Resonator Types	70
4.1	4-Vane RFQ	70
4.2	Ladder RFQ	74
4.3	CH RFQ	78
4.4	Discussion	81
5	Power Tests of the 325 MHz 4-rod Prototype	83
5.1	Low Power Conditioning	83
5.2	High Power Tests	86
5.2.1	Optimization of the 4-rod RFQ	87
5.2.2	High Power Conditioning	89
5.2.3	Measurement of the Shunt Impedance	90
6	Conclusion	95
6.1	Summary	98
6.2	Outlook	98
	Bibliography	99
	Danksagung	107
	Lebenslauf	107

0 Zusammenfassung

Die vorliegende Arbeit befasst sich mit Untersuchungen zu einem 4-rod Radio Frequenz Quadrupol (RFQ) Beschleuniger für hohe Betriebsfrequenzen, die bisher an dieser Struktur noch nicht realisiert wurden. Benötigt wird ein solcher 325 MHz RFQ am FAIR Projekt der GSI zur Beschleunigung von Protonen.

RFQ Beschleuniger sind das Bindeglied zwischen der Protonenquelle und den Driftröhrenbeschleunigern. Sie fokussieren, bunched und beschleunigen den Strahl mit Hilfe des elektrischen Quadrupolfeldes, so dass die Teilchenpakete von den Driftröhrenstrukturen aufgenommen, durch diese weiterbeschleunigt, und mit magnetischen Linsen fokussiert werden können.

Beim Ausbau der Beschleunigeranlage der Großforschungseinrichtung GSI (GSI Helmholtzzentrum für Schwerionenforschung GmbH) im Rahmen des FAIR (Facility for Antiproton and Ion Research in Europe GmbH) Projekts wird ein neuer Linearbeschleuniger gebaut. Dieser soll Protonen über eine Länge von etwa 30 m auf etwa 70 MeV beschleunigen. Der Protonenlinac dient als Injektor für das SIS 18, das die Protonen zur Erzeugung von Antiprotonen für spätere Experimente weiterbeschleunigt.

Der RFQ übernimmt dabei die Aufgabe den Gleichstromstrahl der Protonenquelle möglichst verlustfrei und effizient einzufangen, zu fokussieren, zu bunched und auf Energien zu beschleunigen, damit die Protonenpakete von den darauffolgenden Driftröhrenstrukturen (CH-Beschleunigern) verlustfrei und ohne Emittanzwachstum aufgenommen und weiterbeschleunigt werden können. Der RFQ ist in der Lage den Gleichstromstrahl der Quelle komplett einzufangen und gleichzeitig mit, bei kleinen Teilchenenergien sehr vorteilhaften, elektrischen Hochfrequenzfeldern zu fokussieren.

Die Betriebsfrequenz von 325 MHz stellt in sofern eine Herausforderung dar, weil bisher kein 4-rod RFQ bei dieser Frequenz realisiert wurde. Dies liegt unter anderem daran, dass aufgrund der bauartbedingten unsymmetrischen Elektrodenaufhängung und der hohen Frequenz ein, das Quadrupolfeld überlagerndes, Dipolfeld erzeugt wird. Dieses störende Feld kann zu einem ver-

tikalten Versatz der Strahlachse führen. Üblicherweise ist dieser hohe Frequenzbereich den 4-vane RFQs vorbehalten, da diese bei hohen Frequenzen von praktikabler Größe sind und gute Resonanzeigenschaften besitzen. Sie bestehen aus einer anderen Resonanzstruktur, die eine höhere Symmetrie aufweist. Jedoch sind die 4-vane Strukturen komplexer beim Tuning, risikobehafteter in der Fertigung und kostspieliger. Die Motivation einen 4-rod RFQ für 325 MHz zu entwickeln, resultiert aus dem Kostenvorteil und einer besseren Zugänglichkeit zur Wartung und Reparatur. Zudem besteht an der Universität Frankfurt eine sehr lange Erfahrung mit 4-rod RFQs.

Die vorliegende Arbeit befasst sich mit den damit verbundenen Herausforderungen, einen 4-rod RFQ für die geforderte Frequenz von 325 MHz zu optimieren. Es wurden entsprechende Untersuchungen mit Simulationen durchgeführt, Probleme analysiert und Lösungen erarbeitet. Ein Prototyp wurde entworfen, gefertigt, untersucht und mit hoher Leistung getestet. Die wichtigsten Schritte können wie folgt zusammengefasst werden:

- Hochfrequenzsimulationen zur Symmetrie der 4-rod Struktur, insbesondere der Randfeldeffekte und der störenden Dipolfelder, hervorgerufen durch die hohe Frequenz, sowie die Analyse möglicherweise den Betrieb störenden höheren Moden.
- Hochfrequenzdesign und Aufbau eines 4-rod RFQ Prototypen, sowie die Verifikation der Simulationsergebnisse mittels Messungen der HF-Parameter, der longitudinale Spannungsverteilung und der Dipolkomponenten auf Messsenderniveau.
- Hochleistungstests zur Demonstration der Betriebseigenschaften des 325 MHz 4-rod RFQs, einschließlich Messungen der Elektrodenspannung mittels Gammaspektroskopie zur Bestätigung und zum Vergleich der Shuntimpedanz mit unterschiedlichen Messmethoden.
- Untersuchung und Vergleich alternativer RFQ Resonatorkonzepte, sowie die Diskussion deren Realisierbarkeit bei einer Betriebsfrequenz von 325 MHz.

4-rod RFQ Beschleuniger wurden bislang mit einer Frequenz von maximal 216 MHz realisiert. Bei höheren Frequenzen treten Effekte auf, die das Hochfrequenzverhalten nachteilig verändern können. Der hauptsächliche Effekt ist ein Dipolanteil der das Quadrupolfeld der Elektroden überlagert. Dieses Feld wird durch Asymmetrien der 4-rod Struktur hervorgerufen und kann bei kleineren Frequenzen vernachlässigt werden. Bei höheren Frequenzen tritt dieses Feld stärker auf und kann zum Beispiel die Lage der Strahlachse verändern. Um dieses Problem zu lösen, wurden sämtliche frequenzbestimmenden Strukturparameter in Simulationen auf ihren Einfluss auf das Dipolfeld untersucht. Mit der Form der Stützen bzw. des Stützeineinschnitts kann der stärkste Einfluss auf das störende Dipolfeld genommen werden. Deshalb wurde die Stützengeometrie genauer untersucht. Durch diese Untersuchungen konnte der Dipol vollständig kompensiert, bzw. sogar überkompensiert werden. Für die reale Länge des Protonenlinac RFQ, von etwa 3 Metern, wurden auch die Moden höherer Ordnung untersucht. Durch die hohe Anzahl von Hochfrequenzzellen wandern die Frequenzen der höheren Moden in Richtung Grundmode, in der der RFQ betrieben wird, und können zu Störungen dieser führen. In Simulationen konnte eine akzeptable Modenseparation nachgewiesen werden. Für eventuelle Abweichungen der Simulation von einem realen Modell wurden trotzdem Strategien zur Einflussnahme der Moden entwickelt. Im Zuge der Simulationen zur Felddoptimierung in longitudinaler Richtung wurden auch Randfeldeffekte, die nicht in der Strahldynamik berücksichtigt werden, untersucht. Dies sind elektrische Felder zwischen den Elektroden und der Tankwand des Resonators, welche die Strahlausgangsenergie beeinflussen können. Diese Felder treten gleichermaßen bei kleineren Betriebsfrequenzen auf. Diese Ergebnisse tragen generell zur Optimierung des HF-Designs bei 4-rod RFQs bei. Am Beispiel des FNAL RFQs konnten störende Randfelder, die eine Energieabweichung von etwa 50 keV verursachten, nachträglich korrigiert werden.

Aufgrund der beschriebenen Untersuchungen wurde ein Prototyp des 325 MHz 4-rod RFQs entworfen und in der hausinternen Werkstatt des IAPs hergestellt. Nach der Hochfrequenzabstimmung konnten mittels Untersuchungen auf Messsenderniveau die Simulationsergebnisse bestätigt werden. Diese Messungen zeigen die Machbarkeit eines dipolfreien 325 MHz 4-rod RFQs mit insgesamt sehr zufriedenstellenden Hochfrequenzeigenschaften. Ein wichtiger Parameter für die Effizienz eines Beschleunigers ist die Shuntimpedanz. Diese gibt an, wie gut die eingekoppelte Leistung in Resonatorspannung umgewan-

delt werden kann und wird bei 4-rod Strukturen üblicherweise mit der Störkondensatormethode bestimmt. In dieser Arbeit wurde sie jedoch mit Hilfe verschiedener Methoden ermittelt, da selbst eine Störung von nur 1 pF im Vergleich zur Elektrodenkapazität des kurzen Prototyps eine zu große Störung darstellte, um eindeutige Ergebnisse zu liefern. Drei weitere Methoden, die teilweise auf theoretischen Annahmen und Simulationen basieren, wurden untersucht, neben der Messung der Elektrodenspannung bei höheren Feldpegeln. Den bei diesen Simulationen und Messungen gewonnenen Ergebnissen folgte ein weiteres optimiertes Design des 325 MHz 4-rod RFQ, das in dieser Arbeit vorgestellt wird.

Nach der Hochfrequenzabstimmung und den Messungen mit kleinen Leistungspegeln, wurden Tests mit hoher Leistung durchgeführt, um die Betriebs-eigenschaften zu demonstrieren. Hierzu wurde der Prototyp erst mit Leistungen bis 500 W im cw-Betrieb konditioniert und später mit einem 40 kW Verstärker, mit einem Tastverhältnis von 0,3 %, gepulst betrieben. Aufgrund von Problemen mit dem Zirkulator bei etwa 8 kW und kleinen thermischen Beschädigungen am RFQ wurde der Prototyp optimiert. Die Oberfläche aller Teile des RFQs wurde bearbeitet und poliert, zudem führte der Einbau einer neuen Bodenplatte und neuer Tuningplatten zu nochmals besseren Ergebnissen der Hochfrequenzabstimmung. Nach langsamen Konditionieren mit ebenfalls geringer Leistung konnte eine sehr gute Akzeptanz von Leistungen bis 40 kW ohne jegliche Probleme erreicht werden. Dabei wurde die Elektrodenspannung mittels Gammaspektroskopie bei unterschiedlichen in den Resonator eingekoppelten Leistung bestimmt. Mit diesen Ergebnissen konnte die Shuntimpedanz berechnet und mit anderen Methoden zur Bestimmung der Shuntimpedanz verglichen werden. Als Ergebnis konnte eine, zu anderen RFQ Strukturen in einem ähnlichen Frequenzbereich, vergleichbare Shuntimpedanz nachgewiesen werden.

Abschließend wurde der 325 MHz 4-rod RFQ mit alternativen RFQ Resonatoren, bezüglich der Realisierbarkeit in dieser Betriebsfrequenz, verglichen. Dabei wurden ein 4-vane RFQ, ein Ladder RFQ und ein CH-RFQ untersucht. Der 4-vane RFQ ist der Standardresonator bei Frequenzen über 300 MHz. Er besitzt eine praktikable Größe und wurde einige Male in diesem Frequenzbereich erfolgreich realisiert, ist jedoch sehr kompliziert in der Fertigung und eine sehr aufwändige und kostspielige Lösung.

Der Ladder RFQ hat keine störenden Dipolanteile, ist aber bisher nur für niedrigere Frequenzen realisiert worden. Das sind der Linac3 RFQ (101 MHz), der ASAKUSA RFQ (202 MHz) und der Zweistrahl RFQ des Frankfurt Funneling Experiments (54 MHz). Die Ladder-Bauweise stellt eine Option für 325 MHz dar, kann jedoch im Aufbau sehr kompliziert werden. Dies hängt davon ab, wie einzelne Details in der Konstruktion realisiert werden können.

Der CH RFQ wurde ebenfalls, wegen des ausbleibenden Dipolanteils untersucht. Jedoch wird diese Bauart umpraktikabel klein bei dieser Frequenz und ist sehr aufwendig in der Fertigung, bei der für einzelne Details noch Lösungen gefunden werden müssten.

Alle diese RFQ Strukturen wurden im selben Frequenzbereich mittels Simulationen untersucht um deren Hochfrequenzeigenschaften und Tuningmöglichkeiten zu bestimmen. Dabei wurden auch technologische Aspekte, wie die Herstellung und die Zugänglichkeit während der Hochfrequenzabstimmung des Resonators, berücksichtigt. Abschließend wird in einer Diskussion die Realisierbarkeit der einzelnen RFQ Strukturen verglichen.

Als Ergebnis dieser Untersuchungen kann festgehalten werden, dass die 4-rod Struktur durchaus eine Alternative für einen Betrieb bei 325 MHz darstellt. Es konnte gezeigt werden, dass der 4-rod RFQ technologisch sowie bezüglich der Hochfrequenzeigenschaften alle Anforderungen erfüllt und gleichzeitig eine kostengünstige Option gegenüber anderen RFQ Strukturen repräsentiert. Zudem spricht die langjährige Erfahrung an der Universität Frankfurt und die enge Zusammenarbeit mit lokalen Firmen für eine schnelle Realisierung einer 4-rod Struktur für den Protonenlinac des FAIR Projekts.

1 Introduction

Particle accelerators are used to deliver beams for a large variety of applications. In general an accelerator complex consists of some kind of particle source, the accelerating structures, transport and diagnostic sections and a target area depending on the purpose of the application. The applications are generally motivated in fundamental research or making use of the produced particle beam.

Electrons are accelerated for example to serve as synchrotron light sources or as free electron lasers (FEL) to produce light with special characteristics. On the other hand protons and ions are accelerated to produce intense particle beams for experiments in the fields of nuclear and atomic as well as in plasma and astrophysics. To mention just a few examples the beams are used in experiments to produce secondary particles or quark-gluon-plasma, to study particle interactions or exotic nuclei or the verification of the standard model. In addition an application for the accelerated particle beam is the cancer treatment with protons and carbon ions.

The radio frequency quadrupole (RFQ) accelerators are used to accelerate protons or ions at low energies just behind the ion source. It accepts the DC beam from the source, forms the bunched beam and accelerates it to an energy that can be accepted from the following accelerating structures. These structures are usually drift tube accelerators. For further acceleration the beam of the linear accelerator (LINAC) is injected into synchrotron rings.

The RFQ accelerator basically consists of its characteristic four quadrupole electrodes and a resonant structure to produce the electrodes alternating potential. The structure can be realized with different kind of resonator types. Which resonator type is chosen depends on various reasons. These reasons can be parameters determining the performance of an RFQ like for example the frequency and duty factor, but also costs and experience in building a special resonator can be relevant. One important parameter by choosing a resonator type is the operation frequency. Why a certain operating frequency of the linac is chosen, often depends on technical reasons like the availability of the power

supply. In the past often 200 MHz high power transmitter tubes from radio broadcasting applications were used. The frequency of 325 MHz can be realized with klystrons. But also the acceleration efficiency or the shunt impedance is depending on the frequency as well. The frequency choice of a linac is a compromise of various parameters of the complete linac. The Institute for Applied Physics (IAP) at Goethe University of Frankfurt has great experience in the development and building of 4-rod RFQs. These kind of RFQs can be built at relative low costs in comparison to other resonator types, they have good tuning possibilities and are comfortable for maintenance. In addition they show a large variability in the frequency. Nevertheless until now 4-rod RFQs are operating at frequencies up to 216 MHz. Usually the 325 MHz region is the domain of 4-vane type RFQs. This is a complex structure with higher precision requirements. In comparison to the 4-rod RFQ they are often associated with higher risks during fabrications. The welding of the single parts of the RFQ needs to be done with high precision due to the tight tolerances. Several steps of complex metrology are necessary during machining and assembling. Besides this, the resonant structure has intrinsic disturbing TE-modes that need to be suppressed artificially. Although challenges occur in the high frequency region for the 4-rod structure as well the advantages mentioned above motivate this work to make this kind of RFQ operating at a frequency of 325 MHz.

This thesis will proof the feasibility of a 325 MHz 4-rod RFQ planned to be operated at the FAIR proton LINAC. Solutions of the challenges in the high frequency region for this accelerating structure are presented. Detailed investigations regarding the dipole and fringe fields with solutions are shown and have lead to a prototype. Simulations comparing other resonator types and their tuning possibilities in the 325 MHz region are presented as well. A copper prototype has been built at the IAP workshop to verify the simulation results with low level RF measurements. High power experiments confirm the shunt impedance of the structure by measurements of the electrode voltage using gamma spectroscopy and show how much power the prototype can sustain.

1.1 GSI and the FAIR Project

GSI

The GSI Gesellschaft für Schwerionenforschung (later GSI Helmholtzzentrum für Schwerionenforschung GmbH) was founded in 1969 by nuclear physicists with the idea to have a central facility for research. First it was triggered by scientists from Darmstadt, Frankfurt and Marburg, later Gießen, Heidelberg and Mainz joined. Three of the main ideas the GSI has realized is the synthesis of superheavy elements, ion implantation and later the tumor therapy with heavy ions. The GSI operates one of the worlds most powerful accelerator. It is the only facility that allows the acceleration of ions of all chemical elements occurring on earth.

To mention a few milestones, first experiments with the linear accelerator have taken place in 1975. The universal linear accelerator (UNILAC) is able to accelerate ions from hydrogen to uranium up to 11.4 MeV/u [2] at a length of 120 m. In 1981 the first six new chemical elements were produced. Until today (with the fragment separator) hundreds of new nuclide could be produced and analyzed. The discovery of three new forms of radioactive decay is just another example for outstanding research results. In 1990 the first new ring accelerator SIS-18 and the experimental storage ring (ESR) were commissioned. The SIS-18 is a synchrotron accelerator that accepts the beam from the UNILAC and has a circumference of 216 m and a maximum bending power of 18 Tm. It consists of two RF accelerator cavities at 16 kV and about 50 magnets to bend the beam and keep it focused. The beam can be stored in the ESR with 108 m circumference. These ions can be stored at high energy and used for experiments. Cooling systems allow high precision experiments. By using the fragment separator (FRS) also new particles with short live-times like new isotopes can be stored and investigated in the ESR. In 1997 the combination of UNILAC and SIS-18 allowed the successful treatment of patients with tumors by irradiation with carbon ions at beam energies between 200 - 400 MeV/u. Another field of research was provided through the PHELIX laser system which was commissioned in 2008. The Petawatt High Energy Laser for Heavy Ion Experiments is a versatile laser facility delivering intense laser beams with energies up to 1 kJ or likewise powers up to 500 TW. It can be used for experiments like the worldwide unique combination of laser radiation with

heavy ion beams generated by the UNILAC. This enables several experiments in the fields of plasma, atomic and nuclear physics. The laser can also be used in stand alone experiments with intense laser beams for proton acceleration or x-ray laser generation. For moderate beam intensities up to 10 TW an additional pulse compressor and target chamber is available.

FAIR

The project FAIR (Facility for Antiproton and Ion Research) is the large upgrade of the existing GSI accelerator complex shown in Fig. 1.1. Its construction was proposed in 2001 leading to the official start of the project in 2007. The construction works began in 2011. The facility will be able to deliver antiproton and ion beams with unprecedented intensity and quality. The final construction of FAIR consists of eight storage and acceleration rings with up to 1,100 m in circumference, two linear accelerators and about 3.5 km beam transfer lines. The international agreement on the joint construction of FAIR in Darmstadt was signed in October 2010 by nine countries.

The existing GSI accelerators together with the planned proton linac serve as the injectors for the new facility. The double ring synchrotron (SIS-100) will provide ion beams of high intensities and considerably increased energy. Thereby intense beams of secondary particles, like unstable nuclei or antiprotons, can be produced. The system of storage-cooler rings allows a high quality of these secondary beams as their energy spread and emittance is drastically improved. Moreover, in connection with the double ring synchrotron, an efficient parallel operation of up to four scientific programs can be realized at a time. The result of this upgrade is an ion beam with unique properties [15].

Beam Properties

One aspect is the improvement of the **beam intensity**. Higher beam intensities allow higher probabilities of observing rare reactions or reaction products. Secondary beams of unstable nuclei can be studied and the synthesis of heavy elements like in supernova explosions will become available.

To determine the mass of short-lived, unstable nuclei, ion and antiproton beams of the utmost energy sharpness are necessary. Also the search for new particles associated with the strong interaction will benefit from more **brilliant**

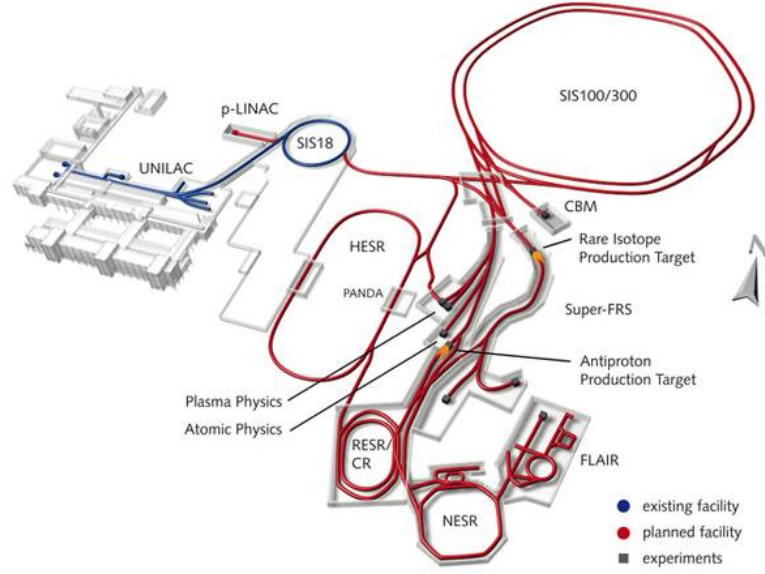


Figure 1.1: Existing GSI facility (blue) and planned FAIR facility (red) [15].

beams. For this the stochastic and electron cooling methods are already in operation at the existing facility. The implementation of this to the higher beam intensities and energies will be one of the big challenges at the planned facility.

In order to produce highly compressed nuclear matter in nucleus-nucleus collisions the double-ring synchrotron will provide much higher **beam energies** than the present GSI facility. This will enable scientists to study the state of matter at the beginning of the universe as well as forms of matter that may exist at the center of neutron stars. The new energy region of FAIR will produce high rates of hadrons with strange quarks. Moreover the energy threshold for the production of hadrons with charm quarks and of antiprotons will be exceeded. Also scientists will be able to produce intense antiproton beams.

The generation of short, high intensity ion pulses is needed to create hot, dense plasmas in bulk matter by ion beam irradiation. Ion pulses with large **beam power** can be generated by the new facility.

The coordination of the accelerators and storage rings and the double ring concept will enable **parallel operation** of up to four different scientific programs with different kinds of ions.

Experiments

The innovations of the FAIR project together with the upgrades of the existing facility will provide a large variety of forefront research in physics and applied science. The scientific program is based on four pillars [5]:

- Atomic and plasma physics, and applied sciences in the bio, medical, and material sciences (APPA)
- Physics of hadrons and quarks in compressed nuclear matter (CBM)
- Structure of nuclei, nuclear astrophysics and radioactive ion beams (NuSTAR)
- Physics with anti-proton beams (PANDA)

One major topic of the FAIR project is physics with antiprotons. The research with antiprotons will be done at the AntiProton ANnihilation at DArmstadt (PANDA) experiment. About 450 physicists from 17 countries are working in the PANDA collaboration [16]. The PANDA detector is located inside the High Energy Storage Ring (HESR), where antiprotons will cycle and collide with protons or other particles. By annihilation or the decay of glueballs¹ particles are created and fly in all directions. Because it is not understood, which types of particles will be created, the PANDA detector has an angular resolution and will be able to measure all types of particles.

One research topic is the so called confinement. The nuclei consists of protons and neutrons. These hadrons are built of quarks and are bound by the strong force. This force is mediated via gluons and shows an unusual behavior. If the quarks are close together the force is small, by increasing the distance of the quarks the force increases as well. By the attempt of separating a quark - anti-quark pair the energy of the gluon field increases until a new quark - anti-quark pair is created. This is called confinement and scientists try to understand this more precisely. But to comprehend it quantitatively by the theory of the strong force, we need a more precise understanding of the strong force at medium and large distances. By colliding protons and antiprotons short living charmonium particles are created. They consist of charm-quarks

¹Glueballs are exotic hypothetical composite particles only consisting of gluons. They are predicted by the theory of the strong force according to quantum chromodynamics [37].

and anti-charm-quarks. Insights into the behavior of the strong force and the origin of the confinement can be provided by the spectroscopy of these charmonium states.

Another research topic with antiprotons is the origin of the hadron masses. Only a few percent of the hadron mass can be accounted from the three valence quarks. It is supposed that the missing amount must be generated in a different way. The only explanation is that the interaction between the quarks must generate this mass. How mass is generated by strong interaction that acts between the quarks will be studied by the PANDA experiment at FAIR.

1.2 Proton Linac

Although the UNILAC is able to provide beams from proton to uranium it is optimized for heavy ion operation. It could provide a proton beam of 18 MeV with currents of 0.25 mA and a normalized emittance of $1 \mu\text{m}$ [14]. However the resulting brilliance is at least two orders of magnitude below the FAIR requirements. Proton beam intensities of $\geq 35 \text{ mA}$ and an energy of 70 MeV are required. [1, 64]. Accordingly a dedicated proton injector linac will be operating independently from the existing UNILAC for heavy ions. It provides the primary proton beam for the production of antiprotons. The linac starts with a proton source followed by a LEBT, where beam diagnostic and focusing magnets are placed. The 325 MHz RFQ is forming and accelerating the beam so that it can be accepted by a drift tube linac (DTL). After this the protons are transferred to the SIS 18 where further acceleration takes place. A schematic drawing is given in Fig. 1.2.

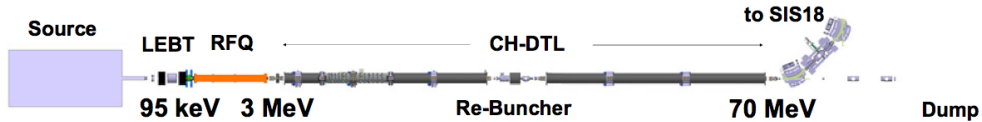


Figure 1.2: Layout of the FAIR Proton Linac [3].

As proton source an electron cyclotron resonance (ECR) type source will be used. An ECR source in principle is a microwave heated plasma chamber. In addition with magnetic fields and the correct gas pressure the electron

cyclotron resonance condition is heating the plasma. The plasma is trapped by to axial (solenoid) and radial (multipole) magnetic fields. The extraction system either with a triode or pentode configuration delivers 95 keV protons with a beam current of 100 mA [34] to the RFQ.

The RFQ is focusing and bunching the beam using electromagnetic fields. This is necessary because magnetic fields are inefficient at low particle energies since the focusing force is depending on the particles velocity. In addition the $\beta\lambda$ length in the low energy region limits the length of magnetic quadrupoles. For example $\beta\lambda$ is about 37 mm for protons at 750 keV and 325 MHz. This is a classical input power for Alvarez drift-tube linacs. A shorter length would lead to a fringe field dominated magnetic quadrupole inside the Alvarez drift tube, unable to achieve a field gradient sufficient to control high space charge forces [59]. The electric quadrupole fields of an RFQ make it very efficient in capturing the beam from the source and accelerating it to an energy of 3 MeV at the end of the RFQ were the DTL starts.

Behind the RFQ the beam is boosted by a DTL from 3 MeV up to 70 MeV. The DTL is divided into two parts. The first part consists of three coupled CH resonators. After a diagnostic section it is followed by three single CH cavities before the beam enters the channel towards the SIS18. This solution allows to achieve the requirements regarding beam intensity and quality of the FAIR project with a reduced number of focusing elements compared to traditional DTLs [9]. A CH cavity is a Cross bar H-mode structure operated in H_{211} -mode [42]. The crossed stem design is increasing the frequency in comparison to an IH cavity (interdigital H-mode), due to a reduced cavity circumference and accordingly a different operating mode, it is advantageous for the proton linac frequency region. Each cavity will be powered by a 3 MW klystron.

2 Theory

2.1 Radio Frequency Quadrupole

The idea of the radio frequency quadrupole was proposed 1970 by Kapchinskiy and Teplyakov at the Moscow Experimental and Theoretical Physics Institute ITEP [22]. A first experimental test at USSR Institute for High Energy Physics in Protvino took place in 1974. A 148,5 MHz RFQ accelerated a proton beam from 100 keV to 620 keV with an efficiency of 50 %.

The idea was picked up by Los Alamos National Laboratory (LANL), they tested the RFQ principle for the application of high-current low-emittance beams and started the development of computer codes for the RFQ design, leading to the program PARMTEQ which is widely used today. 1980 a proof of principle experiment at LANL demonstrated the acceleration of a proton beam from 100 keV to 640 keV with a efficiency of 90 % as predicted by the codes [31] initiated by the American SDI project.

Based on this development many RFQ accelerators are operating across the world. A special type of resonant structure of the RFQ was developed at IAP, University of Frankfurt [48]. The RFQ accelerators have the ability to replace electrostatic accelerators like Van-de-Graaff or Cockroft-Walton. They reduce the size of the accelerators dramatically and increase the beam current (see Fig. 2.1. The RFQ is able to focus, bunch and accelerate a DC beam from the ion source to an energy up to ~ 5 MeV/u [32] with high efficiency and preserving emittance. All these functions are realized by the RFQ fields only [31].

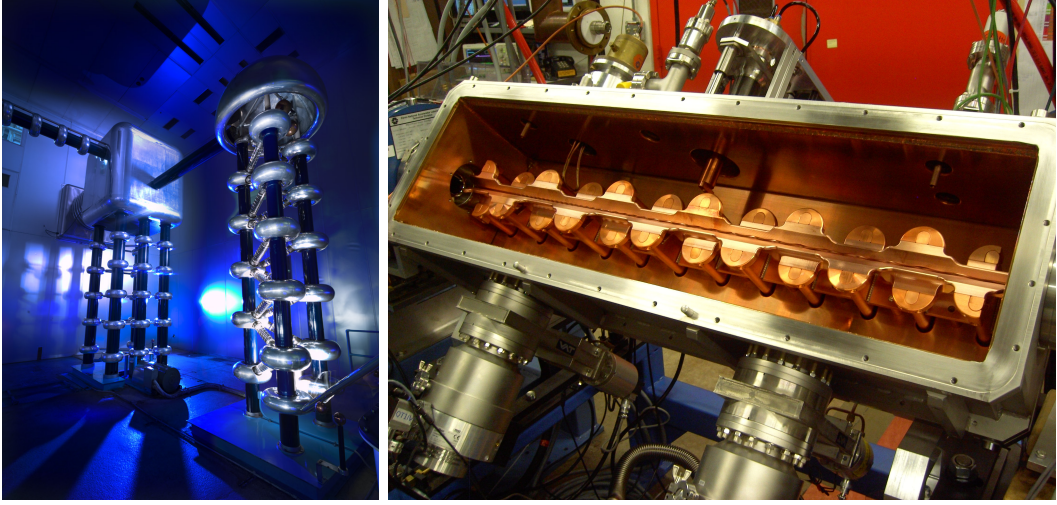


Figure 2.1: Fermilab's old Cockcroft-Walton accelerator has been replaced by the 1.2 m long RFQ.

2.1.1 Principle of an RFQ

To accelerate charged particles one needs an electric potential causing an electric accelerating field. The space charge of the particles is repulsive so one needs in addition focussing fields to compensate this behavior. Especially at low energies the defocussing behavior is very strong due to the large density of particles.

By using a static accelerator, like a Van-de-Graaff accelerator, the maximum beam energy is limited to the maximum voltage the accelerator can provide. In RF accelerators using the Wideroe or Alvarez principle, illustrated in Fig. 2.2, for acceleration, the accelerating voltage can be passed by the particles several times. Hence it is possible to achieve much higher beam energies than in a static process. The RF and respectively the accelerating fields have to be synchronized with the movement of the particles to gain an accelerating field otherwise there would be no benefit of these kind of acceleration. In particular the phase of the particle bunches needs to be synchronized with the electric field for a proper acceleration. In the above mentioned Alvarez accelerator, drift tubes are used to shield the particles from the decelerating field. One drift tube has a positive and a negative potential so that a particle bunch can be accelerated in every gap of the structure. The distance of the accelerated particle bunches is $\beta\lambda$, where $\beta = v/c$ is the ratio of the particles velocity v to the speed of light c and λ is the RF wavelength. In Wideroe structures the

drift tubes are loaded with only a single potential, so particle bunches can be accelerated in only every second gap, but the bunch distance is also $\beta\lambda$. Due to the increasing particle velocity and a fixed resonator frequency the length of the gaps and drift tubes grows to be matched to this speed.

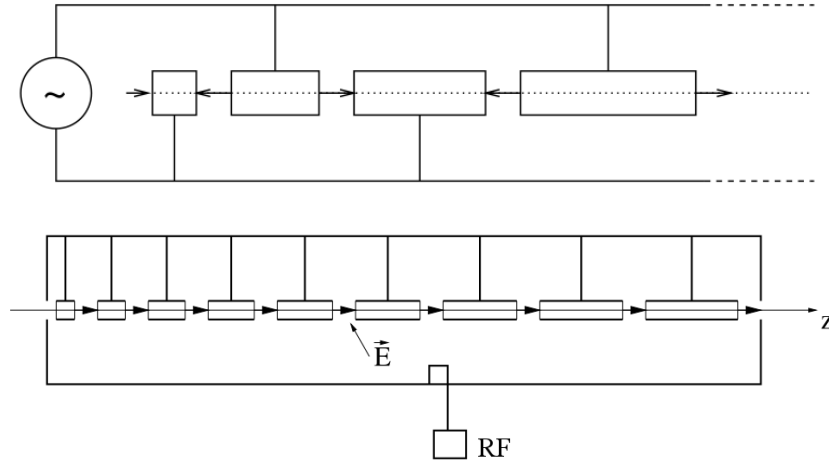


Figure 2.2: The principle of Wideröe (above) and Alvarez (below) accelerating structures [17].

In addition magnets need to be inserted into drift tube structures for focusing of the particle bunches. Like mentioned before the Lorentz force is velocity dependent and magnets are less effective at low beam energies. Electric fields are preferred for focusing in this low energy region. The bunching, accelerating and focussing with only electric fields is realized with the special geometry of RFQ structures. Longitudinal fields are able to accelerate and bunch, transverse electric fields focus the particle bunches.

Focusing

The focusing of an ion beam can be done with either magnetic or electric quadrupole fields. If one uses a chain of static quadrupoles that are alternating in their direction by 90° the focusing and defocusing forces in one plane to the next are alternating as well. This is called the alternating gradient focusing principle.

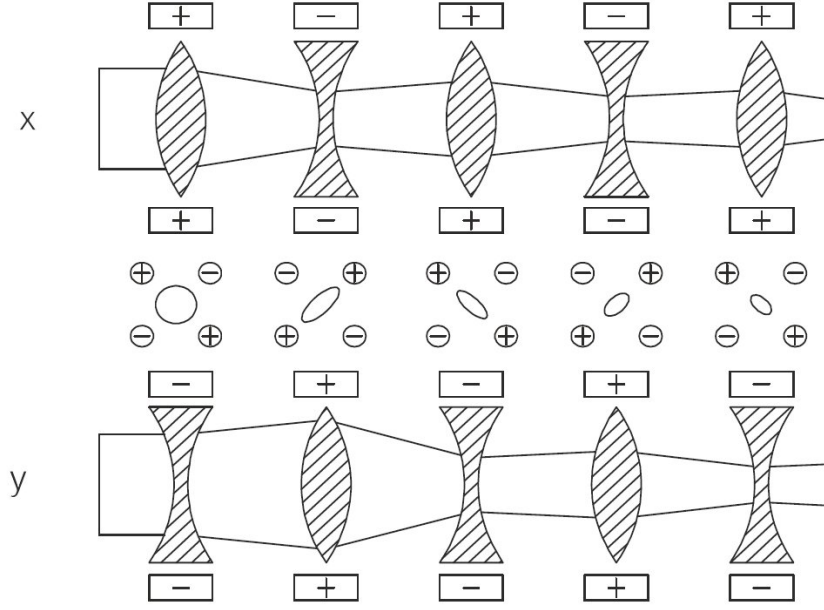


Figure 2.3: Scheme of alternating gradient focusing.

Fig. 2.3 shows a schematic focusing of a beam with a chain of quadrupoles. The quadrupole field is in the x-y plane, representing one pair as x-electrodes and the other as y-electrodes. One can achieve an overall focusing effect by a linear rising force in radial direction passing through several polarities. The alternating direction of the static quadrupoles is realized in an RFQ by alternating the electrodes voltage as represented in Fig. 2.4. This kind of quadrupole is able to only transport and focus charged particles, but not to accelerate them. In an RFQ the alternating gradient focusing is continuous without longitudinal end effects like in static quadrupoles. At low beam energies the static quadrupoles need to be short to fit into a drift tube leading to a fringe field dominated lens. Therefore the continuous focusing of an RFQ is preferred.

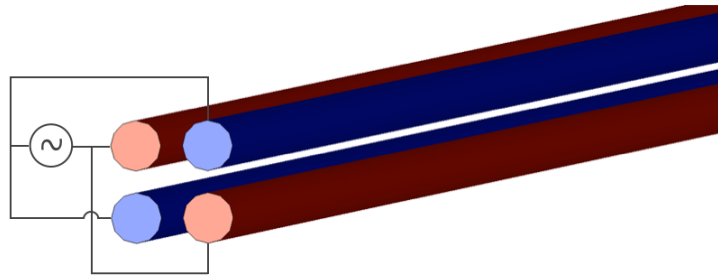


Figure 2.4: Quadrupole with time varying polarity.

Acceleration

The alternating field on the electrodes leads to a transverse focusing of the particles with constant velocity. In order to accelerate and bunch of particles, electric fields in longitudinal direction need to be provided. Therefore a sinusoidal shape, the modulation, is applied on the electrodes causing this longitudinal field component. This shape can be described by the aperture a and the modulation factor m shown in Fig. 2.5. The aperture is the minimal distance of the electrode, the maximum distance is $a \cdot m$ to the beam axis. One acceleration cell is defined by neighboring maximum and minimum in the electrodes modulation profile (see Fig. 2.5) with a length of c_L .

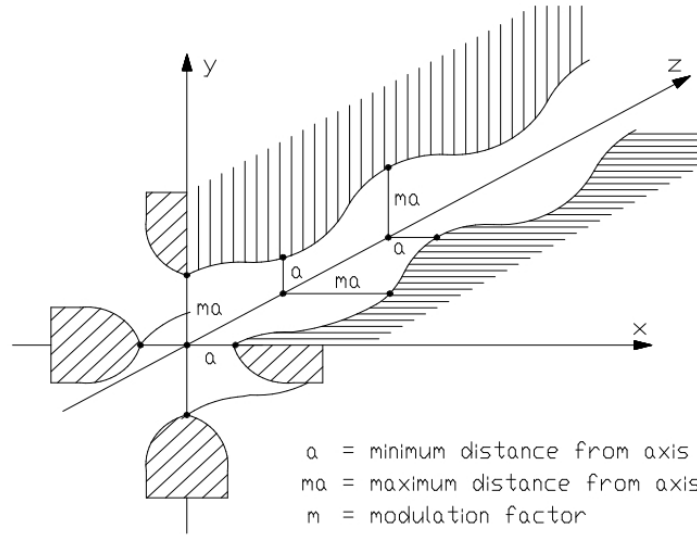


Figure 2.5: Demonstration of the modulation and aperture of the electrodes [58].

After the distance of c_L the vertical and horizontal electrodes have changed a and $a \cdot m$. If this distance is synchronized to the RF field and the particles velocity the particles are accelerated in every second cell. The requirement is $c_L = \frac{\beta\lambda}{2}$. This corresponds to the Wideröe principle. The half of a modulations wavelength equals the length of a drift tube in a Wideröe accelerator. Aperture and modulation are changing along the electrodes. A stronger modulation causes greater acceleration in longitudinal direction, but weaker focusing. This is discussed in more detail in 2.1.3. Typical values for modulation are between 1 and 2.5.

Phase Focusing

The electric field in longitudinal direction is depending on time since the electrodes are part of the RF structure of the RFQ. If a particle enters the RFQ at the beam axis it has a special phase relating to the RF of the structure. The best particle transport is provided if the particle is at synchronous phase ϕ_s shown in Fig. 2.6.

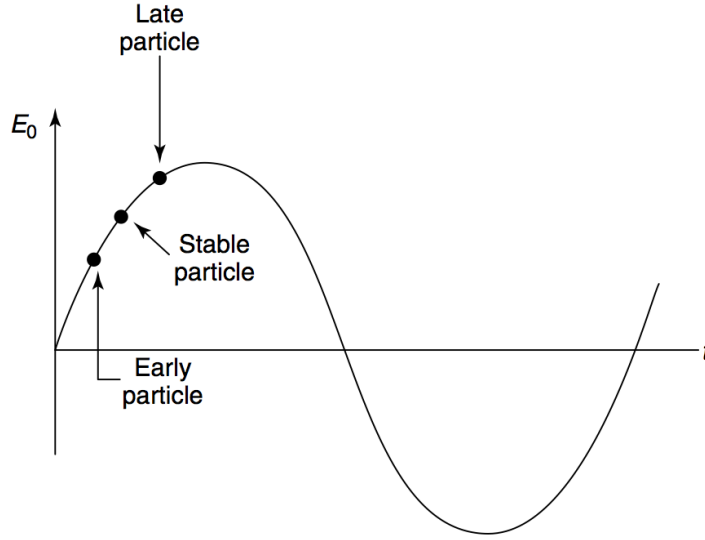


Figure 2.6: Phase of a particle bunch in dependence of the time changing electric field [60].

A faster particle than ϕ_s enters an acceleration cell earlier when the voltage is still rising. It gets less accelerated than a particle at synchronous phase. A later and slower particle sees a stronger field than in synchronous phase and gets more accelerated. The stable oscillations around the synchronous phase correspond to the accepted energy spread that is defined by the separatrix (Fig. 2.7). Particles within the separatrix oscillate around the synchronous phase becoming stable bunches. The largest separatrix can be found at 90° before the maximum. Almost all particles are accepted and bunched at this point but not gain acceleration. If the synchronous phase is 0° the acceleration gets to its maximum, the phase width of the separatrix, in this case, becomes minimal. In the opposite case, if the phase is 90° all particles are captured but without acceleration. A typical acceleration synchronous phase is at $\Phi_s = 30^\circ$ and the separatrix equals three times Φ_s . In comparison without an RFQ and a buncher cavity only $1/4$ of the beam can be captured for a stable acceleration

To ensure this behavior for each bunch the phase has to change every single acceleration cell by 180° . This is the Wideröe condition $L = \beta\lambda/2$; with $\beta = v/c$ and the wavelength of the RF λ . Accordingly for a continuous acceleration particle bunches can be found in every second cell of the RFQ.

The frequency is determining the cell length of the accelerating structure. In order to have efficient structures at high beam energies a high frequency is needed as well as a high charge per bunch ratio leads to the desire to start with an RFQ at 325 MHz.

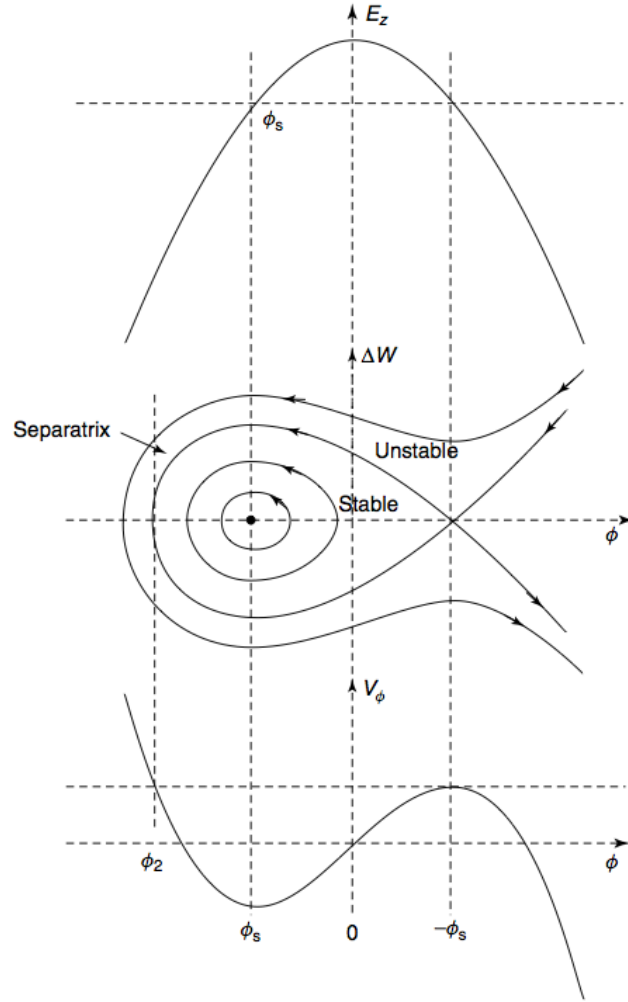


Figure 2.7: The accelerating field as a cosine function of the phase, the longitudinal phase space trajectories including the separatrix (separating stable and unstable range of the particles) and the longitudinal potential [60].

2.1.2 Resonator Concepts

There are several resonator types to load the electrodes to the desired quadrupole potential. The needed parameters lead to a special resonator type. One significant difference between the concepts is the resonant frequency. The frequency range of RFQs in general is between some 10s MHz up to several 100s MHz which makes one chose a special resonator concept. Some other differences are explained in the following.

The 4-vane cavity is mostly used in the high frequency range above 200 MHz, for example at CERN, BNL or SNS. It is the most common structure for light ions, especially protons. The cavity consists of four vanes symmetrically placed within a cavity and is operated in TE_{210} -mode (Fig. 2.8). The magnetic field is localized longitudinal in the four quadrants of the cavity. Its transverse electric field is localized near the vane tips [60].

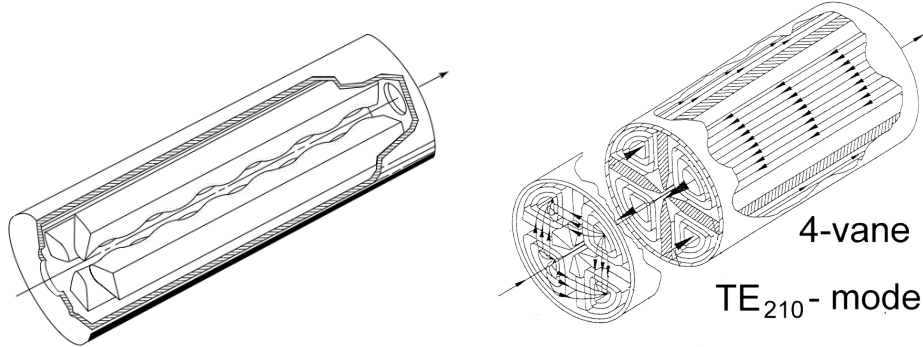


Figure 2.8: 4-Vane RFQ [60] and its magnetic field lines in TE_{210} -mode.

The resonant frequency scales with the geometric size of the cavity. Below a frequency of 100 MHz the dimensions of a four vane type RFQ becomes unpractically big and the 4-rod or IH type RFQ result in smaller structures [32]. For example at 200 MHz a 4-vane structure has approximately a diameter of 40 cm. More details on the resonant structure and its modes are given in chapter 4.1. A 4-rod RFQ is made of a chain of $\frac{\lambda}{4}$ resonators operated in π -0-mode. The $\frac{\lambda}{4}$ resonators are capacitively shortened by the electrodes shown in Fig. 2.9. The connection of the electrodes is made by the stems and the tuning blocks representing the inductivity [48]. Since the 4-rod RFQ is a transmission line resonator its tank has only minor influence on the RF behavior. 4-Rod structures are built for frequencies up to 216 MHz [26]. This thesis will prove the performance of a 4-rod RFQ at 325 MHz.

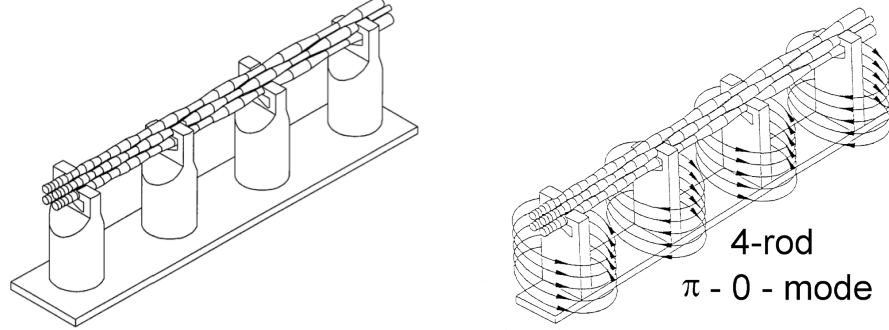


Figure 2.9: 4-rod RFQ structure [32] and the magnetic fields of the transmission line resonator.

The advantages of the 4-rod type RFQ are the great tuning and adjustment possibilities and the easy access to all parts of the RFQ for maintenance and executing the tuning. This advantages leading to lower costs as well. 4-rod RFQs have been realized many times and accordingly there exists a lot experience in building these structures. An overview about 4-rod RFQ projects, mostly for light and heavy ions, of the last years is given in [51].

The IH RFQ is a cavity resonator which is operated in T_{111} mode. The electrodes are fixed on unsymmetric rings which are mounted on the supports. This kind of RFQ has feasible dimensions for lower and medium RFQ frequency ranges.

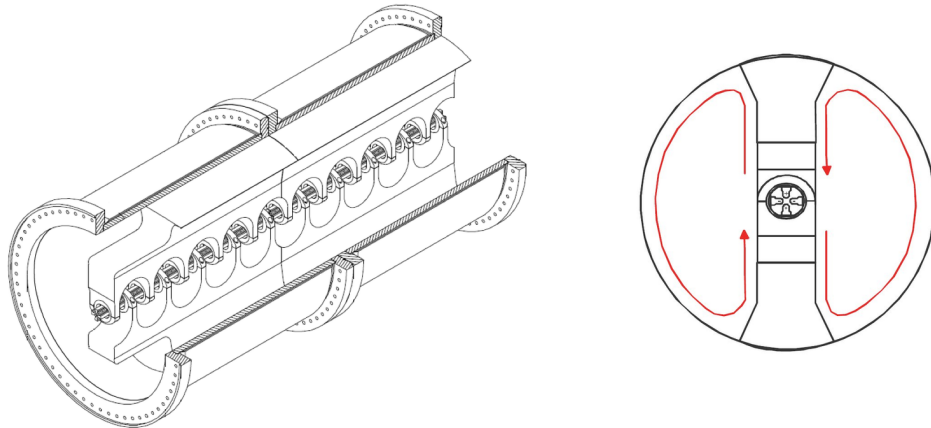


Figure 2.10: Drawing of the 36 MHz IH RFQ at GSI [44] and its current paths.

The Ladder RFQ is similar to a 4-rod RFQ, but with its stems also connected to the cavity lid using doubled $\frac{\lambda}{4}$ plates shown in Fig. 2.11. Due to symmetric charge transportation it has no dipole field. The electrodes are connected to rings as well as the IH-RFQ. Its geometric size and frequency is similar to 4-rod RFQs but not that easy for access for tuning and maintenance. Ladder RFQs have been realized at the CERN antiproton decelerator ASACUSA [30], at Lincac 3 [4] or at the Frankfurt funneling experiment as a two beam RFQ [12, 33].

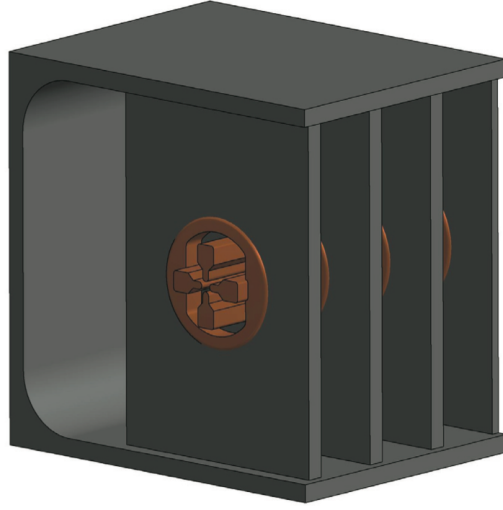


Figure 2.11: 3D drawing of a Ladder RFQ [6].

There are many more RFQ resonator types like for example the Split-Coaxial-RFQ or the Spiral-RFQ. Some examples are given in figure 2.12. The choice of resonator depends on various parameters, like operation frequency, access and input power.

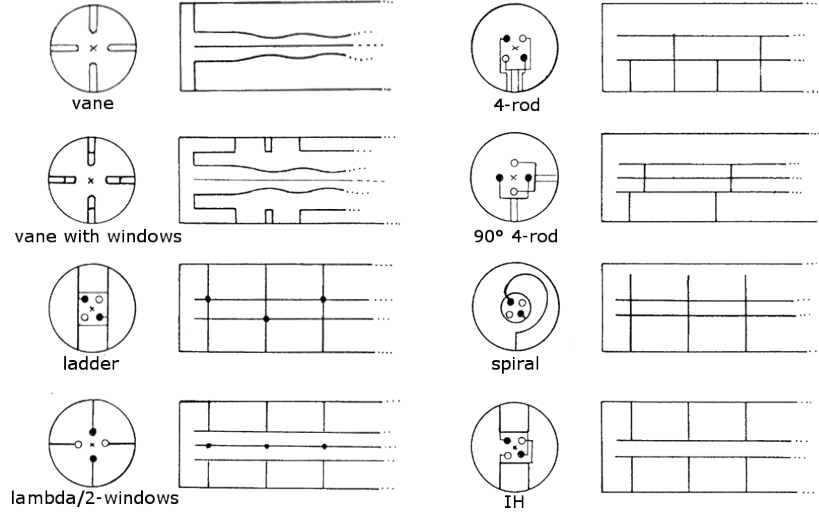


Figure 2.12: Examples of different RFQ resonator types. The special characteristic of each resonator is an optimization for a specific application [49].

2.1.3 RF-Fields in an RFQ

General Potential of an RFQ

To analyze the RF quadrupole structure the quasistatic approximation can be used, which is valid if the main source of the electric field on the electrodes is the electric charge and its dimensions are small compared to the wavelength. In addition the electric fields are negligible small due to the time changing magnetic field. This is valid if the dimension of the geometry of the structure, which is creating the fields, the aperture, is small in comparison to the RF wavelength. Furthermore we assume a constant geometric wavelength of the electrodes modulation. However, because the particles energy should change along the structure, the above mentioned case is only valid if the energy gain per RF period and hence the change of the cell length from one cell to the next is small. Using the quasistatic approximation one can separate the time dependence of the potential and one gets in cylindrical coordinates

$$U(r, \theta, z, t) = V(r, \theta, z) \sin(\omega t + \phi) \quad (2.1)$$

where $\omega/2\pi$ is the RF frequency, ϕ represents the initial phase of the potential and $V(r, \theta, z)$ is a solution of Laplace's equation $\nabla V(r, \theta, z) = 0$, given in cylindrical coordinates

$$\frac{\partial^2 V}{\partial r^2} + \frac{1}{r} \frac{\partial V}{\partial r} + \frac{1}{r^2} \frac{\partial^2 V}{\partial \theta^2} + \frac{\partial^2 V}{\partial z^2} = 0 \quad (2.2)$$

the series expansion of the potential in cylindrical coordinates is in general

$$V(r, \theta, z) = \sum_{s=0}^{\infty} A_{0,s} \left(\frac{r}{a}\right)^{2s} \cos(2s\theta) + \sum_{n=1}^{\infty} \sum_{s=0}^{\infty} A_{n,s} I_{2s}(nkr) \cos(2s\theta) \cos(nkz) \quad (2.3)$$

Two Term Potential

The general solution for the potential 2.3 has not really practical use. One way obtain a self constant solution is to use the the first two coefficients from the general solution for the potential. This approach was used from Kapchinsky and Tepliakov to construct the electrode shapes that conform to the resulting equipotential surfaces and is called the two-term potential function.

$$V(r, \theta, z) = A_0 r^2 \cos(2\theta) + A_{10} I_0(kr) \cos(kz) \quad (2.4)$$

The values of the coefficients A_0 and A_{10} are determined from the boundary conditions appropriate to the electrode geometry. A_0 term refers to a pure quadrupole term being responsible for the transverse field and therefore the transverse AG focusing of the RFQ. The A_{10} term is a monopole term which is responsible for the longitudinal field. The potential can be rewritten in the following sense. At a certain time of the RF period the potential of the horizontal and vertical electrodes are $+\frac{V_0}{2}$ and $\frac{V_0}{2}$. At the longitudinal position $z = 0$ the horizontal vane tip has a distance $r = a$ from the beam axis and the angle $\theta = 0$ [32].

$$\frac{V_0}{2} = A_0 a^2 + A_{10} I_0(ka) \quad (2.5)$$

the vertical vane tip $\theta = \pi/2$ and displacement $r = m \cdot a$

$$-\frac{V_0}{2} = -A_0 (ma)^2 + A_{10} I_0(kma) \quad (2.6)$$

solving equations 2.5 and 2.6 for the constants A_0 and A_{10} leads to

$$A_0 = \frac{V_0}{2a^2} \frac{I_0(ka) + I_0(kma)}{m^2 I_0(ka) + I_0(kma)} \quad (2.7)$$

$$A_{10} = \frac{V_0}{2} \frac{m^2 - 1}{m^2 I_0(ka) + I_0(kma)} \quad (2.8)$$

now the dimensionless constants χ and A can be defined

$$\chi = \frac{I_0(ka) + I_0(kma)}{m^2 I_0(ka) + I_0(kma)} \quad (2.9)$$

$$A = \frac{m^2 - 1}{m^2 I_0(ka) + I_0(kma)} \quad (2.10)$$

the constants correspond to $A_0 = \chi V_0/2a^2$ and $A_{10} = AV_0/2$. Now the complete time dependent potential is

$$U(r, \theta, z, t) = \frac{V_0}{2} \left[\chi \frac{r^2}{a^2} \cos 2\theta + AI_0(kr) \cos(kz) \right] \sin(\omega t + \phi) \quad (2.11)$$

The time dependent voltages on the horizontal and vertical electrodes are $+V_0 \sin(\omega t + \theta)/2$ and $-V_0 \sin(\omega t + \theta)/2$. A more convenient expression for equation 2.11 is in Cartesian coordinates with $x = r \cos(\theta)$ and $y = r \sin(\theta)$ follows

$$U(x, y, z, t) = \frac{V_0}{2} \left[\frac{\theta}{a^2} [x^2 - y^2] + AI_0(kr) \cos(kz) \right] \sin(\omega t + \theta) \quad (2.12)$$

This is the scalar potential. What one needs for calculating beam dynamics are the components of the electric field. One will receive them by taking the partial derivative $E = -\nabla U$ of the potential. These components in cylindric coordinates are

$$E_r(r, \theta, z) = -\frac{\partial U}{\partial r} = -\frac{\chi V_0 r}{a^2} \cos 2\theta - \frac{V_0 A k}{2} I_1(kr) \cos(kz) \quad (2.13)$$

$$E_\theta(r, \theta, z) = -\frac{1}{r} \frac{\partial U}{\partial \theta} = \frac{\chi V_0 r}{a^2} \sin 2\theta \quad (2.14)$$

$$E_z(r, \theta, z) = -\frac{\partial U}{\partial z} = \frac{A V_0 k}{2} I_0(kr) \sin(kz) \quad (2.15)$$

The two term potential is the most simple choice to deal with the problem. In the 1980s when first simulation tools were implemented this two term approach was used. Modern codes use higher order terms up to the order of eight [60]. Besides this, methods like numerical calculation on a grid as described in [32] can be used as well.

Electrode Design

To develop the electrode design of an RFQ several parameters, like the particle energy of the input and output beam, the charge over mass ratio q/A of the particles, the emittance and the beam current, are important. These parameters differ from every single RFQ to another, because every RFQ has its own purpose and has to meet its own requirements. A basic concept to design the electrodes has been developed in the 1980s in Los Alamos. This concept considers all the above mentioned parameters. These parameters together with the resonant frequency enable one to calculate the cell length and the focusing strength. Hence the aperture and modulation can be fixed which defines the acceleration profile. The modulated RFQ is subdivided into four sections performing different tasks. As an example in Fig. 2.13 shows a principle quadrupole electrode modulation. It was a design for a 425 MHz 4-vane RFQ developed in the 1980s at LANL by Crandall, Stokes and Wangler [21]. Another design is presented in [50], that was developed to optimize the design for shorter RFQ structures.

At the beginning the DC beam from the source needs to be captured in the first section of the RFQ. This is the *radial matcher*, which function is to capture the beam with minimum losses. Therefore the phase of the synchronous particle is set to $\Phi = -90^\circ$, where the separatrix captures the maximum ratio of particles [60]. Before bunching the beam it is prepared in the *shaper* section. There the particles are focused transversely and the phase is shifted to

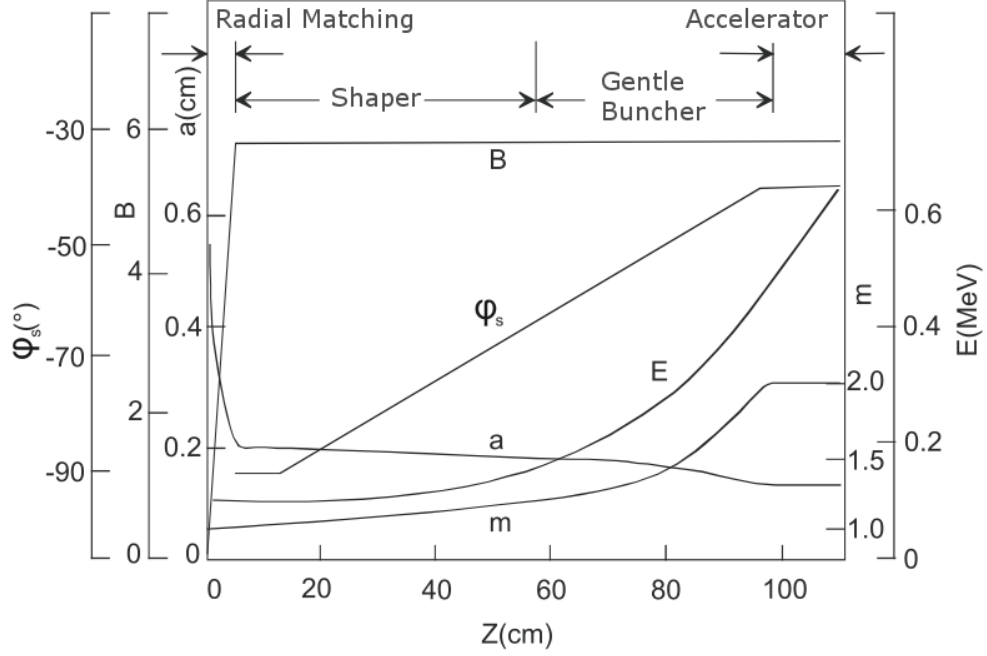


Figure 2.13: "Standard" Los Alamos design for the quadrupole electrode design [21].

about $\Phi = -70^\circ$, that is closer to an acceleration value. The adiabatic bunching described in chapter 2.1.1 takes place in the *buncher* section. The basic concept of adiabatic bunching is to keep the bunches of a geometric constant length by changing the parameters of the acceleration cells from cell to cell. This prevents the bunches from blowing up by its space charge in transverse direction. The synchronous phase is shifted to $\Phi = -60^\circ$ to -30° for example and first acceleration takes place. The last section is the *acceleration* section, where the synchronous phase is constant. The modulation and the aperture is nearly constant and the acceleration is continued until the required energy is reached.

2.1.4 Characteristic RF Parameters

Quality Factor

Resonators currents are excited by the RF on the surface of the structure. During oscillation the energy is dissipated. The quality factor describes the amount of energy which is dissipated during one RF period and is defined by

$$Q_0 = \omega_0 \frac{W}{\overline{N}} \quad (2.16)$$

where ω is the angular frequency, W the energy stored in the resonator and strongly depending on its geometry, \overline{N} is the dissipated power or the dissipated energy times the period. High values of the quality factor correspond to low losses and less needed power to excite a resonator. The quality factor is influenced by material properties and the geometry of the resonant structure. Typical values for the quality factor of normal conducting resonators are between 10^3 and 10^5 and for superconducting resonators between 10^8 and 10^{10} in the frequency range between 20 and 400 MHz [40].

Q_0 is the unloaded quality factor and describes an ideal case without any external excitation by the amplifier and the power coupler that is taken into account by the external quality factor Q_{ext} . Q_0 is measured with only weak coupling β . Q_{ext} are related by $Q_0 = Q_{ext}(1 + \beta)$.

Determination of Q using 3 dB Method One can consider an equivalent circuit of a resonant structure as oscillating circuit with parallel ohmic resistance R , a capacitance C and an inductivity L . This is a good approach close to the resonant frequency. In this circuit the energy is given by $W = \frac{1}{2}LI_L^2$ and the dissipated Energy is $\overline{N} = \frac{1}{2}RI_R^2$ with I as the respective current to the element. If one uses this together with formula 2.16

$$Q_0 = \omega_0 \frac{\frac{1}{2}LI_L^2}{\frac{1}{2}RI_R^2} = \omega_0 \frac{\frac{1}{2}L\frac{U^2}{\omega_0^2 L^2}}{\frac{1}{2}R\frac{U^2}{R^2}} = \frac{R}{\omega_0 L} = \omega_0 C R \quad (2.17)$$

In LRC oscillating circuit the conductance Y , which is defined as the inverse impedance Z , is the sum of the reciprocal of every single impedances. One can write it as follows

$$\frac{1}{Z} = \frac{1}{Z_r} + \frac{1}{Z_C} + \frac{1}{Z_L} = Y \quad (2.18)$$

$$= \frac{1}{R} + j \left(\omega C - \frac{1}{\omega L} \right) \quad (2.19)$$

In case of a resonance the resistance becomes real and current and voltage are in phase. This means $\omega C = \frac{1}{\omega L}$, which leads to the Thomson formula

$$\omega_0 = \frac{1}{\sqrt{LC}} \quad (2.20)$$

The resonance curve represents the field in the resonator around the resonance frequency. To determine the width of the resonance curve one shifts the frequency with $\delta\omega$ around ω . This means ω becomes $\omega_0 + \delta\omega$ formula 2.19 and it follows:

$$Y = \frac{1}{R} + j \left(\omega_0 C + \delta\omega C - \frac{1}{\omega_0 L} + \frac{\delta\omega}{\omega_0^2 L} \right) \quad (2.21)$$

By replacing L and C using formula 2.17 $\frac{1}{Z}$ becomes a function of Q_0

$$Y = \frac{1}{R} \left(1 + 2jQ_0 \frac{\delta\omega}{\omega_0} \right) \quad (2.22)$$

In case of resonance $\frac{1}{Z}$ is becoming real part

$$\Re(Y) = \frac{1}{\Re(Z)} = \frac{1}{R} \sqrt{1 + 4Q_0^2 \left(\frac{\delta\omega}{\omega_0} \right)^2} \quad (2.23)$$

In the case of resonance in an oscillating circuit the voltage is at its maximum. The voltage drops with a factor $\frac{1}{\sqrt{2}}$ if the frequency is shifted about $\frac{\delta\omega}{\omega_0} = \pm \frac{1}{2Q_0}$ from ω_0 . This means the power drops about the half of it. To measure the quality factor one has to plot the resonance curve (see figure 2.14). Then one can measure at which frequency shift $\delta\omega$ the resonance drops about $\frac{1}{\sqrt{2}}$, or about 3 dB respectively, what equals to 1/2 of the stored energy.

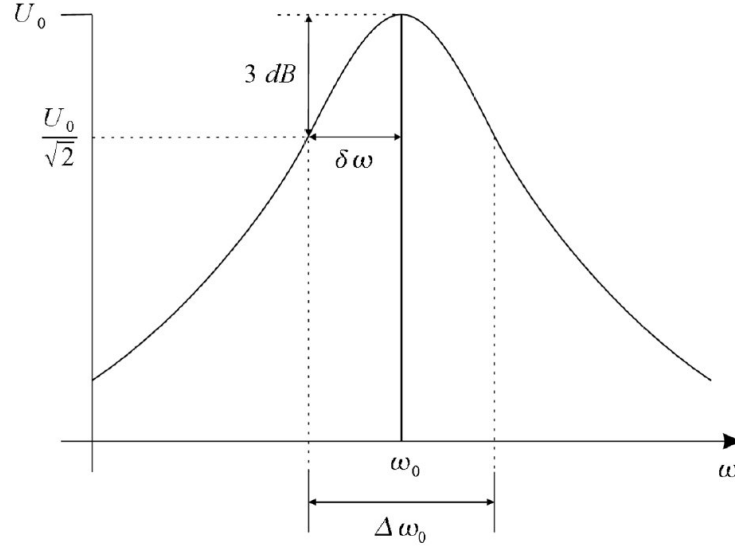


Figure 2.14: Resonance curve - the width of the resonance curve correlates with the quality factor.

Shunt Impedance

Another important RF parameter is the shunt impedance or R_p -value. It correlates the maximum voltage U_{max} at the electrodes to the average dissipated power \bar{N} .

$$R_{p0} = \frac{U_{max}^2}{\bar{N}} \quad (2.24)$$

The shunt impedance is a direct measure of the efficiency of the structure to convert RF power into an electric field between the electrodes. In stationary case the average dissipated power is equal to the power delivered from the amplifier but without beam loading. It is equal to

$$R_p = \frac{2Q}{\omega_0 C} \quad (2.25)$$

where C is the total electrode capacitance. Since the electrode capacitance increases with longer electrodes, the R_p -value is depending on the length. If one multiplies the shunt impedance with the total resonator length the R_{pL} -value enables one to compare RFQs with different length.

$$R_{pL} = R_p \cdot L \quad [\Omega m] \quad (2.26)$$

Perturbation Capacitor Since the fields inside the electrodes area of a 4-rod RFQ are not homogenous instead the common bead pull measurements the perturbation capacitor method is used. To measure the shunt impedance of an RFQ resonator one can add a known perturbation capacitor between the electrodes [48]. This ΔC reduces the resonance frequency of the oscillating circuit to

$$\omega_0^* = \omega_0 - \Delta\omega = \frac{1}{\sqrt{L(C + \Delta C)}}. \quad (2.27)$$

Using the Slater Theorem [55] the frequency shift and the stored energy can be written as

$$\frac{\Delta\omega_0}{\omega_0} = \frac{\Delta W}{W} = 1 - \frac{1}{\sqrt{1 + \frac{\Delta C}{C}}} \approx \frac{\Delta C}{2C} \quad (2.28)$$

With formula 2.25 and the definition of the quality factor 2.16 for the shunt impedance follows

$$R_p = \frac{2\Delta f Q}{\pi \delta C f_0^2}. \quad (2.29)$$

with the undisturbed resonance frequency f_0 and the measured quality factor Q_0 one can calculate the R_p -value of the RFQ.

R/Q -Comparison with Simualtions The measurement presented above is defective due to the small capacitance, which value is hard to validate with high precision. In addition high frequency resonators are more sensitive to perturbations. These perturbations are meant to be small in comparison to the electrodes capacitance. Another way to obtain a quite reliable shunt impedance is the comparison of the R/Q -ratio of measurements and Microwave Studio® simulations. The R/Q -value gives one the ability to characterize and compare the efficiency of resonators independent from parameters like the frequency and

the surface current. This value is only depending on the resonators geometry [42].

$$\frac{R_{MWS}}{Q_{MWS}} = \frac{R_{meas}}{Q_{meas}} \quad (2.30)$$

By experience the quality factor of the simulation is more optimistic than the measurement. This is also true for the shunt impedance. Reliable results can be obtained by the comparison of both ratios. Using the R/Q -value from simulations together with the precise measurement of the quality factor of the cavity one can determine the shunt impedance of the structure.

Electrode Capacitance Another method used to calculate the shunt impedance is to calculate the electrodes capacity, which is quite easy for the 325 MHz prototype, since it has no modulation on the electrodes. The calculation can be derived in [8] using [28] and gives the formula for the electrodes capacitance

$$\frac{C_{RFQ}}{L} = 2 \cdot \pi \cdot \epsilon \cdot \ln^{-1} \frac{\text{aperture} + \text{electrode diameter}}{\text{electrode diameter}} \quad (2.31)$$

with the electrode length L . Using the definition of the quality factor 2.16 and the formula for the energy stored in a capacitor one gets

$$\bar{N} = \frac{\omega_0 W}{Q_0} = \frac{\frac{1}{2} C U^2 \omega_0}{Q_0} \quad (2.32)$$

and inserting into 2.24 leads to

$$R_p = \frac{2Q_0}{C\omega_0} \quad (2.33)$$

that shows the shunt impedance is depending on the electrodes capacitance C , which is approximately proportional to the length of the electrodes.

Gamma Spectroscopy It is also possible to validate the shunt impedance under operation by using the gamma spectroscopy method. This gives one the maximum intervane voltage depending on the input power to calculate the shunt impedance by its definition 2.24. Depending on the electric field strength, electrons are unleashed by field emission and accelerated. When the time of flight, to hit the opposite electrode, of the electrons is small in comparison to the RF period the kinetic energy of the electrons is given by the maximum inter vane voltage.

$$E_{kin} = eU_{max} \quad (2.34)$$

On the adjacent electrode the electrons are captured and produce bremsstrahlung. The expected spectrum is a continuous γ -spectrum. For the measurement of the γ -spectrum one can use a semiconducting detector.

2.1.5 Modes

4-rod RFQ

A 4-rod RFQ can be described as a chain of $\lambda/4$ -resonators. An equivalent circuit of a resonator is a LC oscillator where the electrodes represent the capacitance, while the current path along the stems and the ground plate correspond to the inductance (see Fig. 2.15). Two neighboring stems with the electrodes build one RF cell of the resonator chain.

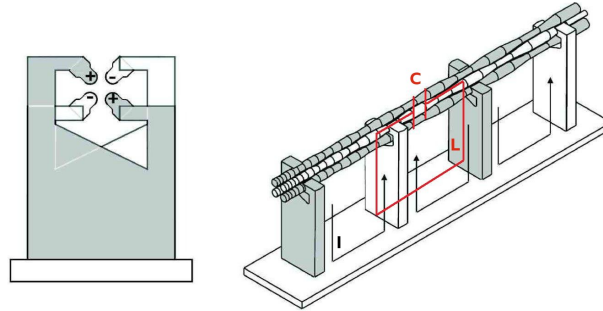


Figure 2.15: Equivalent circuit of an RFQ. One RF cell can be described as a LC oscillator where L is given by the current path and C by the electrodes capacitance.

If higher order modes are close to the operating modes frequency they might be excited as well and can disturb the operating mode. In order to avoid this

it is important to know the frequency spectrum of an RFQ. As an example the quadrupole mode of a 4-vane RFQ and its higher order modes (HOMs) are quite close, like below 1 MHz, to each other and need to be separated artificially by special elements. The higher order modes of a 4-rod RFQ are typically some tens MHz above the operating mode, but this changes with longer electrodes and the number of RF cells. That means one has to take it into account for higher frequencies of 4-rod RFQs. The higher order modes of a 325 MHz 4-rod RFQ are shown in Fig. 2.16.

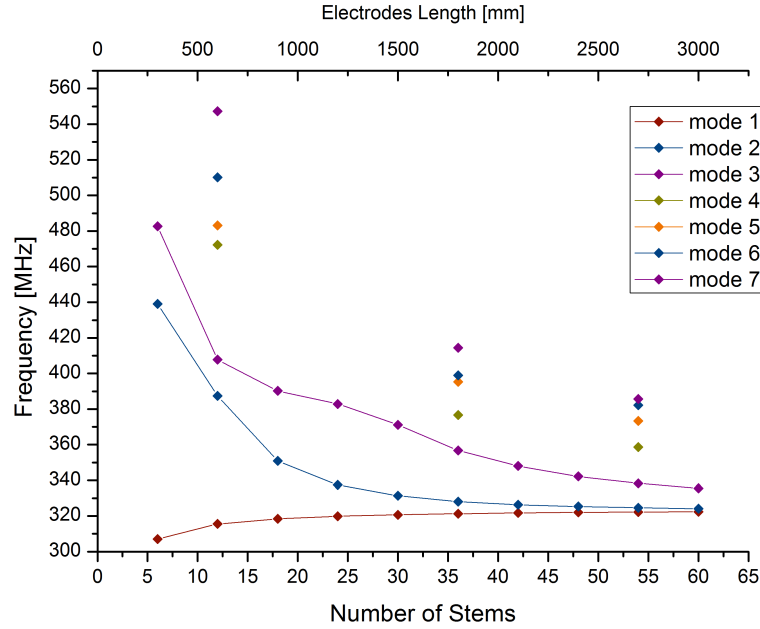


Figure 2.16: Simulation of the frequency of the higher order modes of a 325 MHz RFQ with increasing length and stem numbers.

At a structure length of about 3 m and around 60 RF cells the first higher order mode is only 1.8 MHz above the operating mode. This difference is not perturbing but one needs to keep an eye on it to prevent it from getting closer to the operation frequency. As an example, the Linac4 4-vane RFQ at CERN, with a length of 3 m and an operation frequency of 352 MHz, has a comparable value for the mode separation [38].

An indication of the modes of a 4-rod RFQ spectrum can be based on the phase shift between each RF cell

$$\phi = \frac{q\pi}{N} \quad (2.35)$$

where $q = 0, 1, \dots, N$ is the number of modes given by N the number of RF cells [58]. The operation mode of a 4-rod RFQ is the π -0-mode and its highest mode is the π -mode. In the π -0-mode the electrodes are on an equal potential in longitudinal direction, while at π -mode the potential of the electrodes changes at each RF cell. Fig. 2.17 shows this dispersion relation and the simulation of a modes spectrum of a 4-rod RFQ with 53 RF cells.

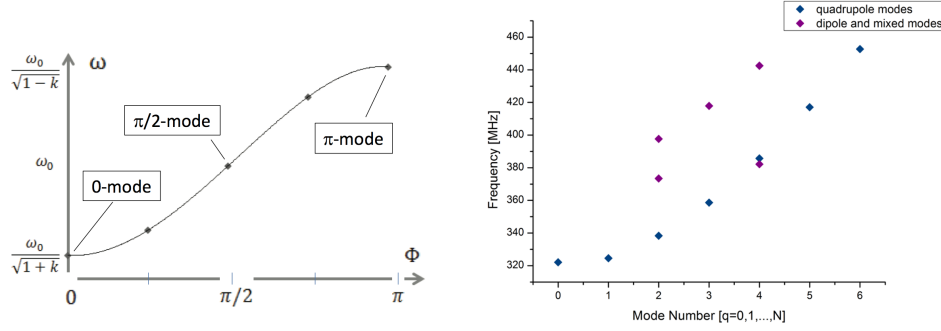


Figure 2.17: Dispersion relation [58] and simulation of the mode spectrum of a 4-rod RFQ with 53 RF cells.

In Fig. 2.18 the normal component of the electric field of the first two modes ($q = 0$ and $q = 1$) of a 12 stem model around 300 MHz is presented. The $q = 1$ mode separates the electrodes potential once. Strongly depending on the geometry and electrode length some other mixed modes occur as well.

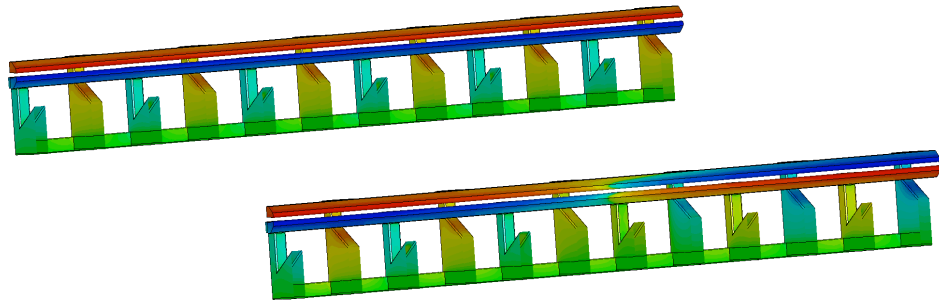


Figure 2.18: Normal component of the electric field of the ground mode and first higher order mode.

4-vane RFQ

A 4-vane RFQ type is a cavity resonator. The currents are flowing azimuthal over the cavity walls to the vane tips. The magnetic field in longitudinal direction is changing in neighboring quadrants. To achieve the best possible field distribution the quadrants need to be very symmetric. The magnetic flux from one quadrant splits in half. Each half flowing around the vane ends into the neighboring quadrants (see Fig. 2.19).

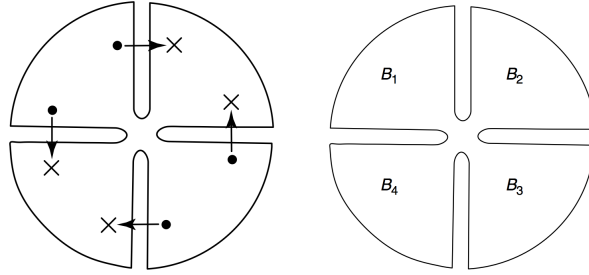


Figure 2.19: Magnetic fields at the end of a 4-vane RFQ splitting in half towards the neighboring quadrants (left). General azimuthal magnetic field pattern in a 4-vane RFQ [60] (right).

The sum of the magnetic flux over the 4 quadrants is zero at any cross section. This condition is true for three independent azimuthal modes, the quadrupole mode (TE_{21n}) and two dipole modes (TE_{11n}) shown in Fig. 2.20.

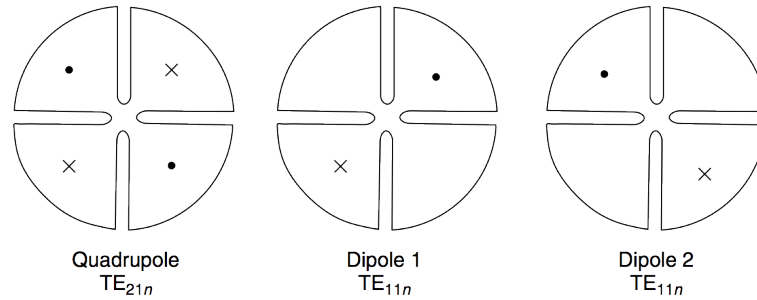


Figure 2.20: Azimuthal modes of a 4-vane RFQ - the quadrupole mode TE_{21n} and two dipole modes TE_{11n} . The n indicates the mode number in longitudinal direction [60].

If the cavity is not properly tuned the magnetic flux will be not equal in each quadrant causing an admixture of the operating mode of the quadrupole and dipole modes. From flux conservation it can be followed

$$B_1 + B_2 + B_3 + B_4 = 0 \quad (2.36)$$

The quadrupole amplitude is proportional to

$$A_Q = \frac{|B_1 - B_2 + B_3 - B_4|}{4} \quad (2.37)$$

and the amplitudes of the dipole modes are

$$A_{D1} = \frac{|B_1 - B_3|}{2} \quad \text{and} \quad A_{D2} = \frac{|B_2 - B_4|}{2} \quad (2.38)$$

A major objective of the cavity tuning, besides the voltage distribution of the vanes, which is assumed to be ideal in the particle dynamics, is to minimize the magnitudes of the dipole modes amplitude to produce the best approximation to a pure quadrupole operating mode. By regarding a 4-vane mode spectrum (see Fig. 2.21) one can see that the cutoff frequency of the dipole modes typically lies only a few percent lower than the quadrupole mode. This implies the possibility of accidental degeneracy between the quadrupole mode and a higher dipole mode. Consequently the structure is very sensitive to dimensional construction errors, that leads to tight tolerances in fabrication and assembly.

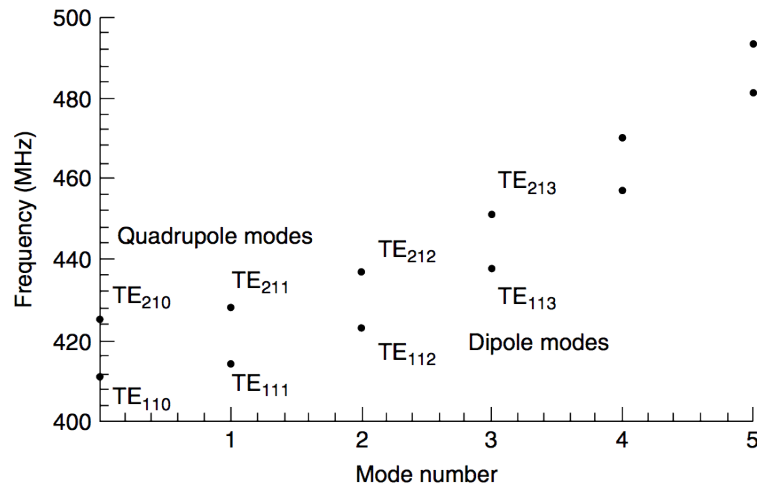


Figure 2.21: Idealized mode spectrum of a 4-vane RFQ. The frequency is plotted against the longitudinal mode number. Higher dipole modes are close to the operation mode TE_{210} [60].

There are several solutions to separate the modes like vane coupling rings connecting the opposing vanes to each other or movable field tuners along the structure as well as tuning rods selectively shifting the frequency of the dipole mode spectrum, so called dipole stabilizer rods or methods like resonant coupling [60]. Another possibility for lower frequencies is to use coupling windows allowing a stronger coupling of the magnetic field between the neighboring quadrants. This is explained in more detail in chapter 4.1.

2.2 CST Microwave Studio

For simulations done in this thesis the 3D simulation code CST Microwave Studio[®] was used. There are a few more codes like SUPERFISH [20], which is a 2D simulation code better used for cavities with cylindrical symmetry. Another code MAFIA, which was the first code based on the finite integral technique has lead to CST Microwave Studio[®] [45]. The basic idea of the finite integral technique is to divide the calculation domain into two orthogonal grids. On the grids edges the electric and magnetic fields are determined by solving Maxwells equations illustrated in Fig. 2.22. More about its numerical methods can be found in [61] and [62].

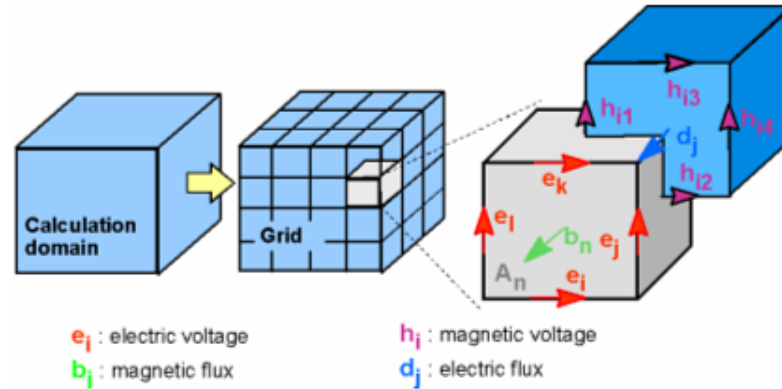


Figure 2.22: Grids of the calculation domain on which the Maxwells equations are solved to calculate the electric fields with CST Microwave Studio[®].

As an example in Fig. 2.23 the meshing of a RFQ is shown. For meshing either automatic fixpoints, user defined mesh refinement or both can be used. Fixpoints are certain points that define edges and details of the resonant structure. On these points the mesh is more concentrated in order to get exact simulation results.

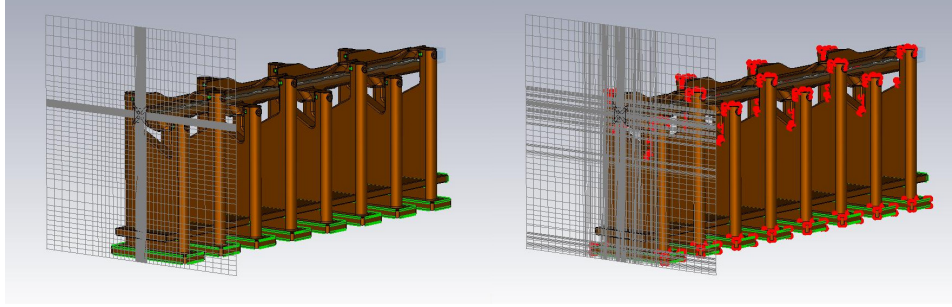


Figure 2.23: Mesh refinement on the electrodes modulation area (left) and meshing based on fixpoints (red) of the structure (right).

Depending on the simulation purpose the mesh can be refined locally. This can be done for example by defining a vacuum block where a certain meshing can be chosen, but it can be excluded simulation of the fields. If one wants to calculate the resonant frequency of an RFQ with modulation or needs a detailed field distribution of a certain region the mesh can be refined in the electrodes area to get a higher resolution of the small geometric shape of it. This method brings accurate results by relatively small solver time. If one would use mesh refinement at the overall structure it might increase the calculation time about a factor 5 to 10. Fig. 2.24 shows the frequency accuracy and the calculation time with the number of mesh cells. With a rising number of mesh cells the accuracy of the frequency increases as well. Depending on the length of the RFQ between 5 and 7 million mesh cells produce adequate results. A typical calculation time for an RFQ with modulation lasts about several hours up to two days, depending on the computing power.

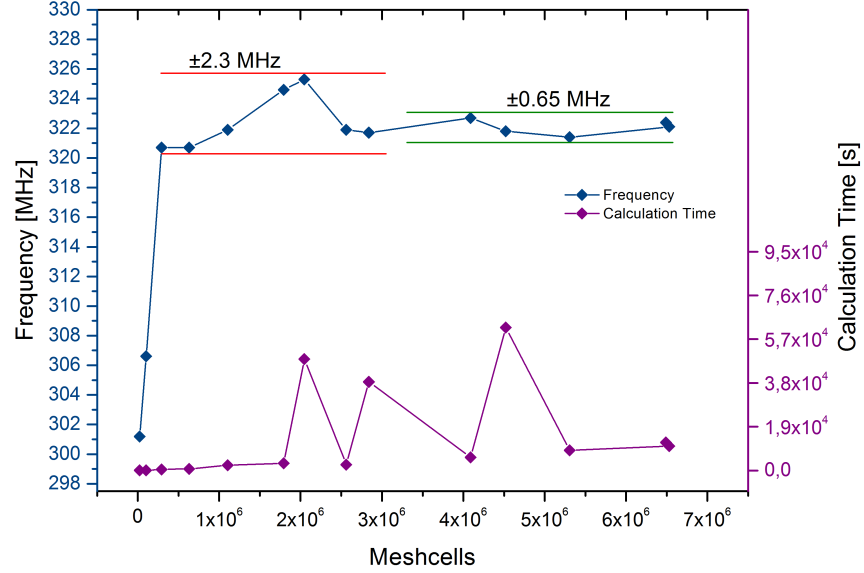


Figure 2.24: Dependency of the calculated resonance frequency and the calculation time on the number of mesh cells on a 4-rod RFQ in the 325 MHz region.

The accuracy of frequency results is strongly depending on the accordance of the simulation model with the real RFQ. With imported technical drawings of an RFQ and a balanced meshing to have a reasonable compromise in solver time a accuracy within 3 - 5 MHz of the resonant frequency can be achieved easily. Since this frequency range is comfortable tunable by the tuning plates, it was not pursued to increase this accuracy.

3 Analysis of the 4-rod Structure at 325 MHz

The particle beam is focused, bunched and accelerated by the electric fields. The particle dynamics as well as the RF design of the RFQ are aiming to provide these fields and one can divide them into transverse and longitudinal field component as seen in Fig. 3.1.

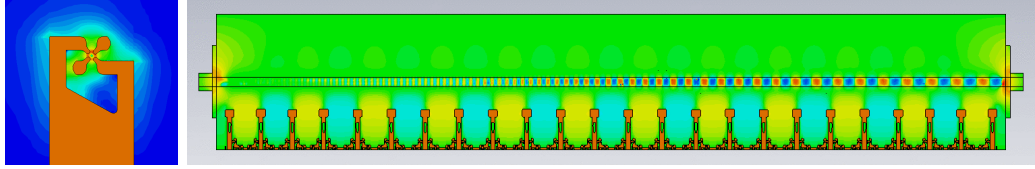


Figure 3.1: Transverse and longitudinal electric field component in an RFQ. View of the quadrupole electrodes along the beam axis (left) and the accelerating field component (right).

The transverse fields are responsible for the focusing and keeping the beam on the beam axis. In a 4-rod RFQ the transverse fields can be influenced by the longitudinal voltage distribution by shifting tuning plates. This allows one to adjust every single RF cell. The longitudinal fields determine the bunching and acceleration of the particles.

All fields are determined by the electrode design, but the resonant structure must provide the proper alternating quadrupole potential to the electrodes. If there is a deviation in the modulation or the resonant structure is not supplying the proper potentials, it can cause problems like a shifted beam axis what can lead to particle losses. Even with perfectly machined electrodes the transverse fields can suffer from the asymmetric shape of the 4-rod structure leading to a dipole field overlaying the quadrupole field. This becomes important in the high frequency case. In longitudinal direction the fringe fields between the electrode and the cavity walls can cause errors in the energy gain of the particles or may be deflected.

3.1 Dipole Field

For a proper working RFQ an accurate quadrupole field of the electrodes is important. This can be perturbed by a dipole field caused by the asymmetric structure of a 4-rod RFQ. But even symmetric structures like 4-Vane RFQs can be disturbed by a dipole field due to higher order modes which are close to the resonant frequency. The asymmetric shape of a 4-rod RFQ results mainly from the electrodes mounted at different heights at the stem. An RF cell of a 4-rod RFQ can be described as a capacitively shortened $\frac{\lambda}{4}$ resonator, where the capacitance comes mainly from the electrodes. In Fig. 3.2 one can see that the current and voltage distribution of a $\frac{\lambda}{4}$ resonator is a function of the stem height.

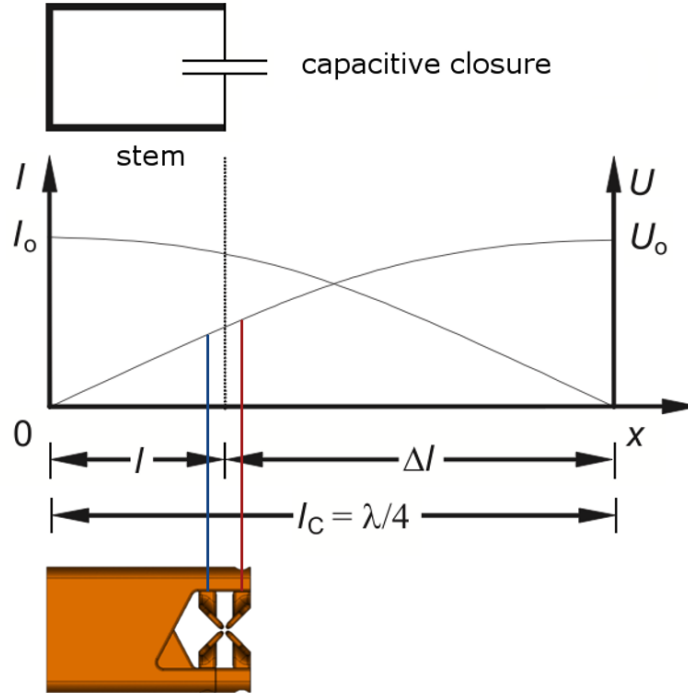


Figure 3.2: Comparison of the electrodes connected to the stem of a 4-rod RFQ to capacitively shortened Lecher wires.

Since one upper and one lower electrode is connected to the same stem the voltage differs. All upper electrodes have a slightly higher voltage than the lower electrodes causing an additional dipole field. The relative difference of these electrode pairs is increasing with higher frequencies because of the

smaller geometric size of the RFQ but about the same electrodes geometry. On the other side, due to the greater sensitivity of a higher frequency structure, the dipole field can be compensated by small changes for example of the stem shape.

3.1.1 RF Design of the Prototype

A 4-rod RFQ at a frequency of 325 MHz becomes quite small in its dimensions, since the resonant frequency scales with the geometry of the structure. In addition it becomes very sensitive on parameter variations in the RF design and later for example by shifting the tuning plates to adjust the RFQs field distribution and resonant frequency, because the number of RF cells is proportional to the resonant frequency. For example an RFQ can be tuned by shifting all tuning plates. The frequency change for a 200 MHz structure is about 10 MHz per 10 mm, while in a 325 MHz RFQ the frequency change is about 25 MHz per 10 mm. This sensitivity enables one to influence quite easily on compensating the dipole field of an RFQ by only small changes on the structures geometry.

At first a basic dipole analysis has been executed with a 6 stem simulation model, together with other parameters before an approach to a possible prototype could be done. After this a prototype based on recent RFQ design strategies has been developed in the simulation program to do further simulations like behavior of the higher order modes (HOMs) with increasing length of the RFQ. Also simulations regarding the fringe fields between electrodes and the tank have been investigated.

3.1.2 Compensation of the Dipole Field

The dipole field can be examined by the longitudinal voltage distribution or so called flatness of the RFQ electrodes by comparison of the upper and lower electrode pairs separately. This can be done in simulations as well as on a real RFQ model using the perturbation capacitance method. In CST Microwave Studio[®] one can draw lines between the electrodes for example where one would place a perturbation capacitor. On these lines the electric field can be integrated giving the longitudinal voltage distribution. This is shown on a model with strong dipole field with a deviation of about 16 % in Fig. 3.3.

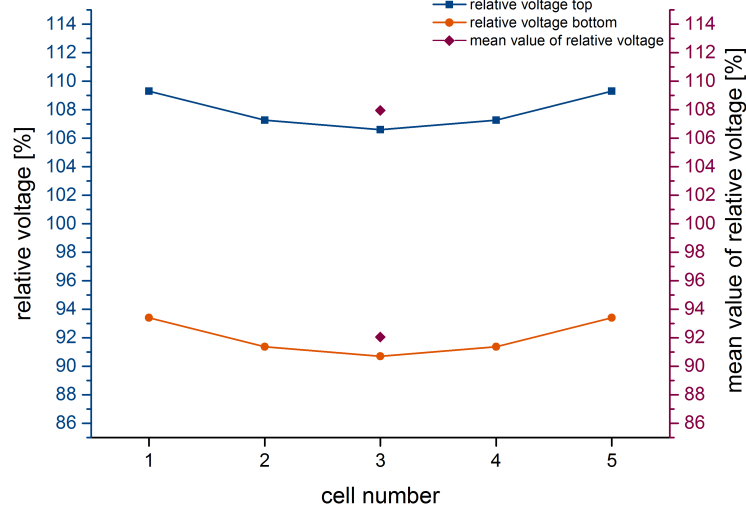


Figure 3.3: Longitudinal voltage distribution of the upper and lower electrodes and their mean value represent the dipole field.

This was calculated for a 5 cell model and shows the flatness curves of the upper and lower electrodes as well as the average voltage distribution for both electrode pairs. Since this calculation model was with unmodulated electrodes the flatness curves are equidistant and one may regard only one line or point along the electrodes to define the dipole field.

Stem Shape

Due to the high sensitivity of the structure at this high frequency one can strongly influence the dipole field for example by the shape of the stems. Different parameter variation are investigated in the following.

As mentioned in the theory part, the dipole field of a 4-rod RFQ is increasing with its frequency and therefore with its reduced geometrical size. However, the smaller an RFQ is the more sensitive it is on geometric changes and therefore it is easier to eliminate the disturbing dipole field. To estimate how one can reduce the dipole field very basic simulations on different variations of stem shapes have been performed. The investigated cuttings are shown in Fig. 3.4, including a straight cutting, an angular cutting with a fixed angle and an angular cutting with a fixed point and a variation of the cutting angle.

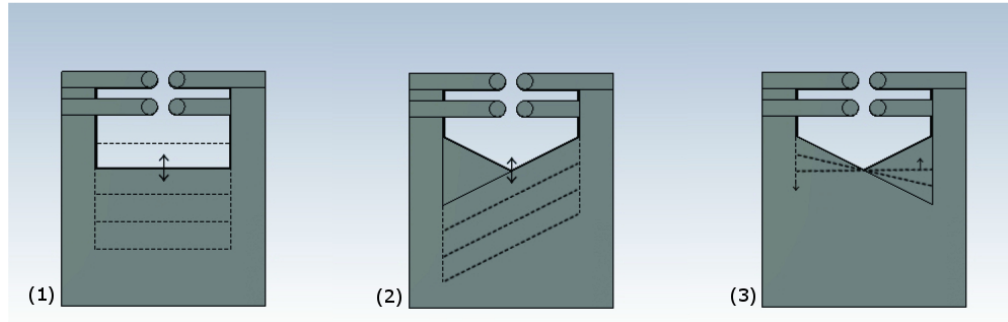


Figure 3.4: Variations of the stem shape to investigate the reduction of the dipole field.

Fig. 3.5 refers to case (1) in Fig. 3.4, there is no compensation of the dipole field at all. This is not surprising because at both stem arms equal space is provided for magnetic field. This field supports the asymmetric charge transportation and increases the dipole field.

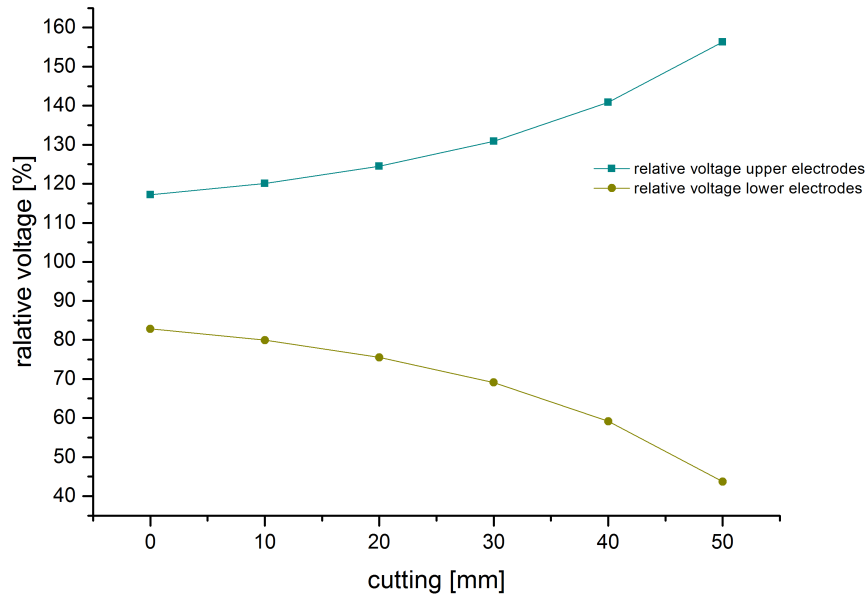


Figure 3.5: Voltage of the upper and lower electrodes in case (1), the straight cutting.

In Fig. 3.6 a fixed angle of the cutting is variated (case (2) in Fig. 3.4) in height and provides more space for magnetic field on the lower electrode side. In contrast to the straight cutting this leads to an unsymmetric charge transportation on the electrodes and at some height to a complete elimination of the dipole field. A deeper cutting leads to an overcompensation of the dipole.

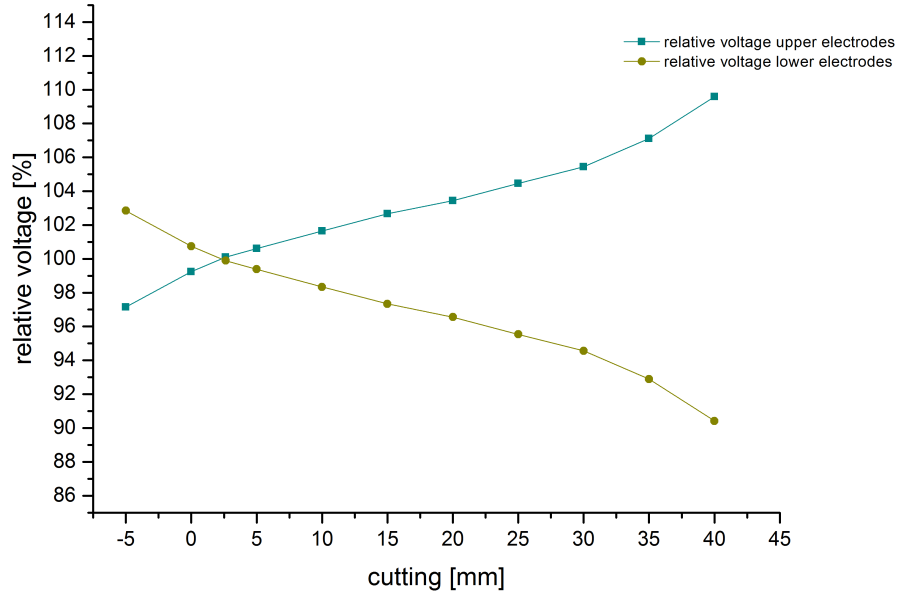


Figure 3.6: Adjustment and overcompensation of the dipole field in case (2), the variation of the fixed angle cutting.

As a next step the variation of a cutting angle at a fixed point in the middle (case (3) in Fig. 3.4) of the stem proves the theory of providing space for magnetic field on the side of the less loaded electrodes. Providing space on the side of the electrodes with higher voltage increases the dipole. Providing it on the lower height and lower voltage electrodes compensates the dipole at some cutting point as shown in Fig. 3.7. This point depends also on the parameter chosen for the electrodes and the clamps that connect the electrodes to the stem.

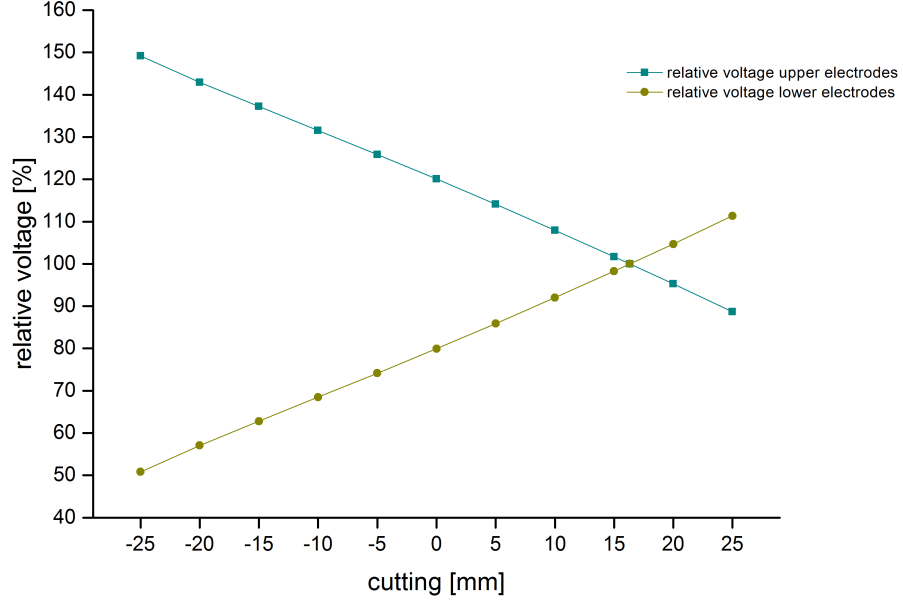


Figure 3.7: Adjusting and overcompensating of the dipole field in case (3), the fixed point angle variation cutting.

In summary more space inside the stem provides more magnetic field which is generating charge transportation up the stem on the electrodes. By the geometry of the cutting one can influence and balance this charge transportation as well as the compensation of the dipole field.

Electrodes Overlap

An increasing electrodes overlap at the ends leads to a higher electrodes capacity and one would expect a decreasing resonant frequency. Fig. 3.8 shows that the average voltage with increasing electrodes overlap stays almost constant. In previous simulations the overlap was set about $\frac{1}{4}$ of a cell length. The potential of the electrodes connected to the last stem is much smaller than on the other electrodes. An ideal overlap would be $\frac{1}{2}$ of a cell length, which leads to $1\frac{1}{2}$ cell length overlap on the electrodes not connected to the last stem and much more capacitance. An overlap of $\frac{1}{4}$ cell length was established by experience in many cases [13]. This is 12.4 mm for the simulation model. Due to the variation of the overlap no change of the dipole field could be observed. That means the additive capacitance of the overlap is uniformly distributed on

all electrodes and has no influence on the dipole but on the resonant frequency. It changes approximately 1.3 MHz per mm. This is caused by the additional capacitance of the electrodes. Apart from this one would expect a stronger unflatness of the structure because of this capacity at the ends of the RFQ.

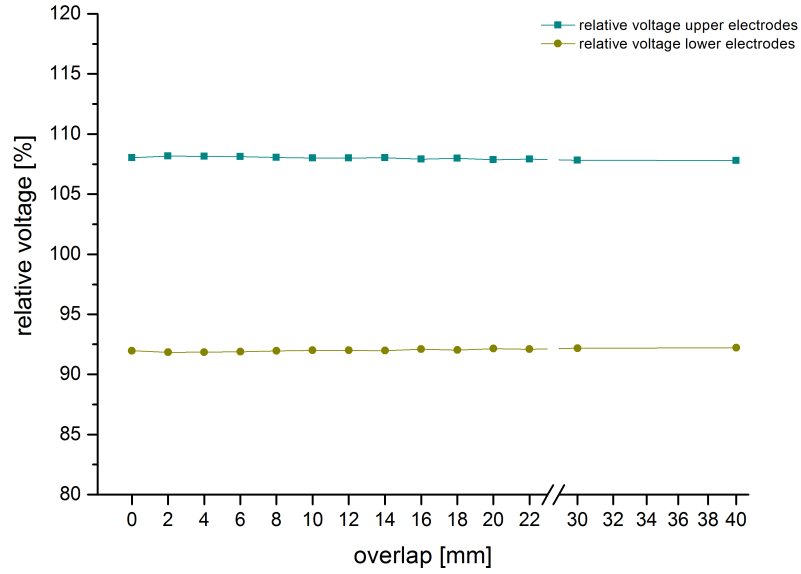


Figure 3.8: Influence of the electrodes overlap on the dipole field.

These simulations have shown that it is possible to compensate the dipole field at this simulation model. The dipole field is eliminated at a stem cutting ratio between the lower and the higher electrode side of about 2, respectively at an angle between 25° to 30° . The deeper the overall cutting is, the steeper the angle needs to be in order to transport more charges to the lower electrodes due to magnetic field. This means if the overall cutting is deeper on both stem arms more charge is transported which needs to be balanced by the angle of the cutting. So there is no particular angle at which the dipole field is compensated, it needs to be fitted by matching the whole stem design and cutting. Limiting effects are that one has to provide at least some space under the electrodes to prevent sparking and field distortion at the electrodes. These simulation results are verified by measurements of a copper model in chapter 3.1.3.

Other Geometric Parameters

Every part of the structure of a RFQ has an either capacitive or inductive influence and hence it might change the resonant frequency and the dipole field. To study this and on the other hand to get to know which influence on the dipole field can be taken by other parts than the stem design (see Fig. 3.9) of the RFQ the following simulations have been done. This is important for the RF design of new structures. This was investigated the first time and becomes more important for the sensitive 325 MHz structure. The several parameters that have been varied are marked in Fig. 3.10.

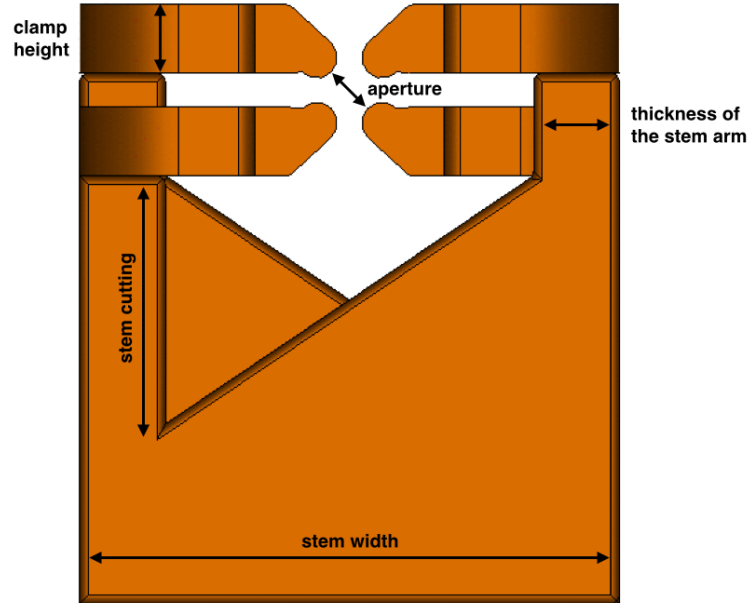


Figure 3.9: Parameter that have been varied in order to investigate their influence on the resonant frequency and the dipole field of the RFQ.

In Fig. 3.10 a rule of thumb of the influence on the frequency and the dipole field is given with arrows showing the direction if it is increasing or decreasing. A quantitative influence of a single parameter can not be given, due to the fact that the single parameter can not be considered individually. The parameters are coupled to each other. This means depending on a chosen setting one parameter has an effect on the sensibility of the next varied parameter. Solving this complex coupled problem is often an iterative process.



















Parameter Variation	Parameter Variation	Frequency	Dipole
Stem Cutting			
Aperture			
Clamp Height			
Width of Stem Arm			
Stem Width			
Stem Distance			

Figure 3.10: Influences of several parameter variations on resonant frequency and the dipole field of the RFQ.

Stem Cutting The stem cutting has a great influence on the dipole field, but lowers the frequency as well. One has to balance all other parameters to have a good dipole compensation and enough space for tuning blocks at the cutting.

Aperture By changing the RFQs aperture one can change strongly the electrodes capacity and accordingly the resonant frequency and the dipole field. If the aperture increases the dipole decreases. A minimum of the dipole field was reached at a $Er/A = 0.5$ (electrode radius over aperture), but usually a ratio of 0.8 is used. Unfortunately the electrode radius and the aperture is determined by the beam dynamics and not by the RF design of the cavity.

Clamp Height With rising clamp height the frequency and dipole decrease. More material at the clamps has a capacitive influence and lowers the frequency. This frequency drop causes slight reduction of the dipole. Further simulations have shown that wider clamps can increase the frequency due to their inductive influence.

Thickness of Stem Arm A thinner stem arm lowers slightly the frequency and the dipole component, but this is almost negligible. More important for the stem arms is to care about a minimum thickness due to stability reasons.

Stem Width Wider stems are reducing the resonant frequency and the dipole field. Since the effect on the dipole field decreases with lower frequencies, wider stems decrease the dipole as well.

With help of these simulations two possible RFQ structures were designed without dipole field at 325 MHz [25]. The parameters are listet in table 3.1. The beam height has also an strong influence on the dipole field that can be explained by the Lecher wire model. However a minimum beam height is neccessary to provide enough space for the tuning plates.

Table 3.1: 325 MHz Structure Types

Parameter	Type I	Type II
Beam Line Position [mm]	75	60
Stem Width [mm]	100	63
Stem Distance [mm]	50	50
Clamp Height [mm]	12	8
Width of Stem Arm [mm]	10	10
Frequency [MHz]	307,5	307,1
U/L	1.05	1.00
Tuning Plate Shift [mm]	15	10
Frequency Shift [MHz]	24,4	26,9

Both prototypes are quite sensitive on changes of parameter. That is also the case for changing the tuning plate height. The tuning of type II has shown a frequency of 323.5 MHz at a tuning plate height of 6.5 mm without a dipole field. In summary the simulations have shown that it is possible to apply the essential parameter settings for a 325 MHz RFQ on the present state of 4-rod design. This means that the desired frequency can be reached without any disturbing dipole field besides an overall fitting field geometry. The frequency adjustment can be done using the tuning plates. This has lead to building the prototype II, due to its stable absence of a dipole field, to proof the achievements by experiments. A further very accurate simulation of the dipole field is shown in Fig. 3.11. The electrode voltage was calculated every 5 mm along the electrodes of the structure. It shows the banana shape overlaid by a sinusoidal shape. The banana shape is caused by the electrodes overlap causing more capacity at the ends of the RFQ. The sinusoidal shape results

from the interaction of the single RF cells. The current flow causing a local maximum on the middle of two neighboring stems that are connected with the same electrode. A maximum voltage between the electrodes is generated in the middle of an RF cell. The dipole has a very small deviation on this structure even if the structure is untuned.

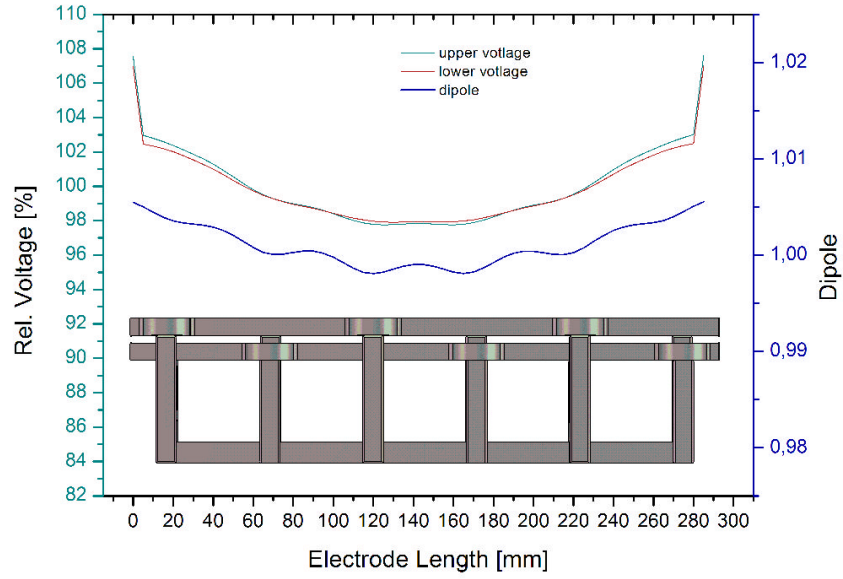


Figure 3.11: Dipole and longitudinal voltage distribution of a 4-rod RFQ at high resolution. The voltage was calculated in 5 mm steps along the electrodes.

For operation of an RFQ a homogenous voltage distribution of its electrodes is required by the beam dynamics design. By changing the height of the tuning plates on the one hand the frequency and on the other the local eigenfrequency of a single RF cell can be adjusted. Hence an uneven voltage distribution, caused by the modulation of the electrodes or the tolerances of manufacturing the RFQ, can be compensated.

3.1.3 Prototype

After the simulation work concerning the dipole investigations a prototype was built in the IAPs workshop. Fig. 3.12 shows the prototype and the simulation model.

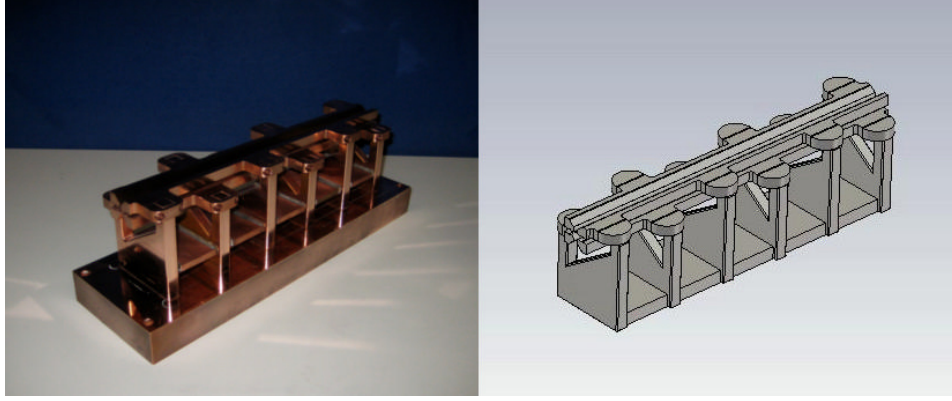


Figure 3.12: Prototype and simulation model of the 325 MHz RFQ.

The prototype is made of copper and has a water cooled ground plate for later power tests. A comparison of the parameter of the prototype and the simulation model in given in table 3.2.

Table 3.2: 325 MHz RFQ Parameter

Parameter	Prototype	Simulation
Beam Line Position [mm]	65	59
Stem Width [mm]	63	63
Stem Distance [mm]	50	50
Mean Aperture [mm]	2.9	3.225
Electrode Tip Radius [mm]	2.5	2.5
Clamp Height [mm]	8	8
Clamp Broadness [mm]	26	
Clamp Radius [mm]		13
Width of Stem Arm [mm]	10	10

There are slight differences between the two models. The beam line position was made a bit higher to ensure the frequency and the tuning possibilities. But with a tuning plate height of 6 mm it is the same as in the simulation. Also the aperture and the clamps geometry (see Fig. 3.13) are adjusted due to machining possibilities of the workshop.

Several low level RF measurements on the prototype have been carried out and compared with the simulations. These measurements were concentrated

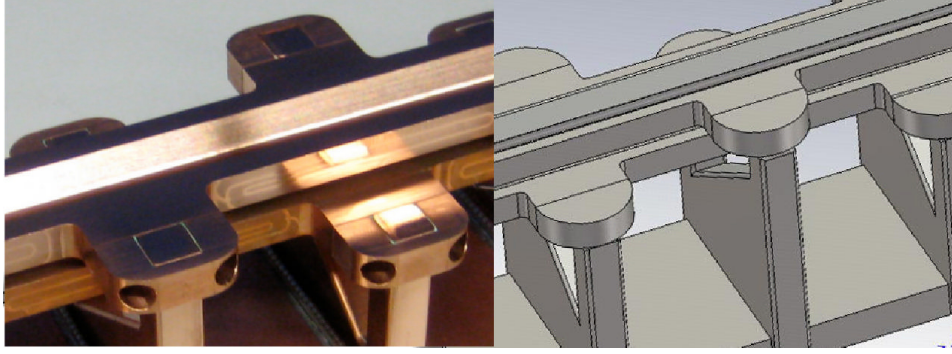


Figure 3.13: Different clamps of the prototype and the simulation model.

on the frequency adjustment, the longitudinal voltage distribution along the electrodes, the so called flatness, and the dipole field. The results can be found in table 3.3.

Table 3.3: RF Measurement Results

Parameter	Prototype	Simulation
Frequency		
Frequency at Beam Line Position 59 mm [MHz]	293.7	290.6
Tuning Range		
Tuning Plate min [MHz]	283.8	290.6
Tuning Plate max [MHz]	335.3	346.0
Tuning Plate Shift [mm]	20.2	18
Frequency Shift [MHz]	51.5	55.4
Dipole		
U/L (<i>upper/lower</i> electrode voltage) TPh min	1.00	1.00
U/L (<i>upper/lower</i> electrode voltage) TPh max	1.03	1.00

As mentioned before, the tuning plates of the prototype were set on 6 mm height to have the same beam line position as it is in the simulation. The difference of the resonant frequency between the simulations and the measurement is about 3 MHz. Regarding the limited machining possibilities in the university workshop for this sensitive prototype and the different clamps, this simulation accuracy is quite good.

The dipole was measured by two longitudinal voltage distribution measurements using a perturbation capacitor for the upper and lower electrodes. The

U/L in the table above is the ratio of these two measurements. Unlike the simulation predicted 0 %, the residual dipole at maximum of the tuning plates was 3%.

By shifting all tuning plates of the prototype to the same height a frequency of 324.3 MHz and a difference of the longitudinal voltage distribution of $\pm 3.4\%$ was measured. This structure is very sensitive to parameter variations. By shifting all tuning plates 1 mm the change of the eigenfrequency is about 2 MHz. Nevertheless after adjusting of the tuning plates the difference of the voltage distribution of the electrodes was only 1.6% (see Fig. 3.14). That is still improvable by further tuning measurements optionally in addition with a piston tuner. Further information about this prototype can be found in [27].

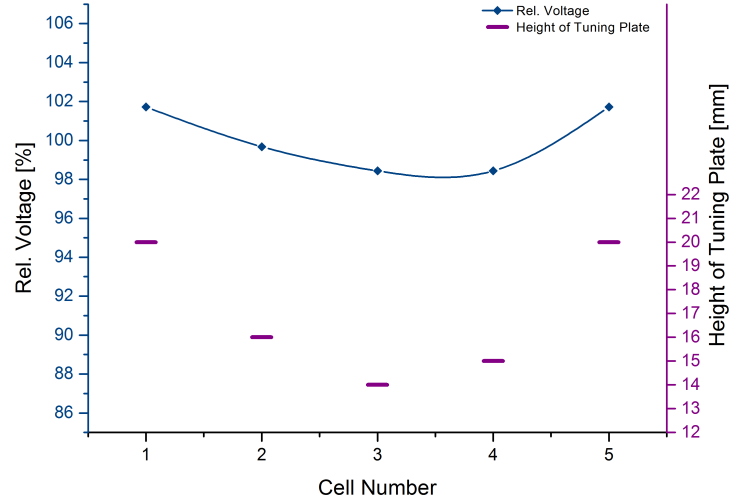


Figure 3.14: Positions of the tuning plates and its corresponding relative longitudinal voltage distribution. The difference of the longitudinal voltage distribution is $\pm 1.6\%$.

3.2 Fringe Fields

3.2.1 Longitudinal Fields

The task of the transverse fields is the focusing of the bunches, while the bunching of the particles and the acceleration is done by the longitudinal fields. Within the electrodes the fields depend on the accuracy of the machining, assembling and the proper potential brought to the electrodes by the resonant structure. Their nominal distribution is determined by the particle dynamics design. Between the electrodes and the cavity wall respectively the beam pipe, the boundaries require a particular consideration. The boundaries depend on a lot of parameters regarding the RF design. The influence of these parameters on the fringe fields is discussed in the following.

From each acceleration cell to the next one, the electric field in beam direction (E_z) has an alternating polarity. An example of this field is given in figure 3.15. In this graph the different parts of the electrode design, the matching, bunching and accelerating section is shown. At the very beginning and the very end there are strong peaks outside the electrodes. These are the fringe fields not considered by the particle dynamics. They form an additional acceleration cell, so that they can have strong influence on the energy gain of the bunches especially at the high energy end of the RFQ. At the low energy side of the RFQ the fringe fields do not have such dramatic impact because of weaker electric fields, a larger aperture and a lower energy of the particles during the adiabatic bunching. In addition when the particles are in the gap the phase is at -90° where the electric field is at its zero point and the particles do not see the peaks of the field. At the high energy end the fringe fields become more serious. The boundary fields are strongly influenced by the electrodes overlap, the last RF cell, the space between electrodes and cavity and the beam pipe respectively the RF shielding.

3.2.2 Boundary Conditions

Since the fringe fields are not included in the particle dynamics they need to be minimized. Different parameter variations of the boundary design to investigate the fringe fields have been performed in simulations. Unlike in Fig. 3.15, simulations without modulated electrodes show clearly the fringe fields, so one can analyze the fields in the gaps without any E_z component inside the electrodes region.

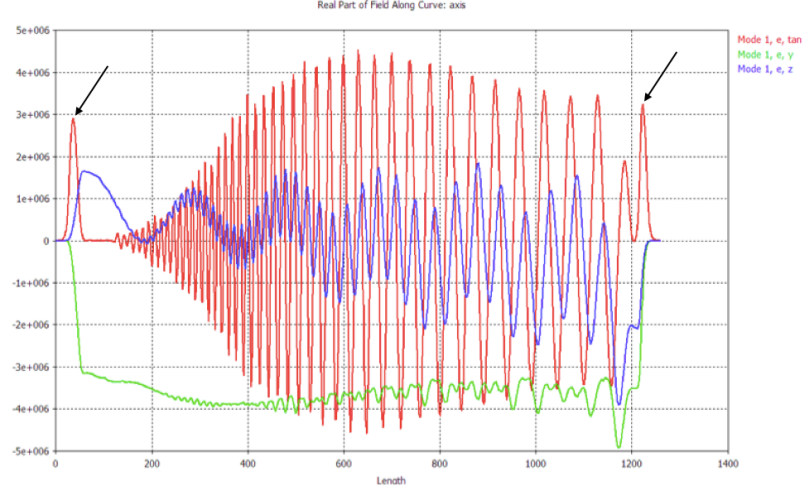


Figure 3.15: Simulation of the electric field in beam direction (red) of the Fermilab RFQ with modulated electrodes [29]. Arrows indicate electric gap field.

Variations of the Boundary Parameters

As first case the electrodes overlap at the ends has been varied as shown in figure 3.16 (overlap + vessel wall) from 0 to 30 mm. With a variation of the gap in this case an overlap and smaller space between electrodes and the cavity wall leads to a rise of the peak voltage as well as the integral over the electric field in the gap. On the other side the cutting of the overlap to zero suppresses the integral on the beam axis by a factor of 1.2.

By varying the overlap with a fixed distance to the cavity wall (Fig. 3.16 (overlap)), what means the vessel was getting larger with the overlap. In this simulation one find a decrease of the integral over the electric field about 5%. If one would go on increasing the overlap the integral drops again. The minimum could be found at an overlap length of about the size of one RF cell. By regarding Fig. 3.11 one can see that the voltage distribution along the electrodes shows local minima at the stems and maxima between the stems. These slight differences are caused by the unsymmetric voltage at the electrodes ends. By comparison to Lecher wires (see Fig. 3.2) one can imagine, that the absolute value at the ends of the electrodes is at its lowest difference at an overlap of about one RF cell length.

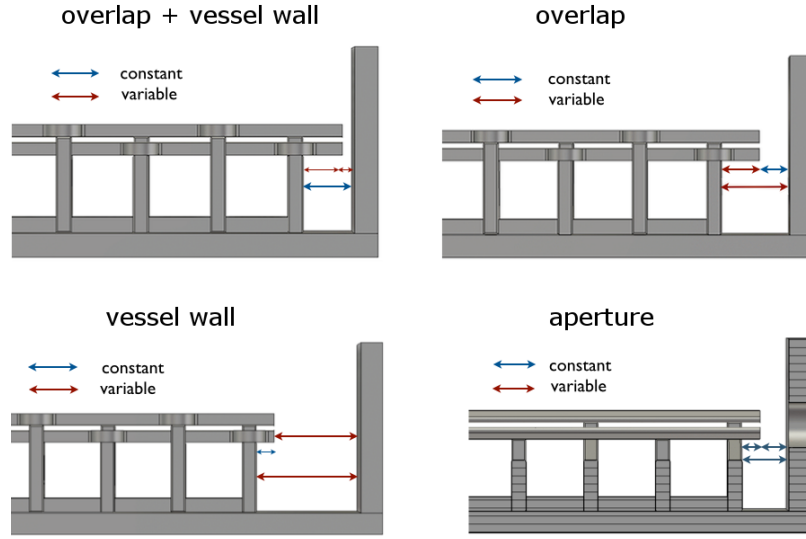


Figure 3.16: Variations of the boundary conditions for investigations of the fringe fields.

In many projects the size of an RFQ is set by the available space in the accelerator complex. So the lack of space leads to short RFQs [50]. In addition the power consumption increases with the length of an RFQ. Due to the particle dynamics one wants to avoid unnecessary drift space especially at the low energy part of the RFQ where the defocusing space charge of the beam is strong. This leads to cavity walls very close to the structure. At the cavity walls currents are induced, that have to be cooled for high duty cycle RFQs [57]. At the boundaries magnetic fields are surrounding the last stem and the electric fringe fields are reaching into the boundary conditions. To investigate this influence only the cavity wall was moved (Fig. 3.16 (vessel wall)). Therefore the overlap was set to a regular size and only the distance to the cavity wall was enlarged. The peak voltage as well as the integral decreases in an exponential behavior. With a large distance between the electrodes and the cavity wall around 70 mm the integral of the electric field would decrease about 20%. The integral of the fields and the electric fields are plotted in Fig. 3.17.

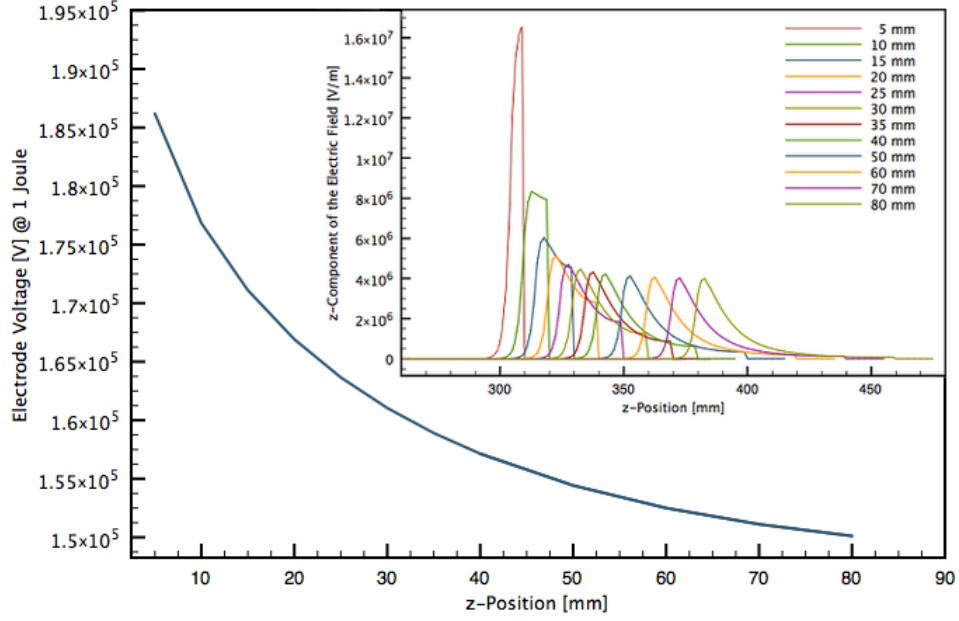


Figure 3.17: Gap voltage and electric fields in the gap in dependence of the cavity walls distance.

In summary these results show a strong impact of the boundary conditions on the gap voltage and consequently the integrated electric field a particle bunch is exposed to. There are possibilities to reduce the gap field, but the disadvantages are that one would have to provide large space the beam would have to travel or besides this a very large overlap of the electrodes. This could cause mechanical instabilities and unwanted movements, like vibrations, of the electrodes during operation. It follows from the above that space around the last stem is needed to establish enough magnetic field (see Fig. 3.18). Small distance between the last stem and the cavity wall suppresses the magnetic field compared to the other RF cells causing a lower potential of the last connected electrodes. This is leading to an unsymmetric field respectively a higher potential on the electrodes not connected to the last stem.

Another parameter that has been investigated was the aperture of the RF shielding respectively the beam pipe at the end of the RFQ (Fig. 3.16 (aperture)). The electric fringe fields of the electrodes are reaching till the boundaries of the cavity, so an opening of the RF shielding can influence these fields. In simulations an opening to 55 mm radius has lead to a reduction of the gap voltage by 10 %. But this shows a strong dependency of the distance of the cavity wall. With larger distances the influence by opening the aperture is reduced.

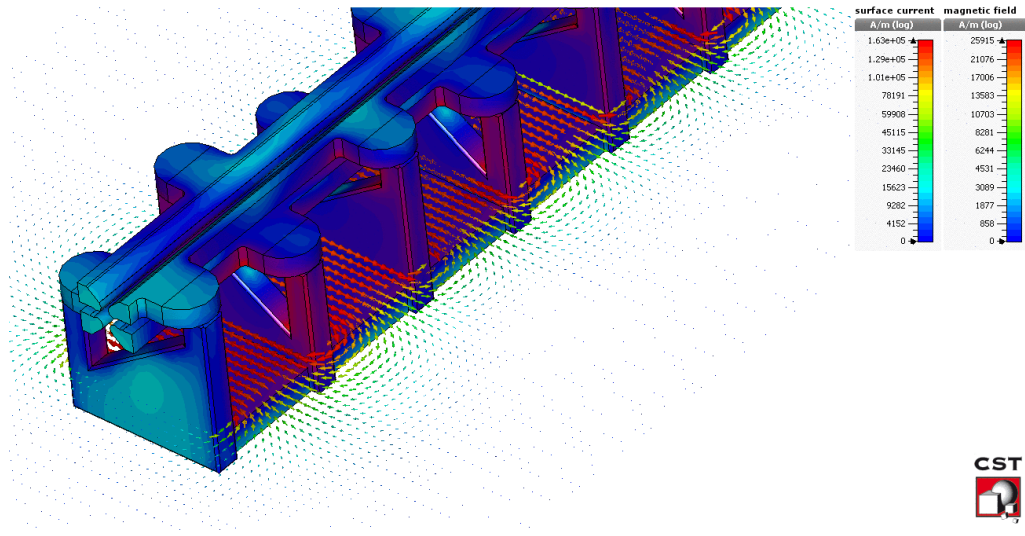


Figure 3.18: Magnetic field lines at a cut plane surface and the surface current at the last stem in comparison to the other stems.

Variation of the Last Stem

Closed magnetic field lines surrounding the last stem are effected by the tuning plates high in the last RF cell. There is no magnetic field under the tuning plates, which leads to a suppressed magnetic field around the stem if the tuning plates are shifted upwards. Simulations have shown a voltage drop of only 2 % by completely removing the tuning plate from its top position. This is only a small improvement due to the already quite small space provided at the stem due to the low beam line, but on RFQs at lower frequencies and hence geometric bigger stems this influence is stronger. This was also studied at a frequency about 200 MHz in [19].

Based on the idea of supplying more space for the magnetic field one can move the last stem towards the second last one making the last RF cell shorter. This has also been investigated in [41]. On the one hand this provides more space between the stem and the cavity wall, on the other hand it increases the frequency of the last RF cell. It has the same effect like a higher tuning plate, what is usually needed for the longitudinal voltage distribution along the electrodes at the end cells. This means in addition the tuning plate can stay on a lower position also supporting the magnetic fields surrounding the last stem. Making the last RF cell shorter about 10 mm leads to a reduction of the gap voltage by 10 % . The z-component of the electric field is shown in

Fig. 3.19.

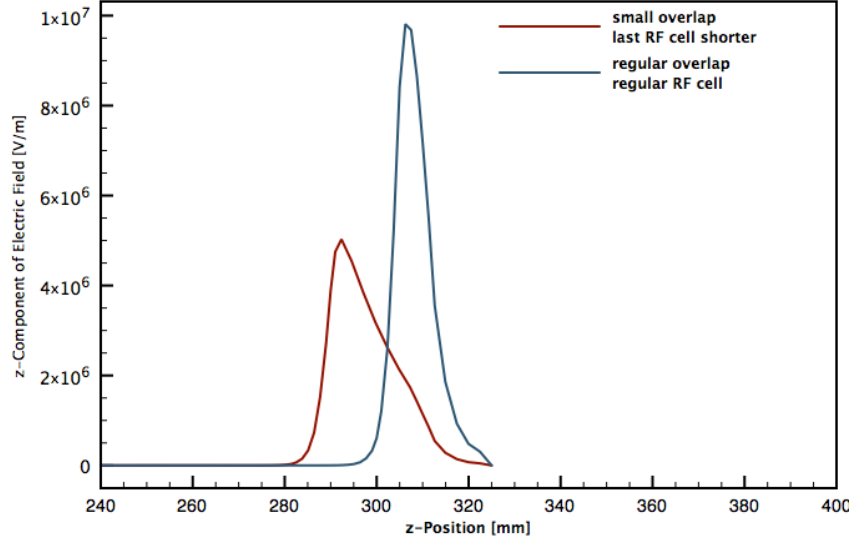


Figure 3.19: z-Component of the electric field of a regular and reduced last RF cell.

The movement of the last RF stem has two advantages. The reduction of the gap field and the adjustment of the longitudinal voltage distribution in advance. Every change of parameter has an influence for example at the frequency, the quality factor or the shunt impedance. For further improvements for example as well of the longitudinal voltage distribution one could move the last and the second last stem changing the last three RF cells to reduce the influence of the capacity of the electrodes overlap.

A further step to receive more magnetic field surrounding the last stem is to improve the stem shape. It was studied what happens to the gap field when the last stem has a wasted shape. In a second step the last stem was getting a waist shape and the second last stem was getting a bulge. Both changes of the shape are shown in Fig. 3.20. By just calculating the influence of the waist shape the gap field was lowered by 3 %. Apparently this shape promotes the evolving of the magnetic field between the last stem and the vessel wall. Simulations of the waist shape in addition of the bulge shape of the second last stem gave an improvement of even 5 %.

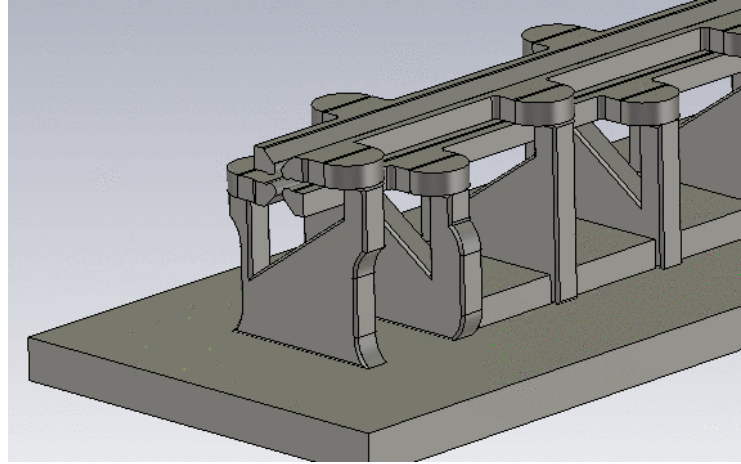


Figure 3.20: Waist on the last and bulge on the second last stem.

Summary

The improvement of the single parameter variations compared to the standard design with a regular electrodes overlap, RF shield aperture, stem distance and shape are listed in table 3.4. The improvement means the reduction of the gap field between the electrodes and the vessel wall.

Table 3.4: Reduction of the Gap Fields Integral

Parameter	Improvement
less overlap	2 - 4 %
more gap space	12 %
more RF shield aperture	10 %
low tuning plate	2 %
shorter last RF cell	10 %
last stem waist	3 %
last stem waist - 2nd last stem bulge	5 %
all together	22 %

In the combination of all of the investigated parameters, it is not possible just to simple add up the single influences. For example the RF shielding aperture has a strong influence as well as providing more gap space. Variations of the RF shield aperture at different gap distances have shown a decreasing influence of the aperture at lager gap distances. So the parameter changes are coupled

to each other and one has to decide what is the best solution depending on the setting of the respective RFQ. For a low frequency and hence larger stem sizes one might prefer the variation of the stem distance. This shows the great possibilities to take influence on the fringe fields, but it needs to conform to the RF layout of the individual RFQ.

3.2.3 Fringe Fields at the FNAL RFQ

Due to the fact that the fringe fields produce electric fields in longitudinal direction in the gap between the electrodes and the vessel wall, one can describe this as an acceleration cell between two drift tubes. The energy gain a particle with charge q will receive in a gap with an average amplitude of the electric field E_0 over the length L is given in 3.1

$$\Delta W = qE_0TL \cos \phi \quad (3.1)$$

The phase shift of the particle at the beginning of the gap compared to the crest of the RF field is represented by ϕ . The energy gain of particles in a time-varying field is always less than in a constant dc field. The ratio of the energy gained in the time-varying RF field to that in a dc field can be described by

$$T = \frac{\int_{-L/2}^{L/2} E(0, z) \cos \omega t(z) dz}{\int_{-L/2}^{L/2} E(0, z) dz} \quad (3.2)$$

The transit-time factor T is a measure of the energy gain reduction caused by the sinusoidal time variation of the field in the gap [60]. The equations show that the impact of the fringe fields depends on the synchronous phase of the particles entering the gap, on the length of the gap and on the operating frequency of the RFQ [10]. 4-rod RFQs at high frequencies with a crandall cell and a short gap between the electrodes and the vessel wall are most sensitive to fringe fields. This gap field can also be influenced by the ending of the electrodes modulation at the high energy part of the RFQ. Either they end with a full acceleration cell, which means that one pair of electrodes is closer to the axis than the other pair or with a quadrupole symmetric ending using

a transition cell. In the case of the transition cell a smooth transition is made from full modulation to zero modulation. The vane tips are ending with quadrupole symmetry and the on-axis potential becomes zero. In addition with the length of the unmodulated part one can take control about when the beam leaves the periodic focusing. This unmodulated part focuses the beam to form a symmetric transverse output distribution of the bunch [11]. When the synchronous particle enters the gap behind the electrodes, the E_z -field is on the rising edge of the RF phase at about 90 % of its maximum amplitude. This refers to the sinus convention. In this case fringe fields can have a strong impact on the output energy of the particles. If the RFQ ends with a full cell the on-axis potential will not be zero. In general fringe fields can be regarded by the particle dynamics simulation software Parmteq, but even if this is done the asymmetries of the 4-rod structure may cause disturbing fields due to different charging of the electrodes ends, like investigated in the chapter before. When particles enter the gap after this full cell the RF phase is at 150° what refers to approximately 50 % of the maximum field amplitude at the falling edge of the RF causing only minor influence if fringe fields can not be compensated. As an example for measurements the beam output energy of the 4-Rod RFQ at Fermilab was measured at the FNAL H^- injector. The setup inside the RFQ is given in Fig. 3.21. The output beam energy was measured before and after removing the RF shielding at the high energy end of the RFQ.

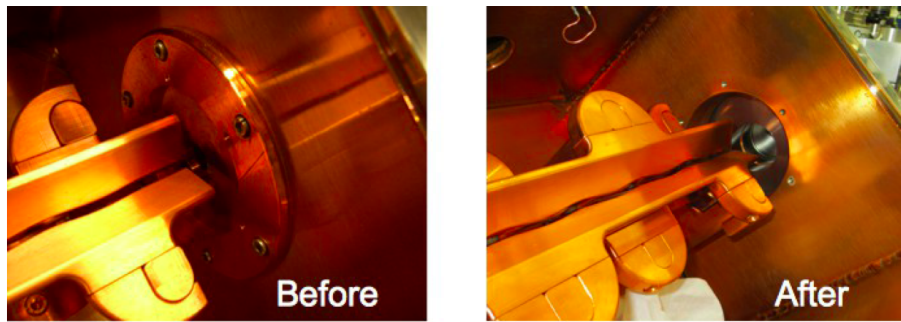


Figure 3.21: High energy end of the RFQ. Measurements were done before and after removing the RF shielding [52].

Fig. 3.22 shows the data results of the energy measurement. The left graph represents the measurement including the RF shielding. The results are time-of-flight measurements using several beam pick up (BPM) positions. The

results of the output energy was 700 ± 17 keV/u. The right graph shows the measurements without the RF shielding. The output energy was measured with a dipole magnet and gave a beam energy of 756.5 ± 0.5 keV/u. In summary the energy deviation in this case could be explained by the gap fields. Also these measurements confirm the influence of the RF shields aperture on the fringe fields and hence the energy gain due to this fields. A careful RF design regarding the fringe fields is important to assure the right output energy of the RFQ. A more detailed view into the studies on the output energy is given in [52].

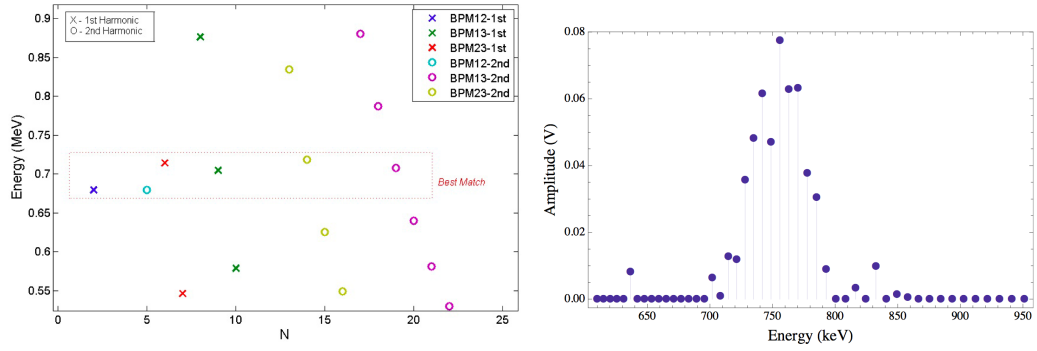


Figure 3.22: Measurement of the output beam energy of the FANL RFQ before and after removing the RF shielding [52].

3.3 Improvement of the 325 MHz 4-rod Prototype

Based on the simulations and measurements of this dipole compensated 4-rod RFQ improvement on this structures have been adapted in simulations. The shape of the stems and the attachment of the electrodes allows an assimilation of the current paths from the bottom to the higher and lower electrodes. This is shown in Fig. 3.23 and makes the structure more symmetric and leads to a stronger dipole reduction. This structure was first investigated by Benjamin Hofmann [18] at 352 MHz. In the following parameter variations are presented for this structure.

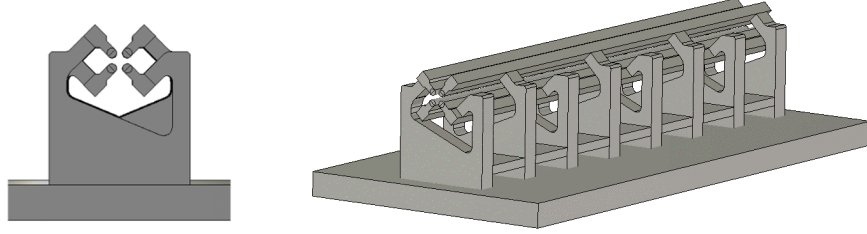


Figure 3.23: Simulation model of the new 325 MHz 4-rod prototype.

3.3.1 Stem Thickness

The stem thickness was varied in order to investigate cooling possibilities inside the stems. Thicker stems providing more space for cooling tubes. The variation of the stem thickness from 10 to 30 mm is presented in Fig. 3.24. Another reason of investigating thicker stems was to have more space for the electrodes connection. At a length about 3 m as for the proton linac at FAIR, it is easier to machine and assemble the electrodes as segments of roughly one meter length. The risk of damage or bending the electrodes is much less and there is no need for special milling machines to handle the electrodes. At the connection of the electrode segments on the RFQ the stems need to be thicker in order to fix them properly. Simulations have shown that if only the stems that connect the electrode segments to each other are thicker, even without fitting the RF cell length, works without problems.

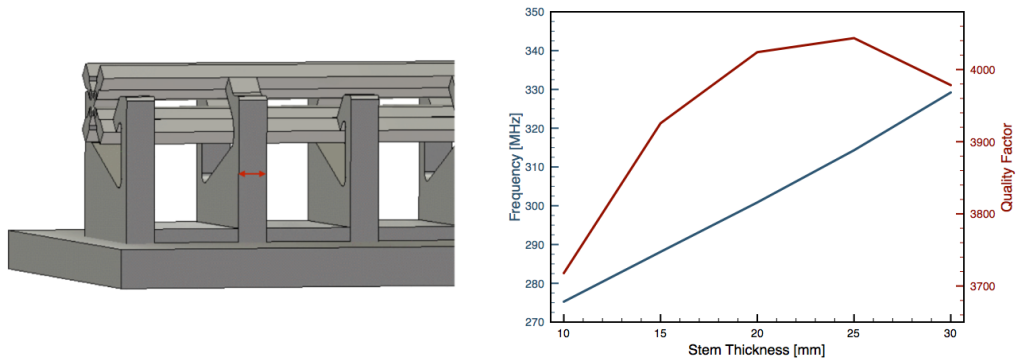


Figure 3.24: Variation and influence of the stem thickness.

3.3.2 Tuning Plate Height

The beam height of this simulation model is quite high with 70 mm. Hence the tuning plates need to be at a certain position to reach the needed frequency. The shift of the tuning plates and the influence on the frequency and quality factor is shown in Fig. 3.25. The frequency shift by moving the tuning plates from 0 mm to 25 mm is from 290 MHz to 345 MHz. That is a shift of 2.2 MHz/mm with an almost linear progression.

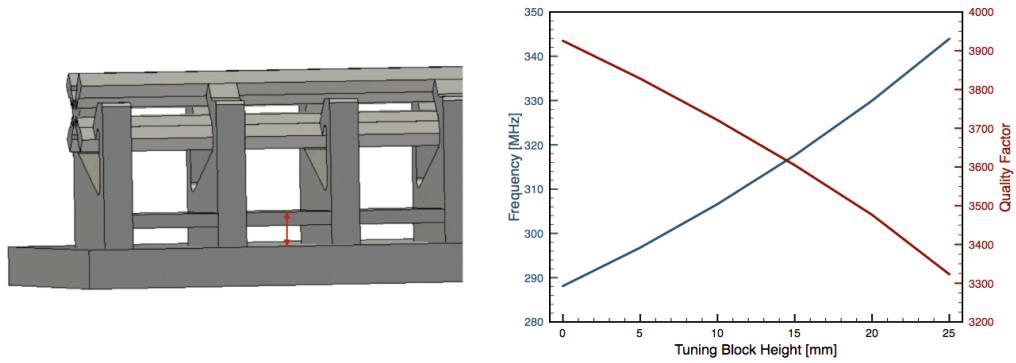


Figure 3.25: Parameter sweep over different tuning plate heights.

3.3.3 Stem Shape

Changes of the angle of the stem cutting have a strong influence on the dipole field discussed in chapter 3.1. The simulations of the left and right side of the cutting (see Fig. 3.26) show that the influence on the frequency is quite small in comparison to the dipole field by changing the cutting of the stem. This enables a comfortable dipole suppression by keeping the resonant frequency at its value.

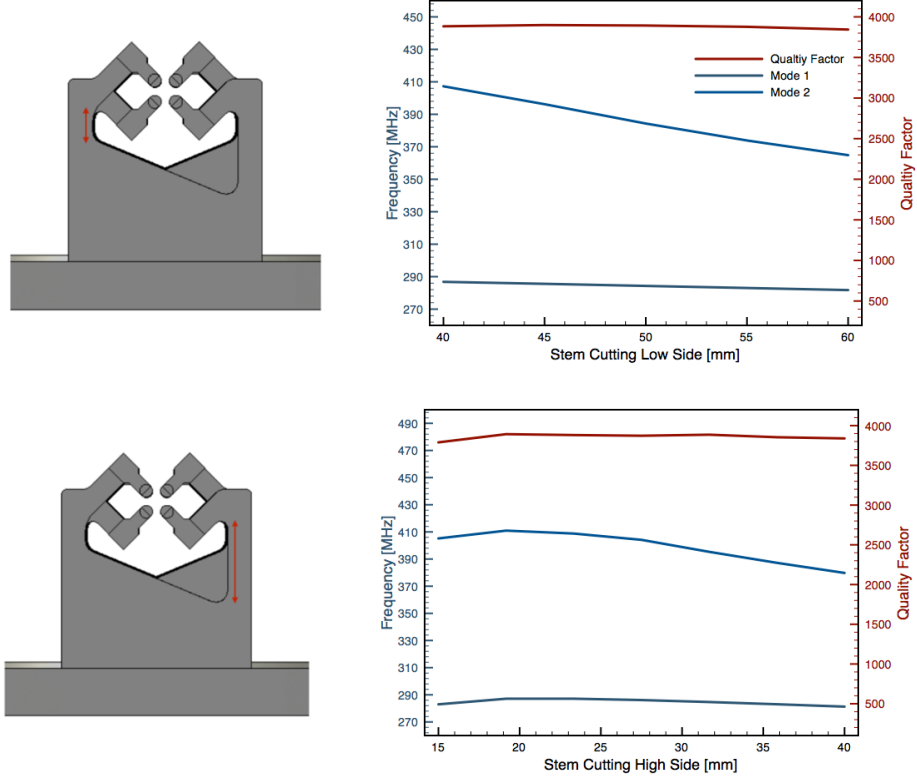


Figure 3.26: Variation of the stem cuttings to the high and low side.

3.3.4 Summary

This dipole and frequency optimized 4-rod structure has the same advantages like usual 4-rod RFQ regarding access and maintenance. Through the stem shape and electrode mounting the current paths are aligned to each other between the left and right side to provide a better dipole compensation in advance. For higher duty cycles the electrodes might need to be water cooled. This can be very challenging with this electrode mounting, but in order to cool the stems one would use a stem thickness of about 20 mm without any problems.

4 Comparison of Alternative RFQ Resonator Types

The 325 MHz operating frequency region in general is challenging in respect of designing, machining, assembling and tuning due to the sensitivity of the resonant structure because of the high frequency. The following chapter describes the different RFQ resonators and compares their feasibility to work as compact proton accelerators at 325 MHz.

For a resonant frequency of 325 MHz different kinds of RFQs can be considered. For operators not only RF design but also reliability, availability, tuning access, efficiency, the capital costs and technological risk can be important. Like mentioned before in the frequency region above 300 MHz usually 4-vane RFQs are preferred because there is a lot of experience for these kind of resonators at high frequencies. Nevertheless besides the 4-vane and 4-rod RFQs also a ladder type RFQ would fit for this frequency. As a fourth type a CH RFQ was considered and investigated. In the following simulations the tuning possibilities of the different RFQ types in the 300 MHz region are presented.

4.1 4-Vane RFQ

4-vane RFQs have been realized many times and are usually the preferred resonators at frequencies above 200 MHz due to its RF power efficiency and its feasible dimensions. This structure consists of 4 symmetrically arranged vanes which are connected to the cavity walls. The 4-vane structure is a cavity resonator operating in TE_{210} -mode. Due to the magnetic fields in longitudinal direction, the current is flowing azimuthal on the cavity walls exciting the vane tips with an RF voltage. The boundary conditions of a closed cylindrical resonator do not allow the TE_{210} -mode because the electric field would be parallel to the end walls. This is solved by undercuts (see Fig. 4.2) at the vane end-

ings allowing the magnetic field flowing from one quadrant to another. This leads to a perpendicular electric field at the end walls [58]. However the structure is very symmetric, a problem of 4-vane RFQs are the dipole fields of the neighboring modes to the operating quadrupole mode. These dipole modes are very close to the operating quadrupole mode and disturb the quadrupole field symmetry. To achieve the required field symmetry the dipole modes need to be artificially suppressed. This is usually realized by piston tuners and dipole stabilizer rods.

The fact that a 4-vane RFQ is a cavity resonator means the size and shape of the cavity is directly influencing the resonant frequency. The 4-vanes cavity size and shape determines the first approach of the frequency. Also the vane thickness and its shape affects the frequency. In Fig. 4.1 some possible parameters to be changed in respect to the frequency are shown.

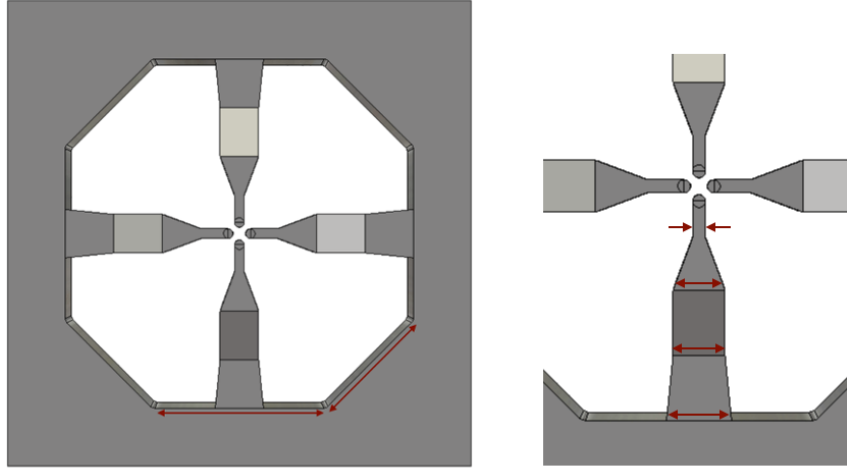


Figure 4.1: Red arrows show possible parameter changes for frequency adjustment of a 4-vane RFQ.

As a rough approximation several centimeters variation of the tank shape can change the frequency up to some tens MHz. If the vane shape is varied about a millimeter the frequency shifts by less than 1 MHz. Every parameter change is strongly depending on the setting of the other parameters. Further influence on the frequency can be taken by the shape of the undercuts at the vane ends or strongly by coupling windows. Coupling windows are holes in the vanes allowing magnetic field propagate also in circular direction.

Undercut

The undercuts are mainly needed to allow the magnetic field to flow into other quadrants to make the operation mode possible. The size and shape of the undercuts has an influence on the frequency and the electric field distribution. The width and height of the undercuts have been varied to quantify their tuning possibilities. The variation of the undercut width (see Fig. 4.2) shows a frequency shift of about 1 MHz/cm. The variation of the undercuts height leads to a frequency shift of 25 kHz/mm.

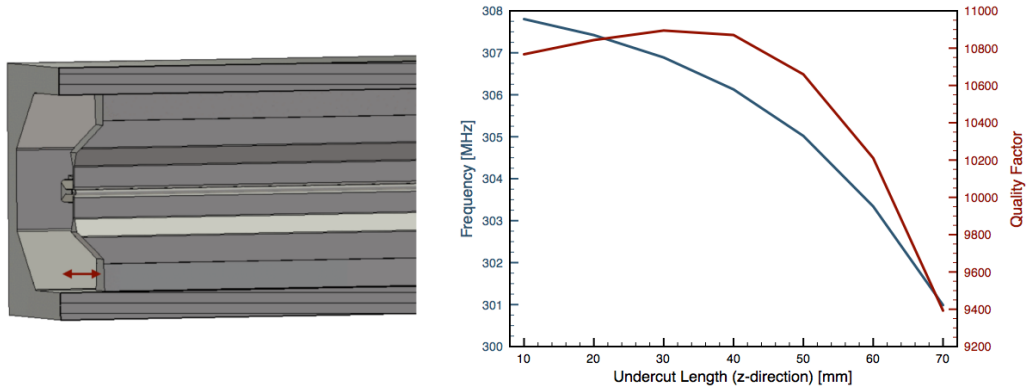


Figure 4.2: Influence of the undercut variation in longitudinal direction on the frequency and quality factor.

Coupling Windows

One can insert windows into the vanes leading to a stronger magnetic coupling between neighboring quadrants. This is similar to a 4-rod RFQ with an angle between the neighboring stems of 90° , shown in Fig. 2.12 (90° 4-rod). The magnetic field is presented in Fig. 4.3. These coupling windows are lowering the frequency of the quadrupole mode in comparison to the dipole modes. This means the separation of the dipole modes from the quadrupole mode results in a lower operating frequency.

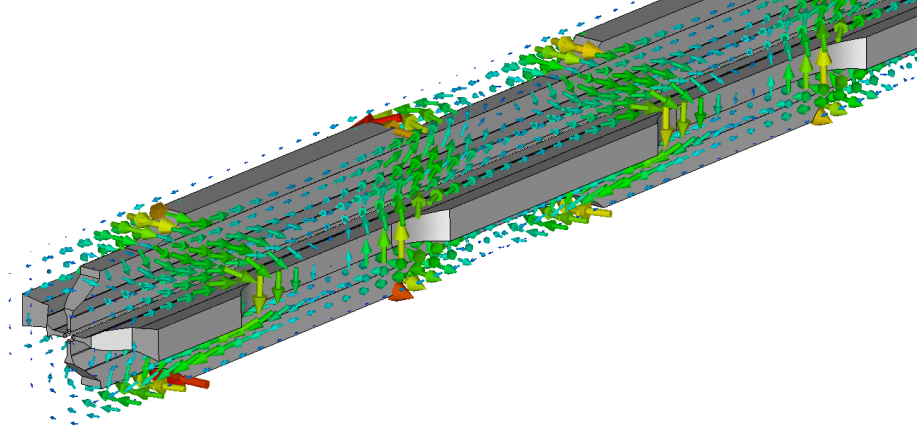


Figure 4.3: Arrows represent the magnetic field lines in a 4-vane RFQ cavity with coupling windows.

The mode separation is even more effective with an antisymmetric window configuration, where adjacent windows are shifted by 180° [60]. In Fig. 4.4 the variation of the width of the coupling window in longitudinal direction is shown. The width was varied from 150 mm to 400 mm lowering the frequency about 60 MHz which is roughly 240 kHz/mm, but this is not a linear behavior.

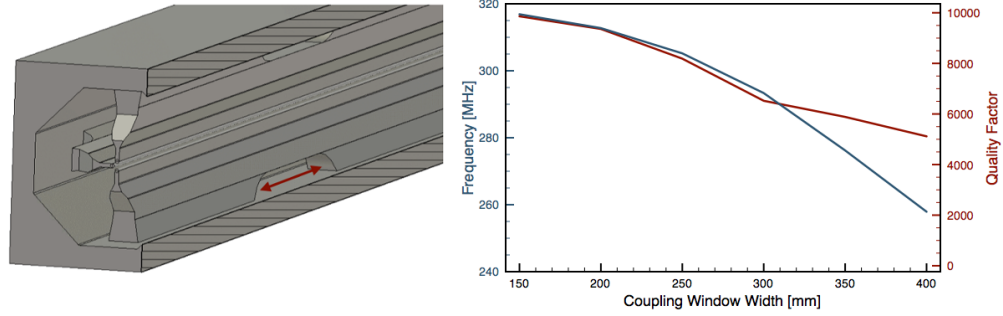


Figure 4.4: Variation of the coupling window width.

The variation of the coupling window height is shown in Fig. 4.5. The frequency shift is about 840 kHz/mm. One can see from this graph as well that the quality factor is rising with higher coupling windows. Wider coupling windows have shown a decreasing quality factor.

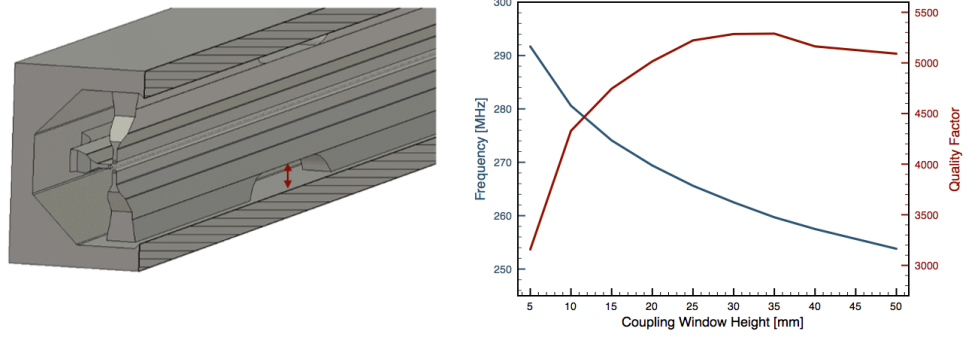


Figure 4.5: Variation of the coupling window height.

Summary

The 4-vane RFQ is well suited for frequencies above 300 MHz. This kind of structure was realized successfully several times for example the LEDA RFQ at LANL [63], the SNS RFQ at ORNL [43], the J-PARK RFQs in Japan [23, 35] or the CRYEBIS-RFQ in Saclay [36]. By now there is a lot of experience in manufacturing of the structure and its dipole suppression. A present example that is quite similar to the proton Linac for the FAIR project is the 4-vane RFQ of the Linac4 project at CERN operating at a frequency of 352.2 MHz. The progress and insights into the development of this RFQ can be found e.g. in [39, 47] and [46].

4.2 Ladder RFQ

The Ladder RFQ consists, similar to a 4-rod RFQ, of 4 quadrupole electrodes. Two adjacent electrodes are connected to one stem and the other electrode pair to the next stem and so on. The electrodes can be mounted directly to the stems or in rings that are fixed to the stems. The advantage of the rings is to have frequency tuning possibilities by varying the thickness of the rings. A disadvantage is, that it might be difficult to receive a good electrical and mechanical connection of the rings to the stems. This construction, using rings to mount the electrodes, relies on the tolerances during fabrication and has been realized for example at the IH-RFQs for the MAFF project of the LMU Munich [54] or for the GSI high current linac. The Ladder RFQ tank is about the same geometric size as a 4-rod RFQ but with each stem connected also to the top of the cavity. The operation mode is similar to a

4-rod type, where two neighboring stems build one RF cell to load the electrodes with the alternating potential. The magnetic field surrounds the quadrupole electrodes passing through the upper gap between two stems. Due to this symmetry the structure has no intrinsic dipole field. Even on 325 MHz the Ladder RFQ has quite appropriate dimensions to handle the assembling. Also the resonant values like the quality factor and the shunt impedance make the Ladder structure competitive in the 325 MHz region.

For the investigation of the tuning possibilities and to study the RF behavior of the structure a Ladder RFQ was analyzed in CST Microwave Studio®. For this it is sufficient to study the structure roughly in the 325 MHz region. Parameter sweeps have been simulated for the electrodes overlap, the ladder width, the thickness of the electrode rings and for piston tuners. The design of the Ladder RFQ which is discussed and investigated refers to the mechanical solution also investigated in [6].

Electrode Overlap

The overlap of the electrodes has been varied in order to investigate the frequency and the longitudinal voltage distribution. The results are presented in figure 4.6. One can identify the, 4-rod RFQ typical behavior, of the decreasing frequency with larger overlaps due to the additional capacitance of the electrodes.

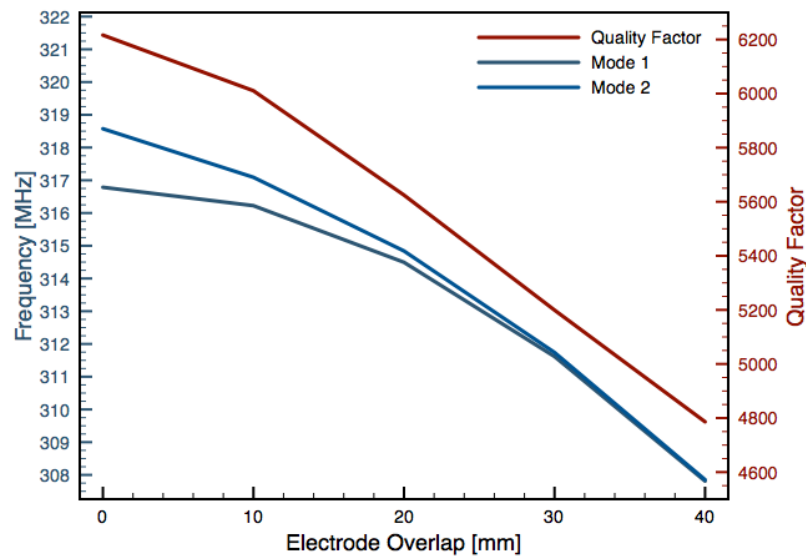


Figure 4.6: Frequency of the first two modes and quality factor in dependence of the overlap of the electrodes.

The Ladder structure has a strong deviation in the longitudinal voltage distribution. This increases in addition with a larger electrodes overlap. The electrodes end asymmetric like at 4-rod structures. Therefore some overlap is desired, due to fringe field reasons (see chapter 3.2). Further simulations proved the adjustment possibilities of the unflatness by shorter stem distances of the last two or three RF cells.

Ladder Width

The variation of the ladder width is shown in Fig. 4.7. By increasing the width of the ladders the frequency as well as the quality factor are rising. The frequency increases with about 0.8 MHz/mm . This behavior makes the ladder width to an important parameter for high frequency Ladder RFQ design, but makes it also inconvenient for measurements with a perturbation capacitor for the flatness or shunt impedance due to less space to access the electrodes.

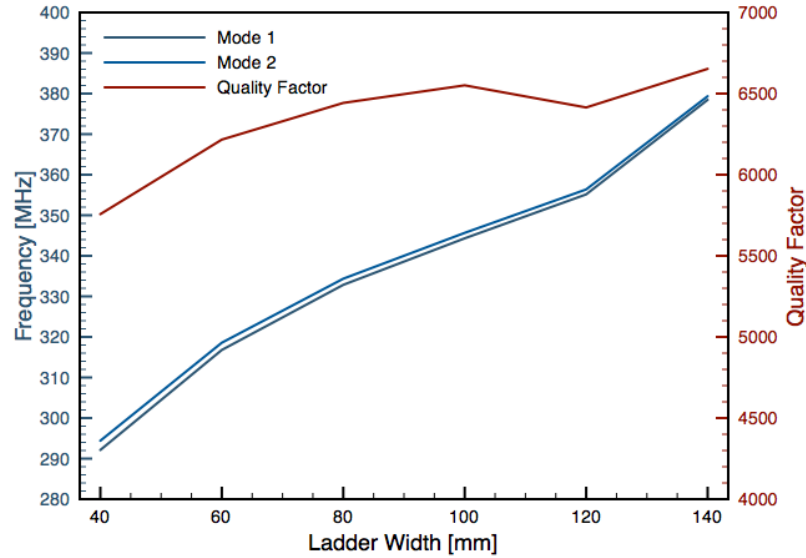


Figure 4.7: Variation of the ladder width and the characteristics of the quality factor and the first two modes of the Ladder RFQ.

Electrode Rings

When the stem size is set, the adjustment of the structure during the tuning process can be done capacitively by changing the thickness of the rings mounting the electrodes. Fig. 4.8 shows the frequency and quality factor by changing

the thickness of all rings at once. For adjustment of the longitudinal voltage distribution single rings of different thickness can be mounted as well.

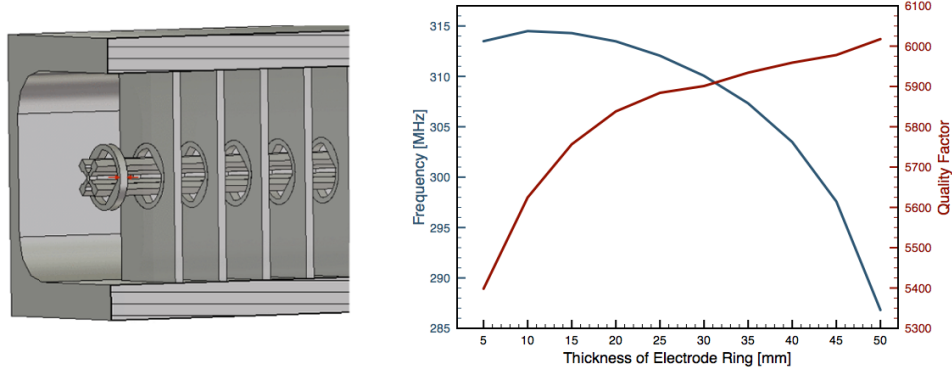


Figure 4.8: Different thickness of the electrodes rings and its influence.

Piston Tuner

As a further tuning possibility piston tuners can be used. For simulations 18 piston tuners have been distributed equally along the structure. These tuners can be moved into the space between the stems to suppress magnetic field and influence the resonant frequency inductively. On a real structure one can either use them as fixed tuners or some of them as movable tuners for frequency adjustment during operation to compensate thermal effects. In order to investigate their tuning range, their depth was varied and plotted against the frequency and quality factor in Fig. 4.9.

Until the tuners enter the ladders they have only minor influence in the kHz region. By entering the stems at 70 mm the tuners can shift the frequency of about 1 MHz.

Summary

The Ladder RFQ has no intrinsic dipole field because of the symmetric shape of the stems but it has also a asymmetric ending of the electrodes like a 4-rod RFQ. Simulations of the structure show quite good results of the resonant values like quality factor and shunt impedance. With respect to this it is quite comparable to 4-rod RFQs. A disadvantages of the Ladder RFQ is the complicated fabrication of the frame that holds the rings. It needs to fit

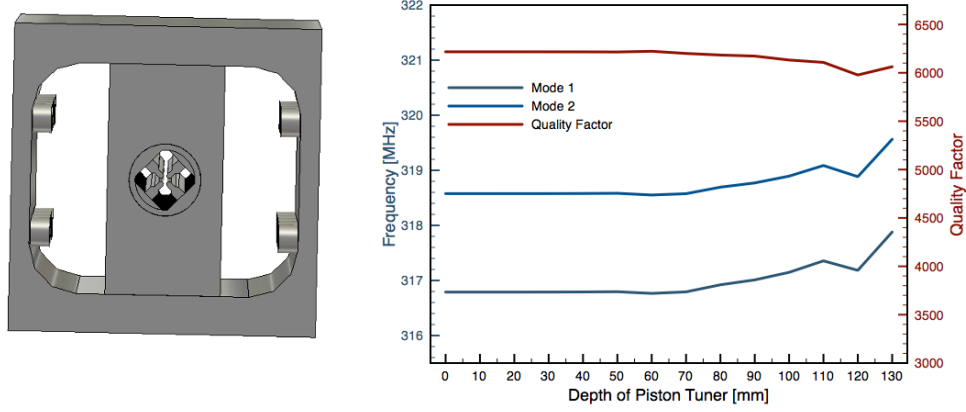


Figure 4.9: Parameter sweep of different piston tuner positions.

very accurate on a large plane area giving pressure on the rings keeping them at their place. Also the construction of the mounted rings with very tight tolerances in the 325 MHz region makes it really challenging. Due to this construction the tuning by the ring thickness is very complex. Tuning is an iterative process where the electrodes have to be dismantled to change the rings. Since the number of rf cells will be about 50 this can be a process of several months combined with high risks of some damage during this procedure. For lower frequencies the tolerances are not that important or if one suggests an alternative tuning instead of the rings would make it much simpler to construct. An alternative could be to use two tuning plates like in a 4-rod RFQ, but in two opposing RF cells each at the same height. This was realized for example at the antiproton decelerating RFQ at CERN with a frequency of 202 MHz [58]. Another alternative realized at the Frankfurt Funneling Experiment is to use capacitive blocks mounted on the ladders.

4.3 CH RFQ

Another type of RFQ that was regarded for 325 MHz is the CH RFQ. Its construction is similar to cross-bar H-mode (CH) drift tube structures. In the investigated case the electrodes are mounted on rings like at the ladder RFQ to benefit from its tuning possibilities. The construction is similar to the Ladder structure but every stem is mounted with an angle of 90° to the adjacent stem. With respect to the RF design the CH RFQ can be regarded as a 4-vane

RFQ but with very large coupling windows. For investigations on the tuning possibilities the shim edges of the tank, the thickness of the electrodes rings and their outer radius was varied.

Shim Edge Length

An approach to the resonant frequency can be done by the variation of the shim edge length but this can be also considered as a general tuning possibility of the structure. Changes of the shim edge length are comparable to the geometric shape of the tank in the 4-vane simulations above. A variation of the shims is shown in Fig. 4.10. The larger the shims, the more magnetic field is suppressed. The frequency increases like in a cavity with smaller diameters. Due to less stored energy the quality factor decreases. In addition the quality factor decreases proportional to the volume filled with electric field [42].

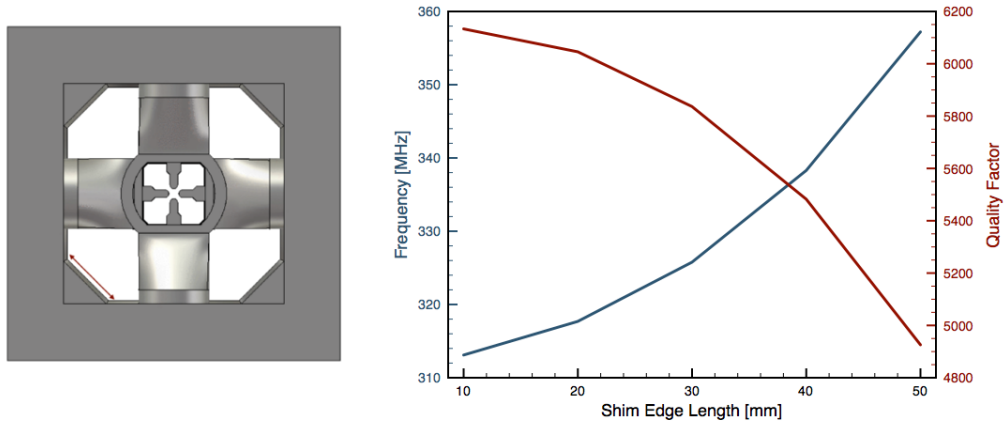


Figure 4.10: Variation of the shim edge length and its influence on frequency and quality factor.

Electrode Ring Width

As a frequency tuning possibility the electrode ring width was studied (see Fig. 4.11). This is similar to the ladder structure but with a different behavior. In both cases the frequency decreases with larger ring thicknesses. The quality factor of the CH RFQ decreases while it increases for the ladder RFQ.

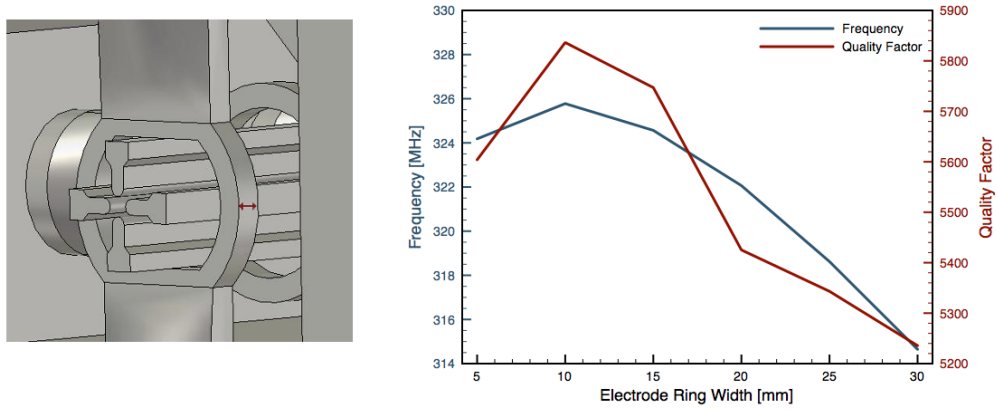


Figure 4.11: Parameter sweep of different electrode ring widths.

Electrode Ring Outer Radius

The simulations before have shown that the CH RFQ at 325 MHz is of very compact size. But for the assembly and tuning it needs at least a minimum size to handle it. Therefore the size of the electrode rings was varied. The results are shown in Fig. 4.12.

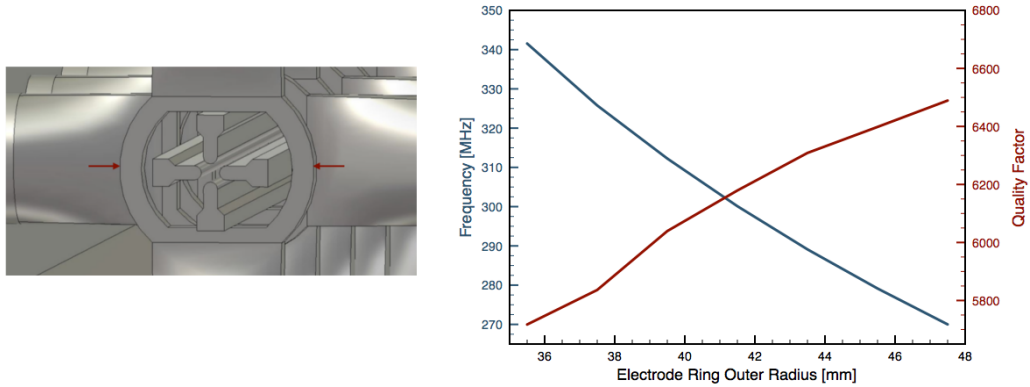


Figure 4.12: Influence of the change of the electrode ring outer radius.

Summary

Although it is very complicated for engineering and assembling the CH RFQ was investigated because of its symmetric structure. Due to this it has non disturbing dipole field and HOMs are quite well separated. The simulations have shown that it becomes impractically small at the desired frequency and

we have not found any proper solution for the engineering. Hence it was not considered anymore for the 325 MHz region but it might be a solution at lower frequencies.

4.4 Discussion

It is difficult to determine which RFQ resonator type is the best for the frequency of 325 MHz, because the costs and production time as well as service inspection possibilities might be relevant for operators of the RFQ. Developing an RFQ is a complex process including RF design, particle dynamics, mechanical engineering, assembly, RF setup, etc. In order to build a well working machine one might rather try to adapt the RFQ requirements on a structure one has experience with than developing a new structure type.

The 4-vane RFQ is the only structure realized and operating at this high frequencies. The production is a complicated and time consuming process, where a lot of experience is needed. Due to the limited access to the structure after production it is very complicated or even impossible to solve potentially damages. This means that the accuracy of the machining needs to be quite high and has to be rechecked several times during production to minimize errors. The 4-vane RFQ is definitely a working but a high priced and more risky solution. For example a replacement for the SNS 4-vane RFQ at ORNL has been built due to a frequency shift caused by cooling problems [7].

The Ladder-RFQ has no dipole field and is of feasible dimensions. The access is limited but better than at the 4-vane resonator. That means it might be possible to fix production errors afterwards. For measurements of the field flatness and the shunt impedance using a perturbation capacitor it is very difficult because of the narrow ladder distance and the limited access possibilities. Using a bead-pull method requires a homogenous field distribution, moreover it is challenging for a 3 m long RFQ with only less space to fit in a bead. The mentioned points refer to a design where the electrodes are mounted on rings that are fixed with to halves of a copper block like in [6]. Overall one might say tuning and flatness measurements are difficult but depend on the solution in detail. For example the tuning of frequency and flatness using the electrodes rings might be hard to realize but using shortcut plates, like it is done at 4-rod RFQs, would make it much easier. The performance of the ladder structure depends strongly on which mechanical design is chosen.

The 4-rod RFQ provides excellent access and is very comfortable for tuning due to its construction. The dipole field can be eliminated at this frequency by proper simulations and RF design of the structure. The RFQ becomes quite small at 325 MHz but due to the fact that it is a transmission line resonator, the cavity can be spacious for comfortable access. Although an operating 4-rod RFQ at 325 MHz does not exist yet, the prototype shows a quite good performance. These results are presented in chapters 3.1.3 and 5. Due to the experience at IAP with 4-rod RFQs the 325 MHz region is challenging but definitely possible.

In summary except the CH RFQ all structures are practicable solutions for 325 MHz. The dipole field and higher order modes will not be a problem and with respect to RF performance all structures are possible. Due to the low duty cycle of lower than 0.1 % [34] no thermal problems are expected for all structures. The differences between the RFQ types are basically in the assembly and tuning as well as repair and maintenance possibilities. Main issues that have to be proven in detail are the alignment tolerances, the RF coupling, tuning of the structure and the capital costs.

5 Power Tests of the 325 MHz 4-rod Prototype

This chapter presents the first power test of a 325 MHz 4-rod structure. The low level RF measurements have shown good accordance with the simulations so the high power tests are the next steps to show the performance of the prototype under real conditions. This test should show how much power the cavity can sustain. The setup with the 40 kW amplifier for the short prototype and corresponds to about 120 kW/m . In addition gamma spectroscopy measurements give information about the electrode voltage of the RFQ. Beyond that gamma spectroscopy enables one to verify the shunt impedance measurements at low power levels.

5.1 Low Power Conditioning

Setup

For low power conditioning a 500 W cw amplifier and N-type coaxial cables as transmission line were used. In the transmission line a circulator with a 2 kW load was mounted to protect the amplifier. A bidirectional coupler as well as a pickup probe on the cavity were used together with power meters to observe the input power by measuring the forwarded, the reflected and the transmitted power. A schematic setup is displayed in Fig. 5.1. On one side of the cavity a glass window was mounted to observe discharges [24].

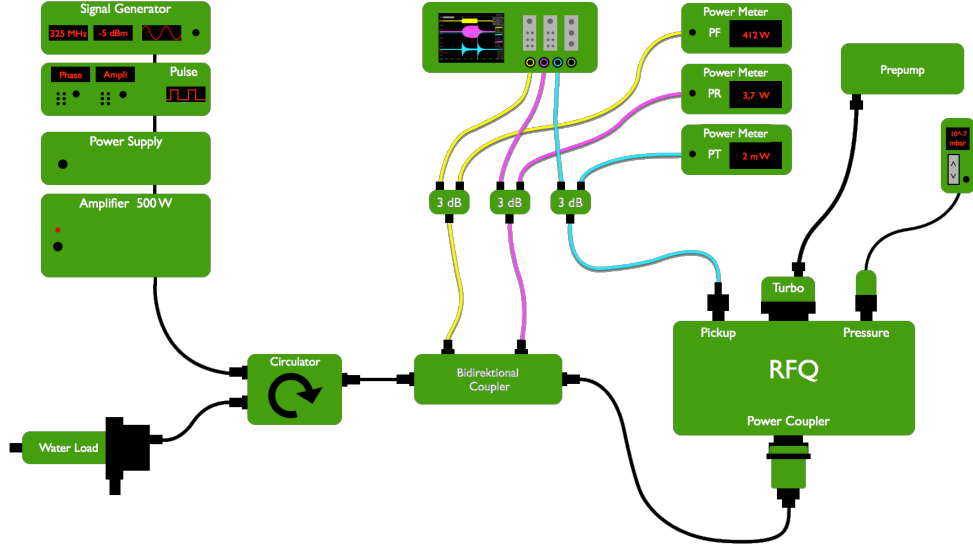


Figure 5.1: Setup for Low Power Conditioning

Low Power Conditioning

Before starting the low power conditioning the vacuum was at an end pressure of $3.6 \cdot 10^{-7}$ mbar. At the beginning almost all forwarded power was reflected and discharges inside the cavity (multitasking) could be observed at very low power levels. The left graph of Fig. 5.2 shows the signal from the uncalibrated pickup probe over a time of about 1.5 hours.

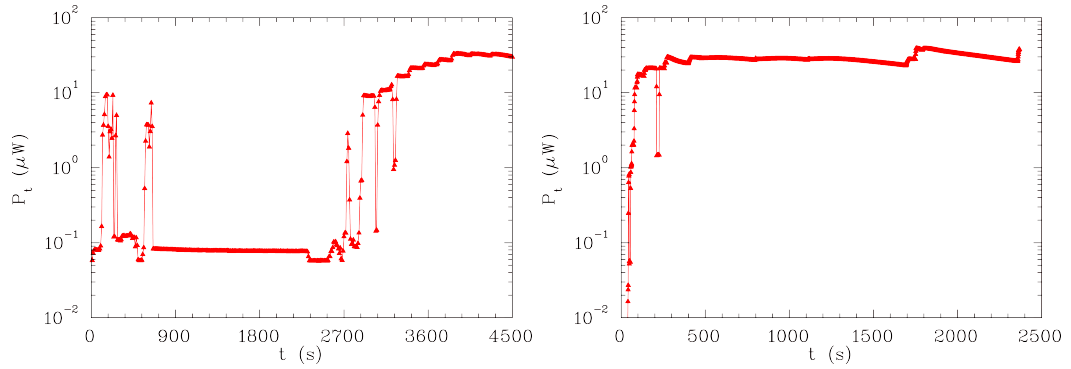


Figure 5.2: Uncalibrated transmitted power signal at day one (left) and day 2 (right) of commissioning.

After providing a forwarded cw power of 2 W overnight the RFQ was accepting an RF level of up to 50 W. Later on that day 350 W accepted power could be reached. But still with glowing discharges causing unstable pressure

in the cavity. Fig. 5.2 (right graph) shows the uncalibrated pickup signal on day two, recorded for about one hour.

The cw power was heating the cavity. There was no water cooling and no piston tuner, so the frequency had to be adjusted manually what made the pickup curve quite unstable. One day later the RFQ was accepting power much better. Up to 450 W cw power was accepted with still some discharges but with mainly stable pressure. The glowing spots during low power conditioning are shown in Fig. 5.3

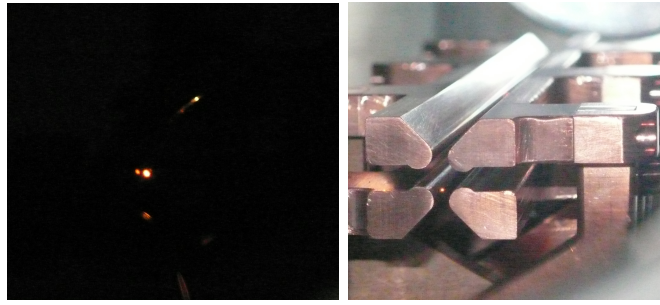


Figure 5.3: Glowing spots and discharges at the RFQ during low power conditioning.

The thermic pictures in Fig. 5.4 were taken at 350 W. They show the temperature of the circulator, the water cooled load and the cavity. There was no water cooling of the RFQ's ground plate at this point but the temperature was below 40°C.

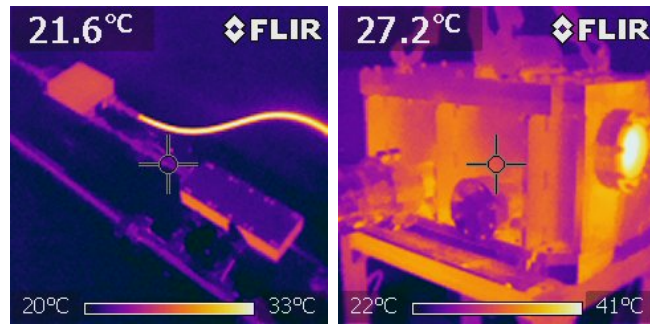


Figure 5.4: Thermal pictures of the 2 kW load on the left and the cavity walls with glas window on the right at 350 W input power.

Fig. 5.5 shows a picture taken by switching from cw to pulsed mode during conditioning. One can see stable pulses at 360 W with a slight overcoupling. From top to bottom the forwarded, the transmitted and reflected pulse is

represented. The low power conditioning was completed by reaching a cw input power of 450 W.

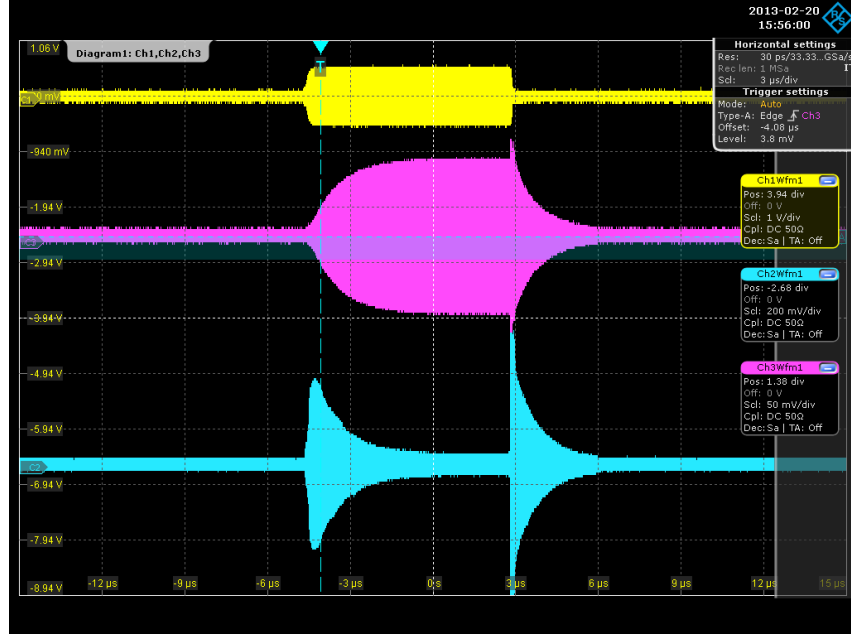


Figure 5.5: Pulse signals of forwarded, transmitted and reflected power (from top to bottom) at 360 W.

5.2 High Power Tests

For the high power tests the same setup was used as for the low power conditioning. The amplifier was changed to a 40 kW pulsed power amplifier made by DB Elettronica, Italy and the N-type cable were replaced by $1\frac{5}{8}$ " inch transmission lines. The 2 kW load had to be replaced by a 10 kW water-cooled load as well.

At the beginning the setup performed quite well, the pulsed power could be increased slowly but after a few days of conditioning and a maximum input power of 12 kW the test was interrupted due to sparking inside the circulator (see Fig. 5.6).

Sparking damages could be found at three spots inside the circulator so that it had to be repaired and optimized by the manufacturer. Due to this shut down also the RFQ was inspected. During conditioning unstable pressure and pulses due to sparking inside the resonator occurred. This was caused by

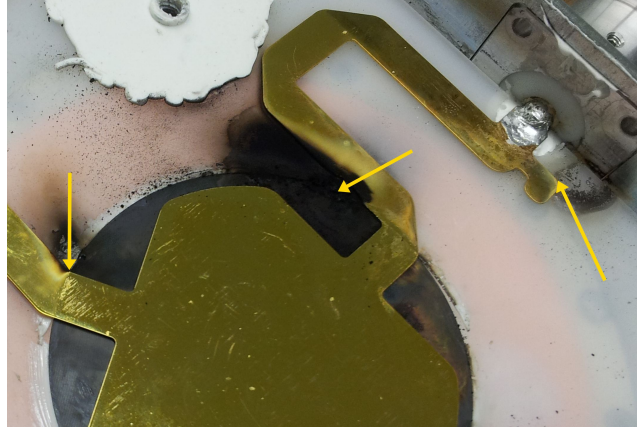


Figure 5.6: Inside of the circulator. Three spots of sparking damage.

problems at the soldering of the cooling channel in the ground plate. The cooling channel was made by milling a contour closed by soldering a copper sheet. The soldering was complicated because of the large surface that needs to be water tight. This led to a surface of the ground plate which was not very smooth. The structure was not cooled and did heat up during low power conditioning. Either the heat of the 450 W cw power or the RF sparking was sprinkling the brazing solder onto the stems, tuning plates and the ground plate. The stained structure by the solder sprinkles can be seen in Fig. 5.7. This led to a disadvantageous RF behavior and the RFQ structure had to be replaced as well.

5.2.1 Optimization of the 4-rod RFQ

In order to find a quick solution it was decided to make a new ground plate without water cooling. This was made of a solid copper block to provide good thermal conductivity. Also the tuning plates were replaced by new ones. The solder sprinkles of the stems had to be removed. The stems and electrodes were dismantled and polished. After reassembling the prototype, shown in Fig. 5.8, the RF setup was done again and optimized as well.

During the new RF setup of the 4-rod RFQ the longitudinal voltage distribution and the dipole tuning was improved. Measurements of the quality factor and accordingly the shunt impedance gave enhanced results as well. A comparison of the results of the RF setup is given in table 5.1



Figure 5.7: Stained structure by solder sprinkles caused by RF and thermal warming.

Table 5.1: RF Parameter of the Prototype before and after Optimization

Parameter	before Optimization	after Optimization
Flatness	$\pm 1.6 \%$	$\pm 0.02 \%$
Dipole	3 %	2 %
Quality Factor	2400	2800
Shunt Impedance	46,8 $k\Omega$	54,6 $k\Omega$

By placing the RFQ structure into the tank the power coupling loop had to be readjusted. The reflection of the power coupler was improved from -20 dB to -30 dB. The low power conditioning was executed with a 50 W amplifier in cw operation. The first time the conditioning was carried out up to 450 W cw power what might have lead to the strong warming of the structure. The duty cycle of 0.3 % with the 40 kW amplifier equals to a thermal power of 120 W what is roughly four times smaller than the low power conditioning before. Thermal problems were not expected this time. Due to the limited availability of the equipment to drive the 40 kW amplifier, the low power conditioning could be done longer as expected over several days very slow with very low power in the mW region. This has lead to an improved acceptance of higher RF levels.



Figure 5.8: Picture of the optimized prototype.

5.2.2 High Power Conditioning

The high power condition was carried out using a 40 kW amplifier in pulsed mode with 1 ms pulse length at 4 Hz. This corresponds to a duty cycle of 0.3 %. The RFQ was accepting about 23 kW within a few hours operation time without any problems like unstable pulses, sparking or unstable pressure within the cavity.

Since there was no cooling of the structure and no piston tuner the frequency was adjusted manually according to the slow warming of the prototype. The frequency was decreasing about 300 kHz during this procedure with an input power of 37 kW. This frequency shift was expected due to thermal simulations with CST Microwave Studio[®]. From the temperature increase the extension of copper was calculated. This was added to the simulation model and the resonant frequency was recalculated. Usually a piston tuner is able to adjust a range of up to 1 MHz at 4-rod RFQs and probably even more in this sensitive 325 MHz region. In addition if the stems would be cooled a much lower detuning is expected.

After acceptance of about half the maximum input power of the amplifier, measurements of the electrode voltage were started.

5.2.3 Measurement of the Shunt Impedance

As described in chapter 2.1.4 the shunt impedance is a important value to determine the efficiency of an accelerating structure. The shunt impedance of the 325 MHz 4-rod RFQ prototype has been calculated using the different methods introduced in chapter 2.1.4 and are compared in the following.

A common way to determine the shunt impedance at low RF levels is to use the perturbation capacitance method. A small known perturbation capacitance, usually 1 pF, is placed between two electrodes of the RFQ. By observing frequency shift one can calculate the R_p -value using formula 2.29. The perturbation needs to be small in order to fulfill the Slater Theorem [55]

$$\frac{\Delta f}{f} = \frac{\Delta \omega}{\omega} = \frac{\Delta W}{W}. \quad (5.1)$$

Therefore the capacitance needs to be small in comparison to the overall electrodes capacitance. Typical electrodes capacitances are 80 - 120 pF/m. This fits also with the electrodes of the prototype but its length is only 0.285 m and the calculated capacitance is only about 46 pF. In addition 1 pF capacitances are the smallest commercial capacitances with rather big production errors of 20 % [32]. Usually the frequency shift in this measurement is about 1 MHz or less. At the 325 MHz prototype the shift is several MHz. Nevertheless the measurement has been carried out giving an R_p -value of $77.8 \text{ k}\Omega \pm 23.3 \text{ k}\Omega$. Altogether at the short prototype this kind of measurement is resulting in very errors bringing only unsatisfactory results. Therefore other types of measurements have been carried out and compared.

Since the electrodes of the prototype have no modulation it is easy to calculate the capacitance by approximation with formula 2.31. This gives one an electrodes capacitance of 45.7 pF. Since the electrode length is 0.285 m this value is comparable to typical 4-rod RFQ electrode capacitances of about 80 - 120 pF/m. Then a shunt impedance of 59.9 k Ω was determined with a measurements of the quality factor using formula

$$R_p = \frac{2Q}{\omega_0 C}. \quad (5.2)$$

Another method to determine the shunt impedance is the comparison of the R/Q -value of simulations with a less defective measure of the quality factor also

described in chapter 2.1.4. By experience this gives one quite accurate results because the ideal behavior of simulations is reduced in the fraction R/Q and scaled with a value from a measurement. The shunt impedance is then given by

$$R_{meas} = \frac{R_{sim}}{Q_{sim}} \cdot Q_{meas}. \quad (5.3)$$

The result of this method is more realistic than the perturbation capacitance measurements and gave an R_p -value of $54.6 \text{ k}\Omega \pm 4.4 \text{ k}\Omega$.

Gamma Spectroscopy

At high RF levels one can determine the shunt impedance directly by measuring the intervane voltage and the RF power level using formula

$$R_{p0} = \frac{U_{max}^2}{N}. \quad (5.4)$$

The voltage can be measured by gamma spectroscopy. Electrons that are produced at one electrode by residual gas ionization are accelerated by the electric field of the intervane voltage. When these electrons hit the copper of the other electrode, bremsstrahlung is generated. This continuous γ -spectrum, as example shown in Fig. 5.9, is measured with a semiconducting detector, which was calibrated with an Am^{241} -probe. Americium emits photons with energies of 26.4 keV and 59.6 keV.

The gamma detector was placed in front of the cavity at the electrode height. It was used a borosilicate glas window flange to receive higher count rates. The window was covered with a metal grid as RF shielding to protect the gamma spectrometer. Measurements of the intervane voltage have been carried out at different RF power levels. These measurements are summarized in Fig. 5.10. This graph shows the intervane voltage depending on the input power as well as the determined shunt impedance at different input power levels.

The RF output level of the amplifier is depending on the operating frequency. Since there was no cooling of the RFQ the frequency was dropping slightly due to a thermal drift of the resonator. The shift of the resonance lead to a lower RF power level. Hence the gamma spectrum was also drifting to lower energies

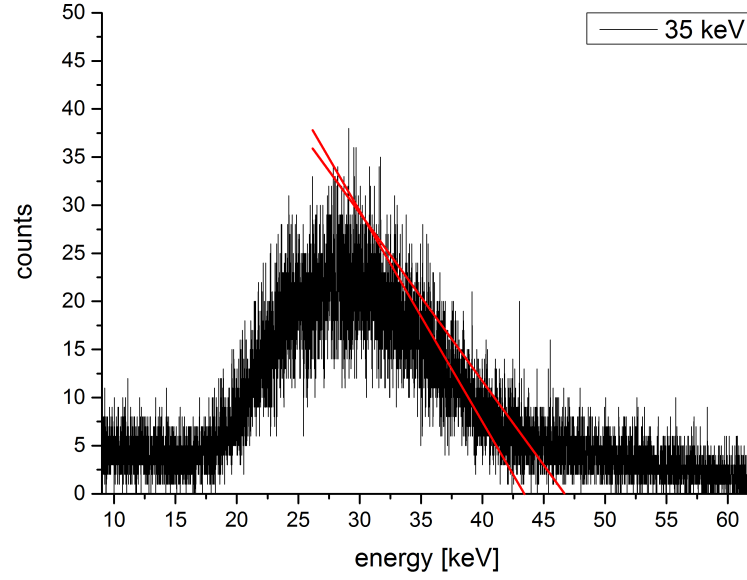


Figure 5.9: Gamma spectrum measured at an input power level of 35 kW.

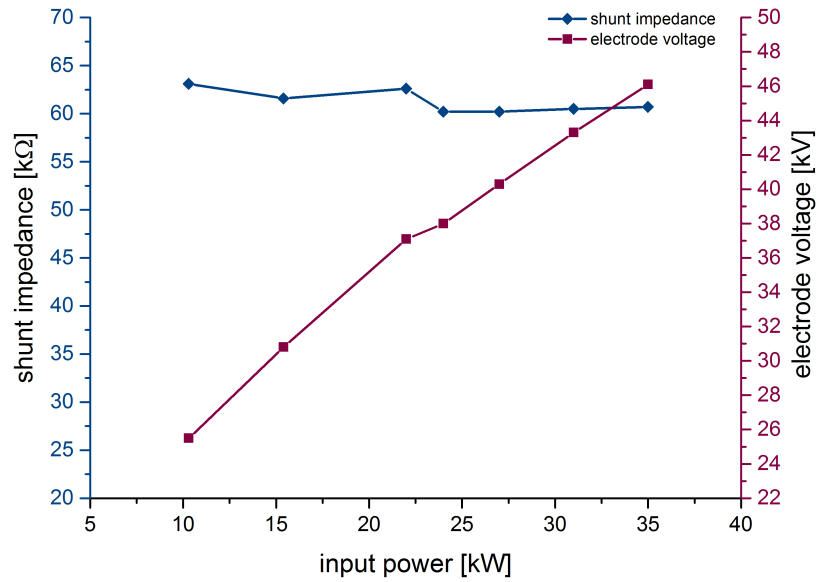


Figure 5.10: Measurement of the electrodes voltage at different input power levels and the determined shunt impedance.

causing less count rates in the interesting area of the photons with the highest energy. These photons are only produced at the maximum amplitude of the sinusoidal voltage. Higher accuracies of these measurements could be reached by using a cooling system and a piston tuner to keep the frequency and the power level more stable.

Summary

The shunt impedances determined with the different methods are summarized in tabular 5.2. The table also includes the shunt impedance calculated from CST Microwave Studio[®] simulations for this prototype.

Table 5.2: Comparison of Shunt Impedance Measurements

Method	R_p -Value	Error
Perturbation Capacitance	77,8 $k\Omega$	$\pm 23.3 k\Omega$
Electrodes Capacitance Calculation	59.9 $k\Omega$	$\pm 4.2 k\Omega$
R/Q -Comparison	54.6 $k\Omega$	$\pm 4.4 k\Omega$
Gamma Spectroscopy	61.3 $k\Omega$	$\pm 6.7 k\Omega$
Simulation CST MWS [®]	72.4 $k\Omega$	

The perturbation capacitance method works quite well if the change of capacity is small in comparison to the overall electrode capacity. In this case a perturbation of several MHz results in errors of 10 % in addition with the error of 20 % of the small capacitance of 1 pF. This measurement is not very accurate for this prototype but might work better if the RFQ would be build in full length of about 3 m. This would increase the electrodes capacitance by a factor of 10 bringing back the requirement of a small perturbation with respect to the total capacitance. The R/Q -comparison delivers good results that fit with the values from gamma spectroscopy. Optimization of the measurements could be done by improving the determination of the dissipated power in the resonator. By cooling the RFQ the frequency would be more stable as well as using calibrated power meters might deliver even more sufficient results. Comparing the shunt impedance with simulation results made with CST Microwave Studio[®] also confirms the expected value. Measurements of the shunt impedance are usually about 70 - 80% of the simulation results by comparison with experimental values of some of the last RFQ projects at the IAP. The graph in Fig. 5.11 shows the shunt impedance depending on the operation frequency of

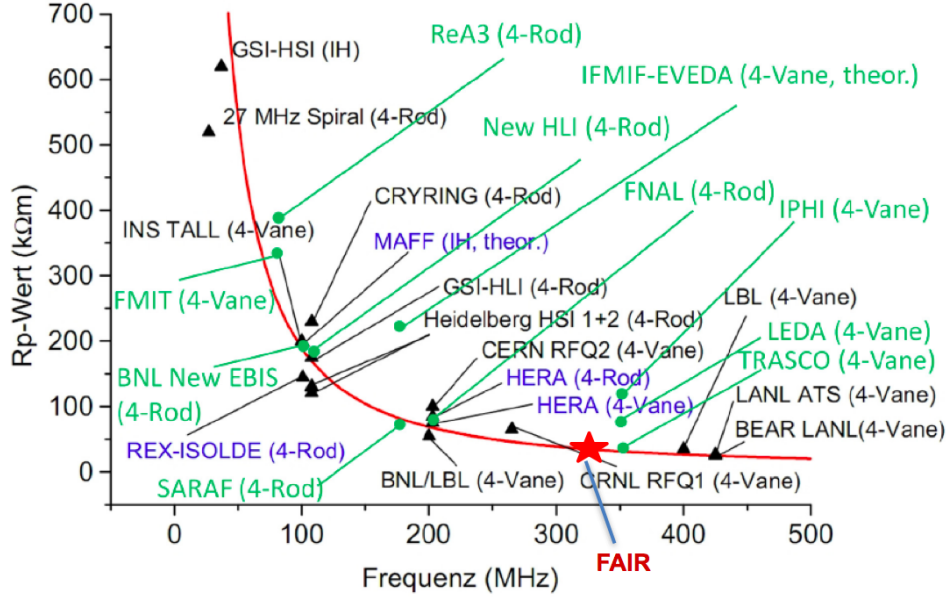


Figure 5.11: Shunt impedance depending on the operation frequency for different RFQs, original from [54] and supplemented by H. Podlech (green).

several realized RFQs of the last three decades. The red line shows the approximated proportionality of $R_p \propto f^{-3/2}$. Because the electrodes capacitance of most RFQs is different due to a different beam dynamics design, only the RFQs in blue are of identical or nearly identical beam dynamics design and are really comparable [54]. At higher frequencies the space between the stems of 4-rod RFQs are becoming closer and hence the current paths on the electrodes shorter. This graph shows that 4-vane and 4-rod RFQ are comparable related to the shunt impedance. Altogether a shunt impedance of around 60 $k\Omega$ fits with the comparison of many operating RFQs worldwide in [54] and is a quite good result for the prototype.

6 Conclusion

The subjects of this thesis are studies on the development of a 4-rod RFQ to operate at a frequency of 325 MHz. An application could be an RFQ accelerator for the proton linac at the FAIR project at GSI. The main tasks this thesis deals with are

- RF simulations on the field optimization of 4-rod RFQs regarding fringe fields and dipole fields due to the high operation frequency and higher order modes that may occur on this RFQ at 3m length due to the number of RF cells.
- RF design and assembly of a 4-rod copper prototype to verify the simulation results regarding the RF parameters and the dipole field at low level RF measurements.
- Power test of the prototype to demonstrate the performance of the 325 MHz 4-rod RFQ at high RF levels including gamma spectroscopy to determine the electrodes voltage and confirm the shunt impedance with different measurement methods.
- Comparison of alternative RFQ resonators and the discussion of their feasibility at 325 MHz.

The highest frequency 4-rod RFQs have been built up to now is 216 MHz. On even higher frequencies asymmetries of the 4-rod structure may cause problems in the RF behavior for example leading to a vertical displacement of the beam axis. A dipole field overlaying the quadrupole field of the electrodes leads to this displacement and is caused by the asymmetric mounting of the electrodes. This effect usually can be neglected at low frequencies, but becomes relatively more serious at above 300 MHz. To solve this problem all typical variations of design parameters defining the frequency of 4-rod RFQ resonators have been studied to determine their influence on the dipole field. In particular the stem shape and respectively the cutting of the stem was investigated in detail as

one of the strongest parameter for the reduction of the disturbing dipole field. Through this a complete dipole compensation or even an overcompensation could be realized. Apart from this for the real length of about 3 m of this RFQ, an investigation on higher order modes due to the large number of RF cells was necessary. Simulations have shown a still acceptable separation of the operating mode from the higher order modes. Also fringe field effects have been studied in order to optimize the longitudinal fields between the electrodes and the vessel walls. This is not only a high frequency problem and helps to optimize 4-rod RFQs in general. The studies of the electrodes overlap, the last stem position and the distance to the vessel wall showed that an enhanced space for the magnetic field around the last stem increases the electric field symmetry of the ends of the RFQ. A further parameter to increase the symmetry is the position and aperture of the RF shielding at the end flanges of the RFQ. The boundary field get less perturbed by more space provided by a larger aperture or more distance to the RF shielding.

Based on these studies a short copper prototype was designed and built in our workshop. With low level RF measurements of the RFQ the simulation results have been successfully verified. The measurements have proofed the possibility of a dipole free 4-rod RFQ at 325 MHz with an overall satisfying RF performance. For the determination of the shunt impedance several methods were investigated and compared.

The already small capacitance of 1 pF for the perturbation method was still too large compared to the small electrodes of the short prototype leading to considerable errors in the measurements. The other methods were based on theoretical calculations or partly on simulations.

Later this values were validated by high power measurements of the electrode voltage of the RFQ using gamma spectroscopy and the determination of the shunt impedance from these results. The findings of this simulations and experiments lead to simulations of an optimized 325 MHz 4-rod RFQ design, that are presented as well.

After the RF setup and low level RF measurements the 4-rod RFQ prototype was tested on high power levels to demonstrate its performance. Therefore it had to be low power conditioned in cw mode to reach an RF power above

multipacting discharge levels. Then a 40 kW amplifier was used for the higher power levels in pulsed mode. Due to problems with a circulator at 8 kW and thermal damages inside the RFQ, the prototype was improved. All parts have been polished and a new ground plate and new tuning plates lead to even better results of the RF setup. After conditioning the prototype again, it was accepting higher power levels up to 40 kW without any problems. The electrode voltage was measured using a gamma spectrometer at several input power levels. From these result the shunt impedance could be determined and compared to other methods of measurement. As a result it could be proven that the shunt impedance of the 325 MHz 4-rod RFQ is comparable to other RFQ structures in this frequency region.

The 325 MHz 4-rod RFQ was compared to alternative RFQ resonators. These are the 4-vane RFQ, the Ladder RFQ and a CH RFQ. All of these structures were analyzed in RF simulations at the same frequency region to determine their RF parameters and tuning possibilities. Also technological aspects like manufacturing and access during the tuning procedures have been regarded. In a discussion the feasibility of the different resonator types has been compared.

The 4-vane RFQ is the state of the art resonator for high frequency applications. It is ambitious in manufacturing and tuning and a rather high priced solution. It has been built successfully several times.

The Ladder RFQ has no disturbing dipole field. It has been realized but never for high RFQ frequencies. These Ladder RFQs are operating at CERN at Linac3 (101 MHz) and the ASAKUSA (202 MHz) decelerator or at the Frankfurt Funneling experiment (54 MHz). It is a possible option for 325 MHz, but its complexity is depending on mechanical solutions in detail.

The CH RFQ was investigated because its dipole free as well, but it becomes unpractical small at this high frequency and is complicated in manufacturing.

6.1 Summary

A basic introduction into RFQ accelerators has been given in chapter 2 of this thesis. In detail the working principle of radio frequency quadrupole accelerators is described and an introduction into important parameters, the electric fields and simulation software is given. Different resonator types to bring the electrodes on the quadrupole potential are introduced.

Chapter 3 describes the main tasks and challenges to approach a 325 MHz 4-rod RFQ including studies on the transversal dipole field and longitudinal fringe fields of the 4-rod structure. Simulations of an improved 4-rod RFQ based on previous simulations and measurements of the prototype are presented.

Alternative RFQ resonator concepts are compared in chapter 4. This work describes the tuning possibilities and basic RF design of the different structures. A discussion based on the feasibility of these structures to work at the 325 MHz frequency is presented.

In Chapter 5 the low power conditioning and high power operation of the prototype is described in detail. Also the optimization of the prototype during this process and the improvement of the RF setup is presented. Measurements of the electrode voltage using gamma spectroscopy lead to a determination of the shunt impedance, which was compared to other shunt impedance measurements.

In summary it has been shown that a dipole free 4-rod RFQ operating at a frequency of 325 MHz at high power levels is possible. Challenges and difficulties have been investigated and options for solutions have been presented and proved with a prototype.

6.2 Outlook

This work has proven the feasibility of a 4-rod RFQ at 325 MHz to operate for the proton linac at FAIR. Further simulations on the dipole compensation are planned. In these simulations the stems are displaced in left and right direction in relation to the beam axis. This shift provides an asymmetric connection to the electrodes and compensates the asymmetries of the current paths. Due to the common RFQ length of 3 m the assembly would be a standard procedure. The electrodes are usually segmented at this length. The

stems and the ground plate are supposed to be milled out of a solid copper block. This provides a higher accuracy of the machining besides a better thermal and electrical connection. Also a thermal extension of the material will be more homogenous avoiding local thermal stress on the structure. This ground plate and stem combination will be segmented as well due to machining reasons. A segment will end in the middle of one stem to ensure a good electrical contact at the connection of two half stems. Only cooling of the stems is designated due to the low duty cycle. Since the number of RF cells is about 50 the iterative tuning process is very elaborate. To improve this a first start of the tuning plate distribution may be predicted using the tuning studies presented in [56, 53] and might speed up the tuning process.

Bibliography

- [1] BARTH, W.: *The Injector System of the FAIR Project*. In *Proceedings of LINAC 2008, Victoria, BC, Canada*, 2008.
- [2] BARTH, W., W. BAYER, L. DAHL, L. GROENING, S. RICHTER and S. YARAMISHEV: *Upgrade Program of the High Current Heavy Ion UNILAC as an Injector for FAIR*. Elsevier Science, 2001.
- [3] BARTH, W., B. SCHLITT, G. CLEMENTE, W. VINZENZ, S. MICKAT and L. DAHL: *Future Heavy Ion Linacs at GSI*. In *Proceedings of the International Accelerator Conference, San Sebastian, Spain*. GSI, Darmstadt, Germany, 2011.
- [4] BEZZON, G. P., A. M. LOMBARDI, G. PARISI, A. PISENT, M. WEISS, P. BOURQUIN and M. VRETENAR: *Construction and commissioning of the RFQ for the CERN lead-ion facility*. In *Proceedings of LINAC 1994, Tsukuba, Japan*, page 722, 1995.
- [5] BOINE-FRANKENHEIM, OLIVER: *The FAIR Accelerators: Highlights and Challenges*. In *Proceedings of the International Accelerator Conference, Kyoto, Japan*. GSI, Darmstadt, Germany, 2010.
- [6] BRODHAGE, R., RATZINGER U and A. ALMOMANI: *Desing Study of a High Frquency Proton Ladder RFQ*. In *IPAC 2013, Shanghai, China*, 2013. IAP, Universität Frankfurt, Germany.
- [7] CHAMPION, MARK S., ALEXANDER V. ALEKSANDROV, DALE HEIDENREICH MARK CROFFORD, YOON W. KANG, JOHN MOSS, TOM ROSEBERRY and JAMES SCHUBERT: *Plans for an Integrated FRONT-END Test Stand at the Spallation Neutron Source*. In *Proceedings of LINAC 2012, Tel-Aviv, Israel*, 2012.
- [8] CHILL, FREDERIC: *Untersuchungen zu den Einflussfaktoren auf die Strom- und Spannungsverteilung im 4-Rod RFQ*. Master's thesis, Goethe Universität, Frankfurt am Main, 2010.

- [9] CLEMENTE, G., W. BARTH, L. GROENING, R. HOLLINGER, P. FORCK, M. KAISER, J. PFISTER, S. YARAMISHEV, W. VINZENZ, Z. ZHANG, R. BRODHAGE, B. KOUBEK, H. PODLECH, R. TIEDE, A. SCHEMP, U. RATZINGER, B. LAUN, J. LESREL, N. CHAUVIN, O. DELFERRIERE, O. TUSKE and C. SIMON: *Beam Dynamics Errors and Loss Investigation of the FAIR Proton Injector*. In *Proceedings of IPAC 2013, Shanghai, China*. GSI Helmholtzzentrum für Schwerionenforschung, Darmstadt, Germany, 2013.
- [10] CRANDALL, K. R.: *RFQ Radial Matching Sections and Fringe Fields*. In *Proceedings of LINAC 1984, Seeheim, Germany*, 1984.
- [11] CRANDALL, K. R.: *Ending RFQ Vanetips with Quadrupole Symmetry*. In *Proceedings of LINAC 1994, Tsukuba, Japan*, pages 227–229, 1994.
- [12] FIRJAHN-ANDERSCH, A., J. MADLUNG, A. SCHEMP and H. ZIMMERMANN: *A Two-Beam RFQ and a Novel Design for Ion Beam Funneling*. In *Proceedings of EPAC 1996, Barcelona, Spain*. Johann Wolfgang Goethe-Universität, Frankfurt am Main, Germany, 1996.
- [13] FISCHER, PHILIPP: *Ein Hochleistungs-RFQ-Beschleuniger für Deuteronen*. PhD thesis, Goethe Universität, Frankfurt am Main, 2007.
- [14] GROENING, L., W. BARTH, L. DAHL, R. HOLLINGER, P. SPÄDTKE, W. VINZENZ, S. YARAMISHEV, B. HOFMANN, Z. LI, U. RATZINGER, A. SCHEMP and R. TIEDE: *A Dedicated 70 MeV Proton Linac for the Antiproton Physics Program of the Future Facility for Antiproton and Ion Research (FAIR) at Darmstadt*. In *Proceedings of LINAC 2004, Lübeck, Germany*, 2004.
- [15] GSI HELMHOLTZZENTRUM FÜR SCHWERIONENFORSCHUNG: <https://www.gsi.de>, 2014.
- [16] GSI HELMHOLTZZENTRUM FÜR SCHWERIONENFORSCHUNG; PANDA EXPERIMENT WEBSITE: <http://www-panda.gsi.de>, 2014.
- [17] HINTERBERGER, F.: *Physik der Teilchenbeschleuniger und Ionenoptik*. Springer-Verlag Berlin Heidelberg, 2008.

- [18] HOFMANN, BENJAMIN: *Untersuchungen an einem RFQ-Beschleuniger für hohe Betriebsfrequenzen*. Master's thesis, Goethe Universität, Frankfurt am Main, 2004.
- [19] J. SCHMIDT, B. KOUBEK, A. SCHEMPP: *Simulations on the Boundary Fields of 4-rod RFQ Electrodes*. In *Proceedings of IPAC 2013, Shanghai, China*. IAP, Goethe University, Frankfurt am Main, Germany, 2013.
- [20] K. HALBACH, R. F. HOLSINGER: *Superfish - a computer program for evaluation of RF cavities with cylindrical symmetry*. pages 213–222, 1976. Particle Accelerators 7.
- [21] K. R. CRANDALL, R. H. STOKES, T. P. WANGLER: *RF Quadrupole beam Dynamics Design Studies*. In *Proceedings of Linear Accelerator Conference, Montauk, NY, USA*. Los Alamos Scientific Laboratory, 1979.
- [22] KAPCHINSKIY, M. and V.A. TEPLIAKOV: *Linear Ion Accelerator with Spatially Homogenous Focusing*. Prib. Tekh. Eksp., (2):119, 1970. Engl. Transl.
- [23] KONDO, Y., T. MORISHITA, K. HASEGAWA, H. KAWAMATA, T. SUGIMURA and F. NAITO: *Recent Progress with the J-PARK RFQs*. In *Proceedings of LINAC 2012, Tel-Aviv, Israel*, 2012.
- [24] KOUBEK, B., H. PODLECH, A. SCHEMPP and J. SCHMIDT: *Power Tests of the 325 MHz 4-rod RFQ Prototype*. In *Proceedings of IPAC13, Shanghai, China*. IAP, Frankfurt am Main, Germany, 2013.
- [25] KOUBEK, B., A. SCHEMPP and J. SCHMIDT: *RF-Design of a 325 MHz 4-rod RFQ*. In *Proceedings of IPAC 2011, San Sebastián, Spain*, 2011.
- [26] KOUBEK, B., A. SCHEMPP and J. SCHMIDT: *RF Setup of the MedAustron RFQ*. In *Proceedings of LINAC 2012, Tel-Aviv, Israel*, 2012.
- [27] KOUBEK, B., A. SCHEMPP and J. SCHMIDT: *Status of the 325 MHz 4-rod RFQ*. In *Proceedings of IPAC12, New Orleans, Louisiana, USA*, 2012.
- [28] KÜPFMÜLLER, MATHIS, REIBIGER: *Theoretische Elektrotechnik*. Springer, 17 edition, 2006.

- [29] KURENNOY, SERGEY: *CST model of FNAL-RFQ: preliminary results*, May 2012.
- [30] LOMBARDI, A. M.: *Decelerating and Accelerating RFQs*. In *Proceedings of LINAC 2000, Monterey, USA*. PS Division, CERN, 1211 Geneva 23, Switzerland, 2000.
- [31] LOMBARDI, A. M.: *The Radio Frequency Quadrupole (RFQ)*. In *CERN Accelerator School Small accelerators*, Zeegse, The Netherlands, 2005.
- [32] MAUS, JOHANNES M.: *Development of RFQ Particle Dynamics Simulation Tools and Validation with Beam Tests*. PhD thesis, Goethe Universität, Frankfurt am Main, 2010.
- [33] MÜLLER, NORBERT: *Untersuchungen zum Funnelling von Ionenstrahlen*. PhD thesis, Goethe Universität, Frankfurt am Main, 2010.
- [34] N. N.: *FAIR Baseline Technical Report*. Technical Report, FAIR, Darmstadt, Germany, 2006.
- [35] OGURI, H.: *Power Upgrade of J-PARK LINAC*. In *Proceedings of IPAC 2013, Shanghai, China*, 2013.
- [36] OLIVIER, M.: *First Heavy Ion Accelerator in Saturne at 1 GeV/AMU using the CRYEBIS-RFQ Preinjector Hyperion II*. In *Proceedings of the LINAC 1984, Seeheim, Germany*, 1984.
- [37] PELIZÄUS, MARC: *3rd Joint Helmholtz Rosatom Lecture Week on FAIR Physics*. Lecture, November 2013.
- [38] PIQUET, O., M. DESMONS, A. FRANCE, Y. LE NOA, J. NOVO and C. ROSSI: *RF Tuning of the LINAC4 RFQ*. In *Proceedings of IPAC13, Shanghai, China*. CEA, IRFU, Gif-sur-Yvette, France, CERN, Geneva, Switzerland, 2013.
- [39] PIQUET, O., A. M. LOMBARDI, M. VRETENAR, O. DELFERRIÈRE, M. DESMONS, A. FRANCE and C. ROSSI: *The RF Design of the LINAC4 RFQ*. In *IPAC 2010, Kyoto, Japan*, 2010. CEA Saclay, France, CERN, Geneva Switzerland.

- [40] PODLECH, H.: *Anwendung der Supraleitung in Beschleuniger- und Fusionstechnologie*. Vorlesungsskript, IAP, Univ. Frankfurt, Germany.
- [41] PODLECH, H., M. GRIESER, R. V. HAHN, R. REPNOW and D. SCHWALM: *Electrodynamic Calculations of the 4-Rod-RFQ Resonator for the Heidelberg High Current Injector*. In *Proceedings of the 2001 Particle Accelerator Conference, Chicago*, 2001.
- [42] PODLECH, HOLGER J.: *Entwicklung von normal- und supraleitenden CH-Strukturen zur effizienten Beschleunigung von Protonen und Ionen*. Habilitationsschrift, 2008.
- [43] RATTI, A., J. AYERS, L. DOOLITTLE, R. DIGENNARO, R. A. GOUGH, M. HOFF, R. KELLER, R. MACGILL, J. STAPLES, R. THOMAE, S. VIROSTEK and R. YOURD: *The SNS RFQ Commissioning*. In *Proceedings of LINAC 2002, Gyeongju, Korea*, 2002.
- [44] RATZINGER, U.: *The New GSI Prestripper Linac for High Current Heavy Ion Beams*. In *Proceedings of the Linear Accelerator Conference, Geneva, Switzerland*. IAP, Univ. Frankfurt, Germany, 2006.
- [45] REHBERG, JANA MARLIES: *Untersuchungen zur Frequenzanpassung des MAFF-IH-RFQ*. PhD thesis, Goethe Universität, Frankfurt am Main, 2008.
- [46] ROSSI, C., P. BOURQUIN, J. B. LALLEMENT, A. M. LOMBARDI, S. MATHOD, M. TIMMINS, G. VANDONI, M. VRETENAR, S. CAZAUX, O. DELFERRIÈRE, M. DESMONS, R. DUPPERIER, A. FRANCE, D. LEBOEUF and O. PIQUET: *The Radiofrequency Quadrupole Accelerator for the LINAC4*. In *Proceedings of LINAC 2008, Victoria, BC, Canada*, 2008.
- [47] ROSSI, C., M. VRETENAR, L. ARNAUDON, G. BELLODI, J. BROERE, O. BRUNNER, A. M. LOMBARDI, J. MARQUES BALULA, P. MARTINEZ YANEZ, J. NOIRJEAN, C. PASQUINO, U. RAICH, F. RONCAROLO, M. DESMONS, A. FRANCE and O. PIQUET: *Commissioning of the LINAC4 RFQ at the 3 MeV Test Stand*. In *IPAC 2013, Shanghai, China*, 2013.

- [48] SCHEMPP, A.: *Beiträge zur Entwicklung der Radiofrequenz (RFQ)-Ionenbeschleuniger*. Habilitationsschrift, 1989.
- [49] SCHEMPP, A.: *The Application of RFQs*. In *Proceedings of Linear Accelerator Conference, Ottawa, Ontario, Canada*, 1992.
- [50] SCHEMPP, A.: *Design of Compact RFQs*. In *Proceedings of LINAC 1996, Geneva, Switzerland*. IAP, Johann Wolfgang Goethe Universität, Frankfurt am Main, Germany, 1996.
- [51] SCHEMPP, A.: *Overview of Recent RFQ Projects*. In *Proceedings of LINAC 2008, Victoria, BC, Canada*, 2008.
- [52] SCHMIDT, J. S., B. KOUBEK, A. SCHEMPP, C. Y. TAN, D. S. BOLLINGER, K. L. DUEL, P. R. KARNS, W. A. PELLICO, V. E. SCARPINE, B. A. SCHUPBACH and S. S. KURENNOY: *Investigations of the output energy deviation and other parameters during commissioning of the four-rod radio frequency quadrupole at the Fermi National Accelerator Laboratory*. Phys. Rev. ST Accel. Beams, 17:030102, Mar 2014.
- [53] SCHMIDT, JANET SUSAN: *Tuning and Optimization of the Field Distribution for 4-Rod Radio Frequency Quadrupole Linacs*. PhD thesis, Johann Wolfgang Goethe-Universität, 2014.
- [54] SIEBER, THOMAS: *Entwicklung von 4-Rod- und IH- Radio- Frequenz-Quadrupol (RFQ)-Beschleunigern für radioaktive Ionenstrahlen bei REX-ISOLDE und MAFF*. PhD thesis, Ludwig-Maximilians-Universität München, 2001.
- [55] SLATER, J. C.: *Microwave Electronics*. D. van Nostrand Co. Inc., New York, 1950.
- [56] TAN, C. Y., J. S. SCHMIDT and A. SCHEMPP: *Simple lumped circuit model applied to field flatness tuning of four-rod radio frequency quadrupoles*. Phys. Rev. ST Accel. Beams, 17:012002, 2014.
- [57] U. BARTZ, A. SCHEMPP: *A CW RFQ Prototype*. In *Proceedings of PAC 2011, New York, NY, USA*. IAP, Goethe University, Frankfurt am Main, Germany, 2011.

- [58] VRETENAR, M.: *Low-beta structures*. In *CERN Accelerator School RF for accelerators*, Ebeltoft, Denmark, 2010.
- [59] VRETENAR, M.: *The radio-frequency quadrupole*. In *CERN Accelerator School High Power Hadron Machines*, pages 207–223, Bilbao, Spain, 2011.
- [60] WANGLER, THOMAS P.: *RF Linear Accelerators*. Wiley-VHC, 2008.
- [61] WEILAND, T.: *A discretization method for the solution of Maxwells equations for six-component fields*. Electronics and Communication (AEÜ), 31:116–120, 1977.
- [62] WEILAND, T.: *Time domain electromagnetic field computation with finite difference methods*. International Journal of Numerical Modelling, 9:295–319, 1996.
- [63] YOUNG, L. M., L. J. RYBARCYK, J. D. SCHNEIDER, M. E. SCHULZE and H. V. SMITH: *High Power Operations of LEDA*. In *XX International Linac Conference, Monterey, California*, 2000.
- [64] ZHANG, CHUAN: *Beam Dynamics for the FAIR Proton-Linac RFQ*. In *Proceedings of IPAC 2014, Dresden, Germany*, 2014.

Danksagung

Meinem Doktorvater Prof. Dr. A. Schempp danke ich für die Aufnahme als letzten Doktoranden in seiner Arbeitsgruppe, aber besonders für die gute Betreuung, Unterstützung und Förderung während meiner Doktorandenzeit. Ebenfalls besonderer Dank gilt Prof. Dr. H. Podlech für sein Interesse an meiner Arbeit und die enge Zusammenarbeit und Unterstützung im Rahmen des 325 MHz RFQs.

Danke sagen möchte ich meiner Arbeitsgruppe, den ehemaligen und den aktuellen Mitgliedern, M. Baschke, U. Bartz, P. Till und besonders bei J. Schmidt für die tolle Zeit und die nicht nur physikalischen gemeinsamen Erlebnisse, die regelmäßigen Stammtische und Kaffeepausen.

Für die gute Zusammenarbeit, und der oftmals schnellen Erledigung des einen oder anderen Auftrags, bedanke ich mich bei der Werkstatt unter der Leitung von Sven Reploeg. Dieser Dank gilt ebenso D. Bänsch, T. Metz und J. Jaitner für die technische Unterstützung bei verschiedenen Projekten.

Stephan Klaproth danke ich für seine tatkräftige Hilfe bei der Gammaspektroskopie. Vielen Dank auch an J. Häuser für die engagierte Zusammenarbeit. Der guten Seele des IAPs, A. Hergt, möchte ich danke sagen, dass sie immer mit Rat und Tat zu helfen weiß.

Vielen Dank auch an meine Kommilitonen und die Mitglieder des IAPs, besonders B. Klump, die mich so viele Jahre begleitet haben. Danke für die tolle Arbeitsatmosphäre und Zusammenarbeit.

Darüber hinaus gilt mein Dank meinen Eltern, meiner Familie und Freunden, besonders E. Mauch und meiner verstorbenen Mutter, dir mir mit Geduld den Rücken stärkten und immer für mich da sind.

Lebenslauf

Persönliche Daten

Name Benjamin Koubek
Geburtsdatum 11. August 1980
Geburtsort Schwäbisch Hall, Deutschland

Doktorarbeit

2010/04 - 2014 Doktorand am Institut für Angewandte Physik (IAP)
Goethe Universität Frankfurt
Betreuer: Prof. Dr. A. Schempp

Akademische Lehrer

H. Appelshäuser, J. Baumeister, A. Bechthold,
C. Blume, T. Boller, R. Dörner, C. Gros, W. Hofstetter,
M. Huth, M. Iberler, J. Jacoby, O. Kester, P. Kopietz,
M. Lang, H.-J. Lüdde, G. Marinescu, J. A. Maruhn,
H. Podlech, U. Ratzinger, H. Roskos, O. Rosmej,
A. Schempp, R. Schmidt, H. Ströbele, J. Wachtveitl,
J. Weidmann, H. Zimmermann

Auslandsaufenthalte

2008 Pohang Accelerator Laboratory, Pohang, Süd Korea
DAAD-KOSEF Summer Institute Program (2 Monate)
2002 - 2003 Working Holiday Scheme, Neuseeland (1 Jahr)

Ausbildung

2010/02 Abschluss: "Diplom Physiker"
2004 - 2010 Physikstudium and der Goethe Universität Frankfurt
(Nebenfach: Chemie und Astrophysik)
2002 Abitur, Hessenkolleg Wiesbaden